Publication Language: English, Turkish

Published date: 04.04.2025

Privilege Owner: Prof. Dr. Mehmet ÖZASLAN

Website: tr: http://dergipark.org.tr/tr/pub/zbs

en: http://dergipark.org.tr/en/pub/zbs

Editorial Board

Table of Contents (İçindekiler)

Volume (Cilt): 6 Number (Sayı): 2
April (Nisan), 2025

ZEUGMA BIOLOGICAL SCIENCE

ZEUGMA
BIOLOGICAL SCIENCE

2025
v:6 n:2 p:1-6

The Investigation of CA 15-3 Antigen Levels in Local and Immigrant Women Patients Diagnosed with Breast Cancer in Gaziantep

M.A. Dagdeviren, M. Özaslan
Department of Biology, Gaziantep University, Gaziantep, Türkiye

aydin_dagdeviren@hotmail.com

Introduction

Cancer, like in the rest of the world, represents a significant public health issue in Turkey and is considered the second leading cause of death after cardiovascular diseases. Globally, cancer ranks second among causes of death, and according to projections, it is expected to become the leading cause by 2030 (1). An epidemiological study has found that breast cancer accounts for 25% of all cancer cases and 15% of cancer-related deaths among women (2). Since breast cancer is the most common type of cancer among women, raising awareness for early detection and strengthening screening programs are of utmost importance. In Turkey, the incidence of breast cancer, which was 24/100,000 according to data from 1993, had risen to nearly 50/100,000 by 2010 (3). A study conducted in 2019 reported that approximately 4,300 women lost their lives due to breast cancer in Turkey (4). CA 15-3 antigen is an epitope located on a large mucin-like glycoprotein encoded by the MUC-11 gene. MUC-1, encoded by the MUC-11 gene, is a glycoprotein with intense O-linked glycosylation on its extracellular domain (5). MUC-1 proteins are normally found in the glandular epithelium of various organs, providing a protective and lubricating effect to the surrounding cells. Furthermore, MUC-1 proteins play a role in protecting the body from infections by covering the apical surfaces of epithelial cells in the stomach, intestines, lungs, eyes, and other organs, preventing pathogens from reaching the cell surface (6). CA 15-3 is a mucin antigen particularly associated with breast cancer, and its use in detecting cancer-related changes is becoming increasingly important. MUC-1 proteins bind pathogens through oligosaccharides, preventing them from reaching the cell surface and serving a protective role in the extracellular space (6). Overexpression of MUC-11 has been frequently associated with colon, breast, ovarian, lung, and pancreatic cancers (6). A study conducted by Kozan and colleagues in Turkey found that BRCA mutations increased the risk of breast cancer in women, particularly with advancing age (7). Moreover, in another study, the ratio of CEA and CA 15-3 antigens was compared, and it was observed that this ratio was significantly higher in breast cancer patients (8). These findings support the role of CA 15-3 antigen as an important biomarker in the diagnosis and follow-up of breast cancer and emphasize its clinical value.

The aim of this study is to examine the relationship between clinical-pathological characteristics, such as age, and CA 15-3 antigen levels in immigrant and local female patients diagnosed with breast cancer. Additionally, by evaluating the diagnostic and prognostic value of the CA 15-3 biomarker, the study aims to determine the effects of age and clinical features on CA 15-3 levels and explore the role of this biomarker in the clinical management of immigrant and local female patients. Through the findings, the study aims to contribute to the development of strategies for breast cancer diagnosis and treatment based on the demographic

https://doi.org/10.55549/zbs.1623868

and clinical characteristics of immigrant and local female groups from a public health perspective.

Materials and Methods:

This study is based on the results of blood samples sent for CA 15-3 test analysis in a hospital in Gaziantep, which were obtained from patients diagnosed with breast cancer. Our study is a retrospective study, and the results of CA 15-3 tests routinely requested from the Obstetrics and Gynecology outpatient clinic were retrieved from the hospital archive covering a 10-year period. The analysis of the CA 15-3 test was performed using the Beckman DxI 800 analyzer, employing the chemiluminescence immunoassay method, with a kit specifically produced for the Beckman autoanalyzer under the name Br 15-3.

The data obtained from the study were analyzed using SPSS 20.0 software. Descriptive statistics such as mean, standard deviation, and percentage distributions were provided. Independent samples t-test was used for the comparison of variables consisting of two parameters, while chi-square analysis was used for the comparison of categorical variables, and the results were evaluated at a 95% confidence level ($p<0.05$).

The study was conducted in accordance with international declarations and guidelines and was approved by the Gaziantep University Ethics Committee and Research Institute, under approval number 2023/186.

Results

As shown in Table 1, an independent samples t-test was performed to determine whether CA 15-3 results differ by age groups among Turkish citizens. The test revealed that the mean CA 15-3 antigen level was significantly higher in women aged 50 and older ($p<0.001$).

Table 1. Comparison of CA 15-3 levels according to age in Turkish women diagnosed with breast cancer

Age	N	Mean	Std. Deviation	t	p
>50	6778	25,58	58,45	4,826	.001
<50	5273	20,71	50,35		

The chi-square analysis performed in Table 2 also showed that CA 15-3 levels were significantly higher in Turkish patients over the age of 50 compared to those under 50 ($p<0.001$).

Table 2. Comparison of CA 15-3 level difference according to age in Turkish women diagnosed with breast cancer

https://doi.org/10.55549/zbs.1623868

		Result_Grup		Total	χ^2	p
		Normal	High			
Age_Grup	<50	4859	414	5273	66,762	0.001
	>50	5935	843	6778		
Total		10794	1257	12051		

Table 3. Comparison of CA 15-3 levels according to age in Syrian women diagnosed with breast cancer

Syrian age grup	N	Mean	Std. Deviation	t	p
>50	97	42,58	91,295	0,667	0,167
<50	143	35,66	69,126		

In Table 4, an independent samples t-test conducted between Turkish and Syrian patients aged 50 and over found that the proportion of Syrian women was statistically significantly higher than that of Turkish citizens (p>0.05).

Table 4. Comparison of CA 15-3 antigen elevation in Turkish patients over 50 years age and Syrian patients over 50 years age.

Nationality	N	Mean	Std. Deviation	t	p
TC	6778	25,5894	58,45148	2,815	0,005
Syrian	97	42,5806	91,29527		

However, an independent samples t-test conducted to determine the difference in CA 15-3 levels between Turkish and Syrian patients under 50 showed that the difference between the groups was not statistically significant (p>0.05) (Table 5).

Table 5. Comparison of CA 15-3 antigen elevation in Turkish patients under 50 years of age and Syrian patients under 50 years of age

Nationality	N	Mean	Std. Deviation	t	p
TC	5273	20,7103	50,35687	2,569	0,001
Syrian	143	35,6643	69,12602		

Another independent samples t-test performed on Turkish and Syrian patients showed that the mean CA 15-3 level was higher in Syrian women than in Turkish women, and this difference was statistically significant (p<0.05) (Table 6).

https://doi.org/10.55549/zbs.1623868

Table 6. Comparison of CA 15-3 antigen mean of Turkish and Syrian patients

Nationalty	N	Mean	Std. Deviation	t	p
TC	12051	23,4545	55,10725	2,938	0,004
Syrian	240	38,4597	78,73056		

Additionally, the chi-square analysis showed that CA 15-3 levels were higher in Turkish patients compared to Syrian patients, and this difference was statistically significant ($p<0.05$) (Table 7).

Table 7. Comparison of CA 15-3 antigen mean difference between Turkish and Syrian Patients

		Result_Grup CA 15-3		Total	χ^2	p
		Normal	High			
Nationality	TC	10794	1257	12051	11,026	0,001
	Syrian	199	41	240		
Total		10993	1298	12291		

In Table 8, the chi-square analysis conducted on all female patients showed that CA 15-3 antigen levels were statistically significantly higher in patients aged 50 and over compared to those under 50 ($p<0.001$).

Table 8. Comparison of the mean elevation of CA 15-3 antigen in all female patients in patients over 50 years of age compared to patients under 50 years of age

		Result_Grup CA 15-3		Total	χ^2	p
		Normal	High			
Age Grup	<50	4976	440	5416	60,857	0,001
	>50	6017	858	6875		
Total		10993	1298	12291		

As seen in Table 9, an independent samples t-test conducted to determine the difference between the groups revealed that the mean CA 15-3 level in the patient group was statistically significantly higher than that of the control group ($p<0.001$).

Table 9. Comparison of the CA 15-3 antigen mean of the patient group and the healthy group

https://doi.org/10.55549/zbs.1623868

Grup	N	Mean	Std. Deviation	t	p
Patient	12558	23,6341	55,57289	3,967	0,001
Control	514	13,9079	6,47944		

Discussion

Although CA 15-3 antigen has been studied in many breast cancer studies using blood samples, it has been emphasized that this antigen alone is not sufficient for the diagnosis of breast cancer. Therefore, despite studies that use different tumor markers along with CA 15-3 antigen, the significance of high levels of this antigen in the prognosis of breast cancer patients still remains relevant. In our study, we investigated the relationship between the elevation of CA 15-3 antigen and age in breast cancer patients.

A similar study was conducted by Park and colleagues in 740 breast cancer patients, where no significant relationship was found between CA 15-3 levels and age in patients above and below 35 years old. However, in our study, it was determined that CA 15-3 antigen levels were significantly higher in breast cancer patients aged 50 and over ($p<0.01$) (Table 1). The possible reason for the differing results in Park and colleagues' findings could be the smaller sample size compared to our study and the average age being 35. Additionally, we believe that the statistical findings obtained in our study are more meaningful.

When examining the CA 15-3 antigen results in immigrant Syrian patients living in our region, we observed that patients aged 50 and over showed higher values compared to those under 50. However, this difference was not statistically significant. Interestingly, we found that CA 15-3 levels were significantly higher in Syrian women compared to Turkish women with breast cancer (Table 4). Although there are no studies in the literature regarding this, it can be hypothesized that Syrian patients' inadequate knowledge about breast cancer prevention, early lactation due to early marriages, and the effects of climate change on the MUC-1 gene could explain these findings. Additionally, the smaller sample size of Turkish patients compared to Syrian patients might have led to the statistical significance of these differences.

In conclusion, this study demonstrates that age and ethnicity may affect CA 15-3 levels in women diagnosed with breast cancer. Specifically, it was found that CA 15-3 levels were higher in women aged 50 and over, higher in Turkish women compared to those under 50, but higher in Syrian women compared to Turkish women. Furthermore, the higher mean CA 15-3 levels in the patient group compared to the control group highlight that cancer may have different effects in different groups, emphasizing the importance of personalized health approaches. These findings suggest that public health policies should develop individualized approaches to minimize health inequalities between local and immigrant populations.

References:

1. TC Sağlık Bakanlığı, 2018 Ulusal Kanser Kontrol Planı. 2013; 2021.

2. Torre LA, Bray F, Siegel RL, Ferlay J, Lortet-Tieulent J, Jemal A. Global cancer statistics, 2012. CA: a cancer journal for clinicians. 2015;65(2): 87-108.

https://doi.org/10.55549/zbs.1623868

3. TC Sağlık Bakanlığı, Halk Sağlığı Genel Müdürlüğü, and Kanser Daire Başkanlığı. Türkiye kanser istatistikleri, Ankara 2018.

4. B. Başara, B. S Çağlar, İ. Aygün, A. Özdemir, T, A. Kulali ve ark. S. B. (2019). TC Sağlık Bakanlığı Sağlık İstatistikleri 2018.

5. Dalziel M, WhitehouseIan C, Farlane M, Clausen H, Taylor J.The Relative Activities of the C2GnT1 and ST3Gal-I Glycosyltransferases Determine O Glycan Structure and Expression of a Tumor-associated Epitope on MUC1. Journal of Biological.2001; 276.14: 11007-11015

6. Croce MV, Isla-Larrain MT, Price M, R. Segal, Eiras, A. Detection of circulating mammary mucin (Muc1) and MUC1 immune complexes (Muc1-CIC) in healthy women.The International journal of biological markers. 2001;16(2): 112-120.

7. Kozan R; Tokgöz V. Türkiye'de meme kanseri farkındalığı ve tarama programı Acıbadem Üniversitesi Sağlık Bilimleri Dergisi. 2016;7.4.

8. Safi, F. Kohler, I., Beger, H. G., & Röttinger, E. The value of the tumor marker CA 15-3 in diagnosing and monitoring breast cancer. A comparative study with carcinoembryonic antigen Cancer. 1991;68(3): 574-582

9. Park, B-W., et al. Preoperative CA 15-3 and CEA serum levels as predictor for breast cancer outcomes Annals of oncology. 2008; 19.4: 675-681.

10. Duffy M. J. Shering, S. Sherry F. McDermott E. O'higgins N. ,CA 15–3: A prognostic marker in breast cancer. The International journal of biological markers. 2000;15(4): 330-333.

11. Topuz E, Güzel Ö, Töre G, Aldemir O, Bilge N, Kınay M, et al. Ca 15-3'ün Tümör Marker Olarak Meme Kanserlerinde Değeri. Turkish Journal of Oncology. 1988;3, 1-2

https://doi.org/10.55549/zbs.1623868

ZEUGMA BIOLOGICAL SCIENCE

ZEUGMA
BIOLOGICAL SCIENCE

2025
v:6 n:2 p:7-15

Technological Innovations Against Future Pandemics with Novel Strategies for Food Safety

[1]Turgay Çetinkaya, [2]Sibel Bayıl*, [3]Mehmet Özaslan

[1] Istanbul University, Faculty of Aquatic Sciences, Department of Aquatic Biotechnology and Genomics, Department of Aquatic Biotechnology, Istanbul, Türkiye,

[2]Gaziantep University, Department of Medical Services and Techniques, Vocational School of Health, Gaziantep, Türkiye

[3] Gaziantep University, Biology Department of Biology, Gaziantep, Türkiye

bayil@gantep.edu.tr

Abstract

The protection of food safety has been a global concern, especially in light of potential future pandemics. Consequently, food safety issues have been increasingly emerging. Strategies for designing customer experience, such as customer listening strategies should be continuously enriched with innovations in products and services. Nonthermal technologies such as nanotechnology, cold plasma, and ozone applications can be considered and applied to ensure food safety. These are alternative methods for treating virus-contaminated food package surfaces. Electrochemical, optical biosensors, and a combination of nanomaterials, nanomaterials-integrated biosensing approach are promising for fast detection of future zoonotic viruses. These developments will lead to the detection of new zoonotic viruses or variants.

Keywords: Pandemi, nanomaterials,food packaging, biosensor, virus

1. Introduction

Understanding food safety hazards risk is necessary to avoid virus transmission in the food supply chain since there is always a risk of zoonotic virus-based outbreaks (Lu et al., 2021). For zoonotic viruses, food and food packaging materials may be potential long-distance carriers (Ayşen, 2022). Because viruses can be found to remain stable on food surfaces or, food contact surfaces. For instance, after COVID-19 break new variants turned out such as Delta (Who, 2024). New variants are also concern for food safety. For instance, recently it was proved that biofilms could be a reservoir for SARS-CoV-2 Delta variant to spread it throughout meat packaging plants [Featherstone et al., 2024). Therefore, more attention needs to be given to increase the preparedness for pandemic scenarios by the food industry (Li et al., 2021 and Dai et al., 2023)

Zoonotic viruses may transmit through respiration, contact during the production, processing, storage, transportation, and retail of food products (Zhang et al., 2022). Monkeypox virus is one of the examples after the COVID-19 outbreak. On 14th August 2024, WHO declared monkeypox outbreak a public health emergency of international concern (Who,2024). While there isn't enough data to measure the risk of monkeypox virus transmission through food, bushmeat is suspected to be a potential source. An infected food handler could contaminate

https://doi.org/10.55549/zbs.1635953

food through contact with dirty hands, especially if they have lesions, or due to poor hygiene practices. Consequently, monkeypox might stay viable in contaminated food that kept in cold storage and heat treatment may inactivate the virus in food (Chaix et al.,2022).

West Nile is another zoonotic virus which primary hosts are typically wild birds. Species such as sparrows, crows, ravens, and some waterfowl play a significant role in the spread of West Nile virus. Mosquitoes acquire the virus by feeding on the blood of these infected birds and then transmit it to humans and other animals. Riverbanks, puddles formed by rainwater on the ground and rocks, swamps, melted snow waters, and artificial water accumulations are breeding grounds for mosquitoes that transmit the disease (Sağlık bakanlığı, 2022).

According to these concerns more efforts should be undertaken to fight against future zoonotic viruses. In this regard, nonthermal technologies such as nanotechnology, ozone application, and irradiation can also provide promising opportunities (Karuppaiah et al., 2023).

This mini review summarize recent innovative practices in food industry, consumer behaviours, biosensing approaches to detect zoonotic viruses, and offer suggestions for future pandemic situations.

2. Practices Against Future Outbreaks

In a recent survey study, it was stated that, there is a decline in the food safety awareness and practices among consumers (Wang et al., 2024). This leads to a higher perceived frequency new outbreaks attributed to inappropriate food processing. There is a need for government intervention to heighten consumer awareness of food safety, especially for the lower-income, elderly, and non-educated groups who may have less knowledge about food safety practices. Educating these people with some activities is important to mitigate the adverse consequences of unsafe food handling.

On the other hand, consumer habits headed towards healthier foods, vegan meat products, cultured meat, and online sales (Loh et al., 2021 and Ayseli et al., 2024). For instance, improvement in diet quality in Mediterranean countries, and Canada was observed (Mignogna et al., 2022). These approaches can help to decrease the zoonotic transmission risks and ensure food safety.

Restaurant managers should be attentive to customers' needs and aim to provide a high customer experience. Innovations in cuisine and home delivery are essential to meet evolving customer expectations. (Ayseli et al., 2024 and Bonfanti et al.,2023). Adopting new food preparation techniques or new services is crucial for customer experience management. The experiential delivery service can be further enhanced in future pandemics. The physical ambiance is vital for Michelin-starred restaurants as it offers a sense of exclusivity that might be lacking in home delivery. Developing strategies for delivering a luxurious gastronomic experience at home ensures that customers can still appreciate the experiential value of their purchase, even outside the upscale restaurant setting (Bonfanti et al., 2023).

Information about safety procedures implemented in the restaurant should be communicated to target customers on media platforms. These practices are expected to boost confidence in restaurant dining (Arriaga-Lorenzo et al., 2022).

3. Trends in Food Technology Applications and Food Packaging Materials

3.1 Application of Nonthermal Treatments

https://doi.org/10.55549/zbs.1635953

Ready-to-eat food as well as packaged food products should not be ignored as potential vehicles for virus transmission. During COVID-19 pandemic slaughterhouses and meat processing factories have already been faced with a series of outbreaks (Arriaga-Lorenzo et al., 2022 and Matthews, 2020). Furthermore, reports are claiming the stability of SARS-CoV-2 on food products. SAR-CoV-2 could remain viable on salmon at 25 C° and 4 C° for 2 and 8 days respecitvely (Kulawik and Kumar Tiwari 2019). Possible survival on meat and meat-absorbed materials was confirmed by other researchers (Featherstone et al, 2022 and Dai et al 2022). Experimental inoculation of cucumber and lettuce with human COV-229E indicated that human-CoV-229E remains infectious on their surface for 72h (Blondin-Brosseau et al., 2021).

Non-thermal techniques such as ozone applications and UV-based technologies are promising emerging methods for inactivation (Guesmi et.al,2022 and Mortazavi et.al, 2022). New studies are necessary to determine the effects of novel techniques on zoonotic viruses or future foodborne viruses. For instance, ozone could react with the cysteine-rich domain of SARS-COV-2 spike protein and decrease the interaction between CoV and host cells; which decline the infectivity (Criscuolo et al., 2021 and Yao et al., 2020). studied the effect of humidity, temperature, and ozone levels on survival of SARS-CoV-2 and found that higher ozone level (95 $\mu g\ m^{-3}$) decreased spreadness. So, the use of ozone generators in risky environments could be a potential strategy for elimination (Masotti et al., 2020). In this sense, ozonated air may be used to disinfect bulk food shipments which may be virus attachment points.

Irradiation by short-wavelength UV light is another alternative method for inactive zoonotic viruses on solid surfaces like glass. It has been stated that employing 1 min a 275 nm UV-C LED is capable of inactivating 99.9% of SARS-CoV-2 (Lu et al, 2021 and Trivellin et al., 2021 and Biasin et al., 2021) reported that UVC rays are more effective compared to microwave and gamma probably due to SARS-CoV-2 dimensions and genome (Farahmandfar et.al, 2021). E-beam irradiation could be also an efficient treatment inside and outside surfaces of cold chain foods to reduce zoonotic virus contamination. (Luo et al., 2023) completely inactivated the porcine epidemic diarrhea virus and porcine transmissible gastroenteritis viruses, with the treatment of 4–6 kGy e-beam irradiation (Wang et al., 2022) used e-beam irradiation to sterilize plastic and filter paper units under cold-chain temperatures.

As one of the other non-thermal treatments, cold plasma application exhibits great potential to eliminate SARS-CoV-2, since it does not cause secondary pollution (Qin et al., 2021 and Vozzi et al., 2021). It has been proven that cold plasma may fragment the viral capsid protein and damage the RNA of SARS-CoV-2 (Wang et al., 2022 and Guo et al., 2022 and Zhang et al., 2021) have indicated that cold-plasma-treated air was able to inactivate a pseudovirus with SARS-CoV 2S protein (Capelli et al., 2022) Metin girmek için buraya tıklayın veya dokunun.used surface plasma device to decontaminate fresh-cut apple packages inoculated with SARS-CoV-2 RNA extract and stated that 10 minutes of exposure was enough to eliminate the viral RNA from the polyethylene terephthalate and polypropylene film materials. Researchers used click chemistry to attach the angiotensin-converting enzyme 2 protein, which serves as the receptor for SARS-CoV-2, to microalgae. This microrobot successfully eliminated SARS-CoV-2 from wastewater (Huang et al., 2022). Consequently, there is growing interest in developing analytical protocols for detecting viruses in sewage systems (Farahmandfar et al., 2021).

Reported studies indicate that other nonthermal methods (Vijayan et al., 2021 and Zhou et al., 2022) can be effective in avoiding transmission and infections on food contact surfaces and nanotechnology applications, high hydrostatic pressure, pulsed electric field, and their possible

https://doi.org/10.55549/zbs.1635953

combination with novel technologies for stronger elimination should investigated. There still research is required for the development of new approaches to inactivate zoonotic viruses.

3.2 Biobased materials and novel detection methods

Biosensors can be alternative for the detection of viruses (Sadak et al., 2022) Since they overcome the limitations of standard techniques they have become an alternative for large-scale testing. Enzyme-based sensors are commercially electrochemical biosensors and can be modified with the advancement of nanomaterials for better analytical sensitivity, and stability at reduced costs of testing (Zhang et al., 2022). Electrochemical methods such as electrochemical impedance spectroscopy, voltammetry, amperometry, and potentiometry are also promising Karuppaiah et al., 2023).

Nanomaterial-based biosensors are other ideal alternatives to detect zoonotic viruses. (Zhang et. al 2022) developed a low-cost commercial interdigitated microelectrode-based sensor for salmon, scallops, and a packing bag for frozen meat, to recognize the trace S-protein. To construct highly selective and sensitive aptasensors to detect zoonotic viruses aptamers can be also combined with surface plasmon resonance, fluorescence, electrochemical techniques, nanopores Cas (Chen et al., 2021 and Zhang et. al., 2022).

Recent advancements in the CRISPR/Cas, called as emerging clustered regularly interspaced short palindromic repeats, system-based biosensing technology are attracting attention. These systems can be integrated with portable devices such as smartphones, nanopores, lateral flow assays, microfluidic chips developed a CRISPR/Cas12a system on spiked frozen shrimp to test SARS-CoV-2 in shrimp samples. The fluorescence results are visually detected by an UV lamp. Quantum dots and graphene nanomaterials have been used in CRISPR/Cas based biosensors. Therefore, nanomaterials with enzyme activity or fluorescent nanodiamonds still need to be further explored (Maddali et al., 2021) Portable nucleic acid sensors (W. Zhang et al., 2022) and optical biosensors have been also reported as promising devices in the literature (Rabiee et al., 2022).Spectroscopic detection methods proteomics can offer a robust option to detect virus in food products. Mass spectroscopy supports the detection of this virus at the surfaces of foods, and wastewater. Therefore, proteomics and mass spectrometry may play a role in the future possible outbreaks (Qian et al., 2023 and Bojórquez-Velázquez et al., 2022).

Above mentioned studies shows that these novel biosensors with nanomaterials such as nanobiosensor systems and novel spectrometric platforms will lead to efficient detection of future possible zoonotic viruses with high accuracy.

4. Challenges

Detecting zoonotic viruses using sensors is challenging due to the complexity of food products, which may influence sensor performance. Therefore, proper sampling and handling is crucial. Surface plasmon resonances aptasensors have low limit of detection but they are limited by their poor repeatability. Since their responses are influenced easily, optical sensors may not effectively determine small analytes because of weak signals. Other drawbacks of electrochemical sensors are their reduced accuracy and stability with repeated usage and analysis costs. Limited information is available regarding the real-time application in food. The absence of cohesive strategies presents challenge for service providers, stakeholders, policymakers, and governments in improving food supply chains (Gharibzahedi et al., 2024).

5. Conclusion

https://doi.org/10.55549/zbs.1635953

Many lessons learned after COVID-19 outbreak regarding future preventive measures for food safety. A new model of trade regulations must be developed for strict application of hygiene measures at all stages of food processing. Touchable items in food factories or food markets including, knives, chopping boards, scales, and calculators are concerning. Cold chain management practices can be improved by focusing on the analysis of requirements to predict transmission risk. Non-thermal technologies will provide direction for future viral pandemics regarding food safety processing, transport, and handling strategies. Novel biosensing methods should be further explored for the detection of zoonotic viruses. There is a demand for biosensors for early viral detection. Future electrochemical detection systems will be required to detect mutations and variants using associated biorecognition elements. Nanomaterials-based biosensors can be advantageous as an alternate tool for detecting viruses. To better prepare for future outbreaks, the food industry needs to adopt affordable, portable, and reusable biosensing tools for accurate diagnosis.

References

Ayşen Ç. D. (2022). COVID-19, Food Safety, Risk Assessment, and Future Approaches in the Food Industry. Handbook of Research on Global Hospitality and Tourism Management. 115-138. Doi: 10.4018/978-1-7998-9148-2.ch006.

Ayseli MT, Çetinkaya T, Ayseli YI. (2024) Innovative Food Safety Approaches and Nutraceuticals to Promote Children's Health on Future Outbreaks with the Reflection of COVID-19. In : Rezaei N, ed. The COVID-19 Aftermath. Advances in Experimental Medicine and Biology. Springer. : 349–69.

Arriaga-Lorenzo P, de Jesús Maldonado-Simán E, Ramírez-Valverde R, Martínez-Hernández PA, Tirado-González DN, Saavedra-Jiménez LA. (2023). Cold chain relevance in the food safety of perishable products. Foods and Raw Materials 2022 ; : 116–28.

Biasin M, Bianco A, Pareschi G. (2021) UV-C irradiation is highly effective in inactivating SARS-CoV-2 replication. Scientific Reports. 11:1;1–7.

Blondin-Brosseau M, Harlow J, Doctor T, Nasheri N.(2021). Examining the persistence of human Coronavirus 229E on fresh produce. Food Microbiol. 98 : 103780.

Bojórquez-Velázquez E, Llamas-García ML, Elizalde-Contreras JM, Zamora-Briseño JA, Ruiz-May E. (2022). Mass Spectrometry Approaches for SARS-CoV-2 Detection: Harnessing for Application in Food and Environmental Samples. Viruses. 14 : 872.

Bonfanti A, Vigolo V, Yfantidou G, Gutuleac R.(2023). Customer experience management strategies in upscale restaurants: Lessons from the Covid-19 pandemic. Int J Hosp Manag .109 : 103416.

Criscuolo E, Diotti RA, Ferrarese R. (2021). Fast inactivation of SARS-CoV-2 by UV-C and ozone exposure on different materials. Emerg Microbes Infect. 10 : 206–10.

Ceylan Z, Ocak E, Uçar Y, Karakus K, Cetinkaya T. (2021). An overview of food safety and COVID-19 infection: nanotechnology and cold plasma applications, immune-boosting suggestions, hygienic precautions. Environmental and Health Management of Novel Coronavirus Disease (COVID-19). 325–44.

https://doi.org/10.55549/zbs.1635953

Capelli F, Tappi S, Gritti T. (2021). Decontamination of Food Packages from SARS-CoV-2 RNA with a Cold Plasma-Assisted System. Applied Sciences 2021 ; 11 : 4177. **47**. Zhang F, Li Z, Yin L, et al. ACE2 Receptor-Modified Algae-Based Microrobot for Removal of SARS-CoV-2 in Wastewater. J Am Chem Soc. 143 : 12194–201.

Chen Z, Garcia G, Arumugaswami V, Wirz RE. (2020). Cold atmospheric plasma for SARS-CoV-2 inactivation. Physics of Fluids. 32 : 111702.

Chaix E, Boni M, Guillier L.(2022). Risk of Monkeypox virus (MPXV) transmission through the handling and consumption of food. Microb Risk Anal. 22 : 100237.

Chen R, Kan L, Duan F. (2021). Surface plasmon resonance aptasensor based on niobium carbide MXene quantum dots for nucleocapsid of SARS-CoV-2 detection. Microchimica Acta. 188 : 1–10.

Dai H, Tang H, Sun W, Deng S, Han J. (2023). It is time to acknowledge coronavirus transmission via frozen and chilled foods: Undeniable evidence from China and lessons for the world. Science of The Total Environment. 868 : 161388.

Dai M, Li H, Yan N. (2020). Long-term survival of salmon-attached SARS-CoV-2 at 4°C as a potential source of transmission in seafood markets. bioRxiv. .

Farahmandfar R, Asnaashari M, Hesami B. (2021). Monitoring of new coronavirus (SARS-CoV-2): Origin, transmission, and food preservation methods. J Food Process Preserv . 45 : e15564.

Featherstone A.B, Mathijssen A.J.T.M, Brown A, Dass S.C (2024). SARS-CoV-2 Delta variant remains viable in environmental biofilms found in meat packaging plants. PLoS One, 19 : e0304504.

Featherstone AB, Brown AC, Dass SC.(2022). Murine Hepatitis Virus, a Biosafety Level 2 Model for SARS-CoV-2, Can Remain Viable on Meat and Meat Packaging Materials for at Least 48 Hours. Tamber S, ed. Microbiol Spectr .

Gharibzahedi SMT, Altintas Z. (2024). State-of-the-art sensor technologies for tracking SARS-CoV-2 in contaminated food and packaging: Towards the future techniques of food safety assurance. TrAC Trends in Analytical Chemistry. 170 : 117473.

Guo L, Yao Z, Yang L. (2020). Plasma-activated water: An alternative disinfectant for S protein inactivation to prevent SARS-CoV-2 infection. Chemical Engineering Journal. 127742.

Guesmi A, Cherif MM, Baaloudj O. (2022). Disinfection of corona and myriad viruses in water by non-thermal plasma: a review. Environmental Science and Pollution Research. 29 : 55321–35.

Huang X, Kon E, Han X. (2022). Nanotechnology-based strategies against SARS-CoV-2 variants. Nature Nanotechnology. 1–11.

Karuppaiah G, Vashist A, Nair M, Veerapandian M, Manickam P. (2023). Emerging trends in point-of-care biosensing strategies for molecular architectures and antibodies of SARS-CoV-2. Biosens Bioelectron X. 13 : 100324.

https://doi.org/10.55549/zbs.1635953

Kulawik P, Kumar Tiwari B. (2019). Recent advancements in the application of non-thermal plasma technology for the seafood industry. Crit Rev Food Sci Nutr. 59 : 3199–210.

Kulawik P, Rathod NB, Ozogul Y, Ozogul F, Zhang W. (2022). Recent developments in the use of cold plasma, high hydrostatic pressure, and pulsed electric fields on microorganisms and viruses in seafood.

Li X, Wang Q, Ding P (2021). Risk factors and on-site simulation of environmental transmission of SARS-CoV-2 in the largest wholesale market of Beijing, China. Science of The Total Environment. 778 : 146040.

Lu LC, Quintela I, Lin CH. (2021). A review of epidemic investigation on cold-chain food-mediated SARS-CoV-2 transmission and food safety consideration during COVID-19 pandemic. J Food Saf. 41 : e12932.

Loh HC, Seah YK, Looi I. The COVID-19 Pandemic and Diet Change. Progress in Microbes and Molecular Biology 2021 ; 4.

Liu J, Zheng T, Xia W, Xu S, Li Y. (2022).Cold chain and severe acute respiratory syndrome coronavirus 2 transmission: a review for challenges and coping strategies. Medical Review. 2 : 50–65.

Luo Z, Ni K, Zhou Y. (2023). Inactivation of two SARS-CoV-2 virus surrogates by electron beam irradiation on large yellow croaker slices and their packaging surfaces. Food Control. 144 : 109340.

Maddali H, Miles CE, Kohn J, O'Carroll DM. (2021). Optical Biosensors for Virus Detection: Prospects for SARS-CoV-2/COVID-19. Chem Bio Chem. 22 : 1176–89.

Masotti F, Cattaneo S, Stuknytė M, Pica V, De Noni I. (2022). Transmission routes, preventive measures and control strategies of SARS-CoV-2 in the food factory. Crit Rev Food Sci Nutr. 62 : 4821–31.

Mignogna C, Costanzo S, Ghulam A (2022). Impact of Nationwide Lockdowns Resulting from the First Wave of the COVID-19 Pandemic on Food Intake, Eating Behaviors, and Diet Quality: A Systematic Review. Advances in Nutrition. 13 : 388–423.

Matthews A. (2020). EU Food System Strengths and Vulnerabilities during Covid-19. EuroChoices. 19 : 4–12.

Mortazavi M, Bains A, Afsah-Hejri L, Ehsani R, LiWang PJ.(2022). SARS-CoV-2 pseudotyped virus persists on the surface of multiple produce but can be inactivated with gaseous ozone. Heliyon; 8 : e10280.

Wang K, Cong L, Mirosa M, Bai L, Hou Y, Bremer P. (2024). Impact of COVID-19 on Chinese urban consumers' food safety knowledge and behavior – A comparative study between pre and post pandemic eras. Food Res Int. 194 : 114905.

Rzymski P, Kulus M, Jankowski M, et al. COVID-19 Pandemic Is a Call to Search for Alternative Protein Sources as Food and Feed: A Review of Possibilities. Nutrients 2021 2021 ; 13 : 150.

https://doi.org/10.55549/zbs.1635953

Paparella A, Purgatorio C, Chaves-López C, Rossi C, Serio A. The Multifaceted Relationship between the COVID-19 Pandemic and the Food System. Foods 2022 ; 11 : 2816.

Rabiee N, Fatahi Y, Ahmadi S. (2022). Bioactive hybrid metal-organic framework (MOF)-based nanosensors for optical detection of recombinant SARS-CoV-2 spike antigen. Science of The Total Environment. 825 : 153902.

Sağlık Bakanlığı. (2022). Batı Nil Virüsü Enfeksiyonu Vaka Yönetim Rehberi [Internet]. Zoonotik ve Vektörel Hastalıklar Dairesi Başkanlığı. Ankara.

Sadak O, Sadak F, Yildirim O. (2022). Electrochemical Biosensing and Deep Learning-Based Approaches in the Diagnosis of COVID-19: A Review. IEEE Access. 10 : 98633–48.

Thirumdas R, Sarangapani C, Annapure US. (2015). Cold Plasma: A novel Non-Thermal Technology for Food Processing [Internet]. Vol. 10, Food Biophysics. Springer Science and Business Media, LLC , 20151–11.

Trivellin N, Buffolo M, Onelia F. (2021). Inactivating SARS-CoV-2 Using 275 nm UV-C LEDs through a Spherical Irradiation Box: Design, Characterization and Validation. Materials 2021 ; 14 : 2315.

Vozzi G, Thomas S V, Dienger-Stambaugh K. (2023).Inactivation of SARS-CoV-2 on Surfaces by Cold-Plasma-Generated Reactive Species. Bioengineering. 10 : 280.

Vijayan P P, P.G C, Abraham P. (2022). Nanocoatings: Universal antiviral surface solution against COVID-19. Prog Org Coat 2022 ; 163 : 106670.

Vijayan P P, P.G C, Abraham P. (2022). Nanocoatings: Universal antiviral surface solution against COVID-19. Prog Org Coat 2022 ; 163 : 106670.

Yao M, Zhang L, Ma J, Zhou L. (2020). On airborne transmission and control of SARS-Cov-2. Science of The Total Environment. 731 : 139178.

Zhang H, Chen M, Huang L. (2021). Using cold atmospheric plasma treated-air for COVID-19 disinfection in cold-chain environment. J Phys D Appl Phys. 54 : 40LT01.

Zhou C, Lin C, Hu Y. (2022). Sensitive fluorescence biosensor for SARS-CoV-2 nucleocapsid protein detection in cold-chain food products based on DNA circuit and g-CNQDs@Zn-MOF. LWT. 169 : 114032.

Zhang C, Yang Y, Feng Z. (2022). Cold Chain Food and COVID-19 Transmission Risk: From the Perspective of Consumption and Trade. Foods. 11 : 908.

Zhang M, King MD. Temporal Variation of SARS-CoV-2 Levels in Wastewater from a Meat Processing Plant. Microorganisms. 11 : 174.

Zhang J, Fang X, Mao Y. (2021). Real-time, selective, and low-cost detection of trace level SARS-CoV-2 spike-protein for cold-chain food quarantine. npj Science of Food. 5:1 2021 ; 5 : 1–6.

Zhang Y, Juhas M, Kwok CK. (2022). Aptamers targeting SARS-COV-2: a promising tool to fight against COVID-19. Trends Biotechnol..

https://doi.org/10.55549/zbs.1635953

Zhang X, Yang Y, Cao J, Qi Z, Li G.(2022). Point-of-care CRISPR/Cas biosensing technology: A promising tool for preventing the possible COVID-19 resurgence caused by contaminated cold-chain food and packaging. Food Front.

Zhang W, He Y, Feng Z, Zhang J. (2022). Recent advances of functional nucleic acid-based sensors for point-of-care detection of SARS-CoV-2. Microchimica Acta. 189 : 1–18.

Qin H, Qiu H, He ST. (2022). Efficient disinfection of SARS-CoV-2-like coronavirus, pseudotyped SARS-CoV-2 and other coronaviruses using cold plasma induces spike protein damage. J Hazard Mater. 430 : 128414.

Qian S, Chen Y, Wang X. (2023). CRISPR/Cas12a-Assisted Dual Visualized Detection of SARS-CoV-2 on Frozen Shrimps. Biosensors (Basel). 13 : 138.

World Health Organisation. (2024). WHO Director-General declares mpox outbreak a public health emergency of international concern [Internet]. Available from: https://www.who.int/news/item/14-08-2024-who-director-general-declares-mpox-outbreak-a-public-health-emergency-of-international-concern

Wang Z, Liang Z, Wei R.(2022). Quantitative determination of the electron beam radiation dose for SARS-CoV-2 inactivation to decontaminate frozen food packaging. Virol Sin.37 : 823–30.

Wang P, Zhou R, Zhou R. (2022). Cold atmospheric plasma for preventing infection of viruses that use ACE2 for entry. Theranostics. 12 : 2811.

WHO. (2024). COVID-19 variants | WHO COVID-19 dashboard [Internet]. Available from: https://data.who.int/dashboards/covid19/variants

https://doi.org/10.55549/zbs.1635953

ZEUGMA BIOLOGICAL SCIENCE

ZEUGMA
BIOLOGICAL SCIENCE

2025
v:5 n:2 p:16-41

Evaluation of Unripe *Musa paradisiaca* Pulp Extract in Streptozotocin-induced Type-2 Diabetic Rats: *In-vivo* Studies and *In-silico* Modelling

Olasunkanmi Kayode Awote[1]* and Ayomide Aleemat Abass[1]

[1] Department of Biochemistry, Lagos State University, PMB 001, Ojo, Lagos, Nigeria.

olasunkanmi.awote@lasu.edu.ng

Abstract:

Diabetes mellitus is still a major public health problem that comes with a lot of complications in both young and old individuals. *Musa paradisiaca* is abundant in the tropical and sub-tropical regions of Africa and has several medicinal traditional claims. Hence, this study evaluated the effect of *Musa paradisiaca* aqueous pulp extract (MPAPE) in STZ-induced diabetic rats. Bioactive compounds of MPAPE were identified and quantified using gas chromatography-mass spectroscopy (GC-MS) and high-performance liquid chromatography (HPLC) techniques. A total of 24 male Wistar rats were divided into 4 groups (n=6), including control, diabetic-untreated, and diabetic-treated groups (with MPAPE or glibenclamide). Oxidative stress (hydrogen peroxide [H_2O_2], nitric oxide [NO], malondialdehyde [MDA], glutathione [GSH]); lipid profile (total cholesterol [TC], triglyceride [TRIG], high-density [HDL-Chol, low-density [LDL-Chol], and very-low-density [VLDL-Chol] lipoprotein cholesterol; liver antioxidant (superoxide dismutase [SOD], catalase [CAT]); and liver function (alanine [ALT], and aspartate [AST] aminotransferase) enzymes were evaluated using standard biochemical kits and procedures. PyRx and Biovia Discovery Studio were used for molecular docking studies, while SwissADME and ProTox were used to predict the ADME/T properties. The results of the phytochemistry of *M. paradisiaca* pulp showed the presence of alkaloids, tannins, flavonoids, saponins, and phenols, with an abundant polyphenolic content. The administration of MPAPE (300 mg/kg body weight) significantly ($p<0.05$) decreased the high levels of glucose, total-chol, LDL-chol, TRIG, VLDL-chol, H_2O_2, NO, MDA, and the activities of SOD and CAT while, decreasing ALT and AST activities, and HDL- Chol, and GSH levels. In conclusion, MPAPE may possess antioxidant and antidiabetic potentials in the management of diabetes.

Keywords: Traditional medicine, Medicinal plants, Nutraceuticals, *Musa paradisiaca* fruit, Oxidative stress, Diabetes, Liver damage, Antioxidant, Streptozotocin, Phytochemistry.

Introduction

Oxidative stress, an imbalance between oxidants and antioxidants, leads to a disruption in redox signaling and regulation (Azzi, 2022). This results in the overproduction and accumulation of reactive oxygen species (ROS), which play a role in the development of a myriad of maladies, including diabetes, cardiovascular diseases, cancers, neurodegenerative diseases, aging, and respiratory diseases. The source of production of ROS can either be environmental stressors (e.g., ultraviolet light, heavy metals, ionizing radiation, and smoke) or within an individual (i.e, mitochondrial dysfunction, lipoxygenase, cyclooxygenase, and peroxisomes) (Singh *et al*., 2022). Several antioxidants, which can either be synthesized by the cells or obtained daily from diets, have been utilized in recent times to stabilize or deactivate free radicals (Marino *et al*., 2022).

Streptozotocin (STZ), isolated from *Streptomyces achromogenes*, is the most common diabetogenic chemical extensively used in experimental animals for creating animal models of Type 1 and Type 2 diabetes. Proper preparation and administration of STZ are essential for obtaining reliable results from the animal models of diabetes produced by the drugs (Furman, 2015; Ghasemi and Jeddi, 2023).

Diabetes mellitus (DM) is a modern pandemic and consistently high blood sugar (hyperglycemia) metabolic disease caused by a malfunction in either the action or secretion of insulin, or both. Chronic high blood sugar (hyperglycemia) caused by insulin deficiency usually disrupts the metabolism of proteins, fats, and carbohydrates. Tissue or vascular damage develops as the condition worsens, resulting in serious diabetic complications like neuropathy, retinopathy, and cardiovascular problems (Onah and Oguche, 2022). Long-term damages, such as macrovascular and microvascular damage, can both be attributed to the persistent hyperglycemic state that causes the majority of problems associated with DM. Currently, well-recognized macrovascular implications include the increasing prevalence of myocardial infarctions and brain injuries as a result of arteriosclerotic abnormalities of the large-diameter arteries, which induce a progressive reduction in the diameter of the vessels. Microvascular problems, on the other hand, impact the small-diameter vessels and peripheral circulation, affecting the central and peripheral nerve systems, lower limbs, kidneys, and eyes (Ortiz *et al*., 2022). In 2019, 436 million adults worldwide were estimated by the International Diabetes Federation (IDF) to have diabetes, and the number is predicted to nearly double by 2030 (Seedi *et al*., 2019; Adeniran *et al*., 2022). Among the countries in sub-Saharan Africa, Nigeria is currently experiencing an increase in the prevalence of diabetes mellitus, with approximately 3.7% of adult Nigerians (20-79 years) living with DM according to a recent IDF report (Fasula *et al*., 2024).

Conventional antidiabetic drugs such as sulfonylureas, biguanides, α-glucosidase inhibitors, agonists for peroxisome proliferator-activated receptor-γ (PPARγ), inhibitors of dipeptidyl peptidase IV (DPP IV), and inhibitors of sodium-glucose co-transporter-2 (SGLT2) are economical and the prolonged use of these medications has been associated with serious side effects including the risk of coma, edema, hypoglycemia, vomiting, bloating, possible weight gain, and issues with the central nervous and cardiovascular systems (Banu and Bhowmick, 2017, Daliri *et al*., 2017; Padhi *et al*., 2020). Therefore, to alleviate these side effects, new therapeutic approaches are required, and natural products have been reported as safe and natural alternatives (Yedjou *et al*., 2023), including medicinal plants.

Medicinal plants do not only serve as a food source but also for their therapeutic effects, including antioxidant defenses, cell proliferation, expression of genes, and maintenance of mitochondrial integrity (Adetuyi *et al*., 2022). Herbal remedies have been used to treat diseases worldwide since the beginning of time; thus, much attention has been given to natural products influencing the development of new drugs. The plant diversity in West Africa, including Nigeria, is very abundant, and African traditional medicine is one of the most ancient medical systems in the world with its attributed low cost, safe history, and suitability in treating various diseases (Ayeni *et al*., 2022). *Musa paradisiaca* is a member of the family *Musaceae* (Fig. 1). Its species are widely spread in southern Asia, and tropical and subtropical regions of Africa (Kemisetti and Rajeswar Das, 2022). Many parts of this plant serve medicinal purposes, and it has been found to possess antidepressant, antihypertensive, antibacterial, antifungal, anti-ulcer, antioxidant, and anti-diabetic activity (Shree and Selvakumar, 2022). Despite the numerous biological activities attributed to this plant, there is limited information on the antioxidant and antidiabetic effects of MPAPE administration on streptozotocin-induced diabetic rats. Hence, this study is carried out using experimental and computational guided methodologies.

Figure 1: Pictorial view of *Musa paradisiaca* leaf and fruit (Google Search Engine, 2025).

Materials and Methods

Plant Collection and Extraction

Unripe fruits of *Musa paradisiaca* were purchased from a local market, Iyana-Iba market, Ojo, Lagos State, South-western Nigeria (6.4609° N, 3.2053° E), rinsed, cut into smaller sizes using a sterile knife, and left to air dry for 24 hours before homogenizing using a mortar and pestle. The resulting homogenate was weighed using an analytical balance, and 67.70 grams was added to a volumetric flask with 670 mL of deionized water in the ratio 1:10, where it was macerated for 48 hours. The resulting solution was filtered using a Whatmann grade 1 filter paper, heated for 30 minutes in a water bath at 40°C, and then stored in the refrigerator until needed.

Phytochemical Screening

The phytochemical components of MPAPE were determined using the methods described by Awote *et al*. (2024).

Gas Chromatography-Mass Spectroscopy (GC-MS) Analysis of *M. paradisiaca* Pulp Extract

An Agilent 5977B GC/MSD system with an Agilent 8860 auto-sampler, a gas chromatograph interfaced to a mass spectrometer (GC-MS) equipped with an Elite-5MS (5% diphenyl/95% dimethyl polysiloxane) fused a capillary column (30 × 0.25µm ID × 0.25µm df) were used to perform the GC-MS analysis of the extract. An electron ionization device with an ionization energy of 70 eV was used in electron impact mode for GC-MS detection. A split ratio of 10:1 was used with an injection volume of 1µL and helium gas (99.999%) as the carrier gas at a steady flow rate of 1 mL/min. To calibrate the GC-MS, five (5) point serial dilution calibration standards (1.25, 2.5, 5.0, and 10.0 ppm) were made from the 40 PPM stock solution. Temperatures were maintained at 300 °C for the injector, 250 °C for the ion source, and 100 °C (isothermal) for 0.5 min in the oven, with a 20 °C/min increase to 280 °C (2.5 min) for the oven. Mass spectra were obtained at 70 eV with a 0.5 s scanning interval and fragments ranging from

45 to 450 Da. GC/MS ran for a total of 21.33 minutes, with a solvent delay of 0 to 3 minutes (Awote *et al*., 2024).

High-Performance Liquid Chromatography (HPLC) Analysis of *M. paradisiaca* Pulp Extract.

The measurement of flavonoid components in the extracts was carried out using high-performance liquid chromatography (HPLC) on an HPLC-Agilent Technologies 1200 series liquid chromatograph equipped with a UV detector. A Hypersil BDS C18 column (150 × 4.6 mm, 5 µm particle size) prepacked for the reversed-phase was used for the chromatography, which was carried out at 250°C. A (0.1% formic acid in water) and B (HPLC grade acetonitrile) are combined to generate the mobile phase, which has a steady flow rate of 0.75 mL/min. At 0 min, 94% A, 14 min, 83.5% A, 16 min, 83% A, 18 min, 82.5% A, 20 min, 82.5%; 22–24 min, 81.5%; and 27–40 min, 80% A, the linear gradient solvent system began. The detection wavelength was 280 nm (Awote *et al*., 2021a).

***In-silico* Studies: Ligand Modeling**

The GC-MS and HPLC-generated ligands' 3D crystal structures were downloaded in .sdf format from the PubChem database (https://pubchem.ncbi.nlm.nih.gov/). Also, the ligands' canonical SMILES were downloaded from the PubChem database. Biovia Discovery Studios 2021 was used to convert the ligands to .pdb format, and Open Babel (https://openbabel.readthedocs.io/en/latest/Forcefields/mmff94.html) was utilized in optimizing the energy of the ligand molecules. Following energy minimization, the ligand molecules were converted specifically into pdbqt AutoDock ligand format (Awote *et al*., 2024).

Protein (Target) Preparation

The selected protein targets were sourced from the Protein Data Bank (https://www.rcsb.org) and a deposited crystal structure of Homo sapiens was used as a reference to model the 3D structures of these proteins. The protein grid box coordinates were set at x= 8.689, y= -27.9742, and z= 15.7172; x= -12.1777, y= -35.4768, and z= 88.7572; x= 80.183, y= 62.3450, and z= 3.4609; and

x= -0.3408, y= -0.6404, and z= 15. 0471 for human pancreatic α-amylase (PDB ID: 2QMK), human pancreatic α-glucosidase (PDB ID: 5NN8), human pancreatic sorbitol dehydrogenase (PDB ID: 1PL6), and aldose reductase (PDB ID: 3S3G), respectively, to target the active sites of each protein. Biovia Discovery Studio 2021 was used to eliminate heteroatoms, ligand groups, and water molecules from the protein structures and add hydrogen polar to protein structures to prepare them for molecular docking analysis (Awote *et al*., 2024).

Molecular Docking Profiling

The AutoDock Vina tool was utilized for molecular docking studies. The usual diabetes standard drugs, acarbose and tolrestat, and the co-crystallized ligands for the target proteins were utilized. Following the sorting of the ligand molecules according to increasing binding energies, the investigation was based on binding free energy values (Awote *et al*., 2024).

Absorption, Distribution, Metabolism, Excretion & Toxicity (ADMET) Properties Prediction

The top ten ligands were selected based on binding energy, and their drug-likeness parameters,

physicochemical properties, pharmacokinetic properties, lipophilicity, water solubility, medicinal chemistry, and toxicity were predicted using SwissADME and admetSAR. These predictive algorithms were used to evaluate the ligands' general eligibility as possible drug candidates and to offer information about their possible safety, pharmacological characteristics, and therapeutic efficacy (Awote *et al*., 2024).

Experimental Animals

Twenty-four (24) male Wistar rats (8 weeks old), with an average weight of 103 g (range of 100– 105 g), were sourced from the animal house of the Department of Biochemistry, Faculty of Science, Lagos State University, Nigeria. The rats were kept in regular day/night cycles while they were made to have access to clean drinking water and commercial pelleted feed (Vital feed® Nigeria). The current national and international criteria were followed in the care and usage of the Wistar rats during the study. With the ethical approval number LASU/23/REC/055, the Lagos State University Research Ethics Committee authorized the study procedure.

Induction of Type-2 Diabetes mellitus

Type-2 Diabetes Mellitus (T2DM) was introduced into the overnight fasted rats intraperitoneally at a dose of 60 mg/kg body weight of Streptozotocin (STZ) (Sigma-Aldrich Chemicals Company, St. Louis, MO., U.S.A.) dissolved in freshly prepared 0.1 M of iced-cold citrate buffer (pH 4.5) (Ogunyinka *et al*., 2017). To prevent hypoglycemia, the rats were maintained with 20% glucose (Unique Pharmaceuticals, Sango Otta, Ogun State, Nigeria) for six hours following the induction and later with 5% glucose for the following 24 hours. On the third day (72 hours) after induction, hyperglycemia was found to be gradually developing, but by the seventh day, all of the rats had stabilized and were consistently hyperglycemic. The rats exhibiting a fasting blood glucose level of 200 mg/dL or higher by the seventh day were classified as diabetic and included in the investigation. The fourth day after STZ induction marked the start of the treatments, which lasted for 28 days. The blood glucose concentrations were measured after drawing blood from the rats' tails using an Accu-Check glucometer. The success rate of induction exceeded 84.7%.

Animal Groupings and Treatments

Animal groupings and treatment were carried out using the modified method of Ogunyinka *et al*. (2017). Before this study, the rats were fasted overnight and divided into four (4) groups (A–D) of six rats each, randomly selected so that the group mean weights were the same.

Group A (normal control) consisted of non-diabetic rats that received 2 mL/kg body weight/day of distilled water orally for 28 days.

Group B (positive control) = streptozotocin (STZ)-induced diabetic rats orally administered 2 mL/kg body weight/ day distilled water for 28 days.

Group C = diabetic rats orally administered 300 mg/kg body weight/ day of *M. paradisiaca* pulp extract for 28 days.

Group D = diabetic rats orally administered 5 mg/kg body weight/ day of glibenclamide (®Daonil, Hoechst Marion Roussel Limited, Mumbai, India) for 28 days.

Blood Collection

After receiving medication for 28 days, each rat was given an injection of 0.1 mL of ketamine to induce anesthesia and then dissected. The gradual lack of corneal and pedal responses confirmed anesthesia. Afterward, a sterile 21G needle was placed on a 5 mL plunger syringe (Cliniject Hypodermic Syringe, Albert David Limited, Mandideep-462046, Raisen District, India) to collect fresh blood from the heart chamber, which was then stored in plain sample bottles. The blood was centrifuged immediately for 15 minutes at 2500 rpm. The supernatant (serum) was then removed and stored in the refrigerator until required for biochemical analysis.

Biochemical Assays

The effects of MAPAPE on STZ-induced diabetic Wistar rats were evaluated using the following biochemical parameters:

Protein Determination

The protein concentration of the various samples was determined using the Lowry method as described by Lowry *et al.* (1951) with a few modifications. In summary, 400 µL of solution C (200 µL solution B (1% copper sulfate ($CuSO_4.5H_2O$) and 2% sodium potassium tartrate) and 9.8 mL of solution A (0.1 M sodium hydroxide and 2% sodium bicarbonate), 40 µL of folin C, and 25 µL of each sample were mixed with 0.5 mg/mL bovine serum albumin (BSA). After thoroughly mixing, the mixture was left to stand. At 650 nm, the absorbance was measured against a blank that contained 60 µL of solution C, water, or buffer. From the Lowry standard curve, the protein concentrations of each group were extrapolated and expressed in mg/mL.

Catalase (CAT) Activity

Catalase activity was determined according to the method of Oladimeji *et al*. (2022). In summary, 10 µL of the homogenate and 590 µL of hydrogen peroxide (590 µL of 19 mM solution) were pipetted into a 1 cm quartz cuvette. The mixture was quickly swirled to mix it thoroughly, and it was then put in a spectrophotometer. The change in absorbance was measured at 240 nm for 10 seconds for 2 minutes. The extinction coefficient of hydrogen peroxide, which is 240 nm, was used to express catalase activity as µmol/mg protein.

Superoxide Dismutase (SOD) Activity

SOD activity was determined by the Epinephrine method reported by Oladimeji *et al*. (2023). In brief, 2.5 mL of 0.05 M phosphate buffer (pH 7.8) was mixed with 0.1 mL of the tissue homogenate supernatant. At the point of absorbance measurement, which was measured at 750 nm for one minute and thirty seconds at intervals of 15 seconds, 0.3 mL of adrenaline solution (0.059%) was then added. After calculation, SOD activity was then expressed as mmol/mg protein.

Lipid Profile Estimation

Using standard diagnostic test kits (Randox Laboratories, Crumlin, U.K.), the lipid profile (triglyceride (TG), total cholesterol (TC), and high-density lipoprotein cholesterol (HDL-c)) of the treated Wistar rats was analyzed in the liver homogenate and plasma sample. The Friedewald formula was used to determine plasma low-density lipoprotein cholesterol (LDL-c) and very-low-density lipoprotein cholesterol (VLDL-c): LDL-c = [TC- (HDL-c + TG/5)], and VLDL-c = TAG/5, respectively (Awote *et al*., 2021b).

Non-Protein Thiol (GSH) Estimation

The level of reduced glutathione (GSH) was estimated according to Jollow *et al*. (1974). Using Ellman's reagent (DTNB), the glutathione (GSH) content was determined calorimetrically. Sulfa-salicylic (4%) was added to the supernatant in a 1:1 ratio to precipitate it. After being stored at 4°C for one hour, the samples were centrifuged for ten minutes at 4°C at 5000 rpm. Phosphate buffer (0.1 M, 550 µL), 100 µL of supernatant, and 100 µL of DTNB were mixed to make up the assay combination. The absorbance was read at 412 nm, and the results were expressed as µmol of GSH/mg protein.

Nitric Oxide (NO) Estimation

After the Griess reaction, the concentrations of nitrite in serum or supernatants were determined by incubating 250 µL of the homogenate with 250 µL of Griess reagent at room temperature for 20 minutes. The spectrophotometric method was used to measure the absorbance at 550 nm. The absorbance of a standard solution containing known amounts of sodium nitrite was compared to determine the nitrite content; the findings were expressed as mmol/L (Green *et al*., 1983).

Hydrogen Peroxide (H_2O_2) Estimation

The FOX (ferrous oxidation-xylenol orange) assay was used to measure the levels of hydrogen peroxide. In brief, FOX is formed by adding 10 mL of Xylenol, 10 mL of sorbitol, and 50 mL of ammonium ferrous sulfate to 30 mL of distilled water. In the meantime, 10 µL of homogenate and 290 µL of FOX were well mixed by vortexing until foamy. After 30 minutes of room temperature incubation, a faint pink color complex is produced. At a wavelength of 560 nm, the absorbance was measured against a blank (distilled water). The hydrogen peroxide generated was calculated and expressed in mmol/mL (Wolff, 1994).

Lipid Peroxidation Estimation

Lipid peroxidation was determined by measuring the formation of thiobarbituric acid reactive substance (TBARS) according to the method of Varshney and Kale (1990). Briefly, tissue samples were homogenized in 0.1 M phosphate buffer (pH 7.4) in a ratio of 1:5. 200 µL of the stock reagent—an equal volume of trichloroacetic acid (10%, w/v) and 2-thiobarbituric acid (0.75%, w/v) in 0.1 M HCl was added to 100 µL of homogenate, and the mixture was incubated at 95ºC for an hour using a water bath. After cooling, the solution was centrifuged at 3000 rpm for 10 minutes, and the absorbance of the supernatant was measured at 532 nm and 600 nm. Lipid peroxidation was expressed as nmol.

Determination of Enzymatic Activities

Using commercial diagnostic kits (Randox, U.K.), the activities of alanine transaminase (ALT, EC 2.6.1.2) and aspartate transaminase (AST, EC 2.6.1.1) were measured following the manufacturer's instructions (Fagbohun *et al*., 2020). At 340 nm, each enzyme's activity was determined using a spectrophotometer.

Statistical Analysis

The results are presented as Mean ± Standard Error of Mean (SEM). For the descriptive statistics, One-way ANOVA was used to compare the treated and control groups using GraphPad Prism 5.0 (GraphPad Prism Software Inc., San Diego, CA, USA). When comparing

the treated and control groups, statistically significant differences were identified at $p<0.05$ with a 95% confidence interval. When significant, means were separated using the Bonferroni post-hoc test.

Results

The preliminary qualitative and quantitative (polyphenol content) of the aqueous pulp extract of *Musa paradisiaca* is presented in Table 1.1. Alkaloids, flavonoids, phenols, tannins, and saponins are all present. More so, the polyphenolic constituent screening of the extract showed an abundance of flavonoids, followed by phenols and tannins. The bioactive compounds found in MPAPE, as revealed by HPLC analysis, are presented in Table 1.2, with syringin (7.933 ppm) having the highest concentration, followed by kaempferol (6.333 ppm), quercetin (5.516 ppm), and luteolin (5.200 ppm). The bioactive compounds found in MPAPE, as revealed by GC-MS analysis, are presented in Table 1.3. The analysis showed the presence of 13 secondary metabolites with a total of 90.55 area percentages.

Table 1.1: Preliminary Phytochemical screening of *Musa paradisiaca* aqueous pulp extract

S. No.	Phytochemicals	Qualitative	Quantitative (mg/100g)
1	Alkaloids	+	NQ
2	Flavonoids	+	0.945 ± 0.78
3	Saponins	+	NQ
4	Phenols	+	0.641 ± 0.10
5	Steroids	-	NQ
6	Terpenoids	-	NQ
7	Tannins	+	0.182 ± 0.00

KEY: + = Present, - = Absent; NQ: not quantified

Table 1.2: Bioactive compounds of *Musa paradisiaca* aqueous pulp extract (MPAPE) analyzed with HPLC

S.No	Phytocompounds	Concentration (ppm)	Retention time (min)
1	Capsaicin	1.016	7.665
2	Caffeic acid	1.400	2.430
3	Beta-sistosterol	3.483	35.596
4	Apigenin	3.816	19.575
5	Luteolin	5.200	2.293
6	Quercetin	5.516	13.480
7	Kaempferol	6.333	36.260
8	Syringin	7.933	16.546

Table 1.3: Bioactive compounds of *Musa paradisiaca* aqueous pulp extract (MPAPE) analyzed with GC-MS

S.No	Phytocompounds	Molecular Weight*	Molecular Formula	Retention Time	Area (%)
1	1-Methylene-2b Hydroxymethyl-3,3-Dimethyl-4b-(3-Methylbut-2-Enyl)-Cyclohexane	222	$C_{15}H_{26}O$	33.776	5.59
2	3-Decyn-2-ol	154	$C_{10}H_{18}O$	21.296	10.9

3	26-Hydroxy Cholesterol	402	$C_{27}H_{46}O_2$	32.626	6.25
4	Campesterol	400	$C_{28}H_{48}O$	24.40	12.51
5	1,2-Benzenedicarboxylic acid, dioctyl ester (CAS) phthalate	390	$C_{24}H_{38}O_4$	25.768	10.18
6	Acetic Acid, 1-Methylethyl Ester	102	$C_5H_{10}O_2$	2.799	4.31
7	Methyl elaidate	296	$C_{19}H_{36}O_2$	20.605	2.16
8	Octadeca-9,12-Dienoic acid methyl ester	294	$C_{19}H_{34}O_2$	21.253	6.45
9	Hexadecanoic acid, methyl ester (CAS) Methyl palmitate	270	$C_{17}H_{34}O_2$	18.070	2.60
10	Octadecanoic acid, methyl ester (CAS) Methyl stearate	298	$C_{19}H_{38}O_2$	20.892	1.93
11	9-Octadecenamide, (Z)-	281	$C_{18}H_{35}NO$	23.51	15.97
12	Hexadecanoic acid (CAS) Palmitic acid	256	$C_{16}H_{32}O_2$	18.844	4.27
13	β-Stigmasterol	412	$C_{29}H_{48}O$	26.04	7.43

*Molecular weight in g/mol

The complex interaction of quercetin, the ligand with the best binding affinity, and the human pancreatic α-amylase protein is presented in Figure 2.1. The 2D structure illustrated the formation of a Pi-Pi T-shaped bond between the ligand and His201 (amino acids) at the surface of the protein. Additionally, Leu162 formed Pi-sigma and Pi-alkyl interactions with quercetin. Meanwhile, Trp59 forms a conventional hydrogen bond, and Leu165 forms a pi-alkyl interaction with quercetin. Additionally, Try151, Ile235, Glu233, Ala198, Asp197, His101, Glu60, Tyr62, and Gln63 all formed van der Waals interactions with quercetin. Figure 2.2 shows the 2D structure of campesterol – human α-glucosidase (protein) complex interaction. Ala555, Phe525, Trp481, Phe649, and Trp376 formed pi-alkyl and alkyl interactions with campesterol. Meanwhile, Leu650, Asp616, Asn524, Asp404, Asp282, Arg281, Ser253, Met519, Asp518, Arg600, His647, and Trp516 formed van der Waals interaction with the best binding affinity.

The 2D structure of the complex interaction between quercetin (ligand) and the human sorbitol dehydrogenase (protein) is presented in Figure 2.3. Ala254 forms an amide-pi stacked interaction, while Thr250, Leu204, and Ile233 form Pi-sigma and Ala252, Ala258, and Ile231 form Pi-alkyl bonds with quercetin. Additionally, Ser255, Cys178, Pro228, Ser227, and Gly179 formed van der Waals interactions with quercetin, while Thr202 and Glu226 formed a conventional hydrogen bond. Figure 2.4 illustrates the complex interaction between apigenin, the ligand with the best binding affinity, and the human aldose reductase protein. The 2D structure below illustrates the formation of a pi-alkyl bond between the ligand and Pro211 at the surface of the protein. Cys298 formed a pi-sulfur and conventional hydrogen bond with apigenin. Additionally, Trp20 and Tyr209 formed pi-pi stacked and pi-pi T-shaped bonds with apigenin, while Cys298, Ser210, and Asp43 formed a conventional hydrogen bond. More so, Pro215, Gly18, and Lys262 formed carbon-hydrogen bonds and pi-donor hydrogen bonds with the ligand apigenin. Meanwhile, Lys21, Asp216, Ser214, Leu212, Pro261, Thr19, Trp111, Tyr48, Gln183, Lys77, and Ile260 formed van der Waals interactions with apigenin, the best binding ligand.

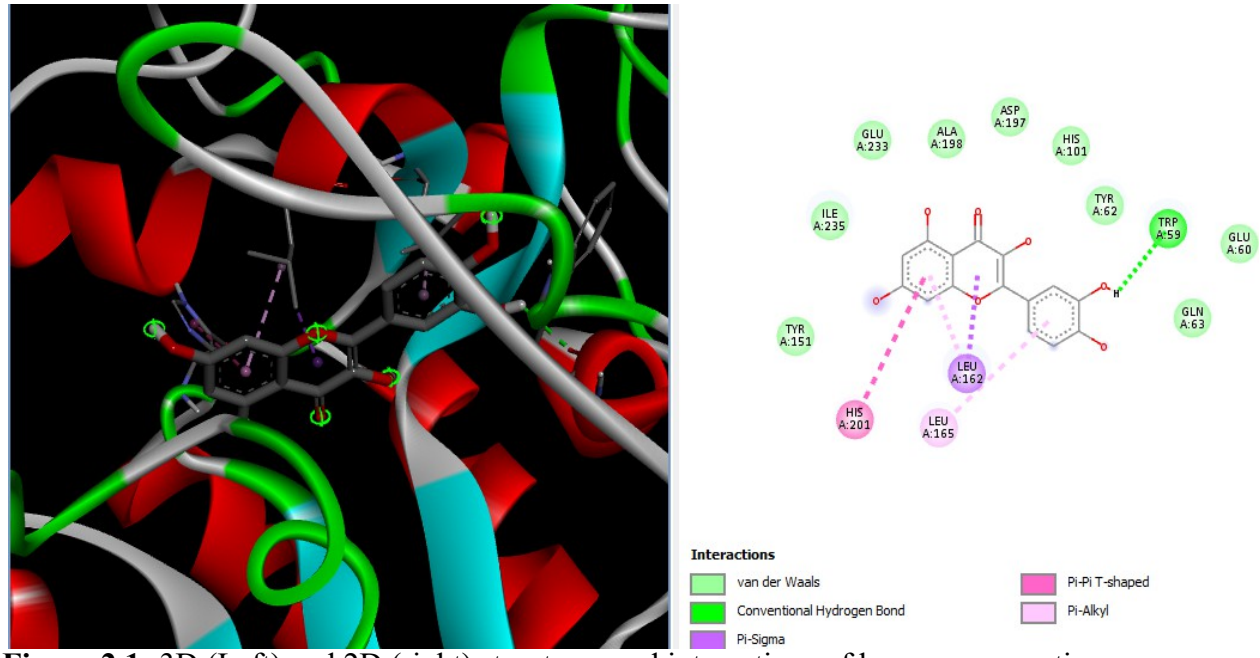

Figure 2.1: 3D (Left) and 2D (right) structures and interactions of human pancreatic α-amylase docked with quercetin

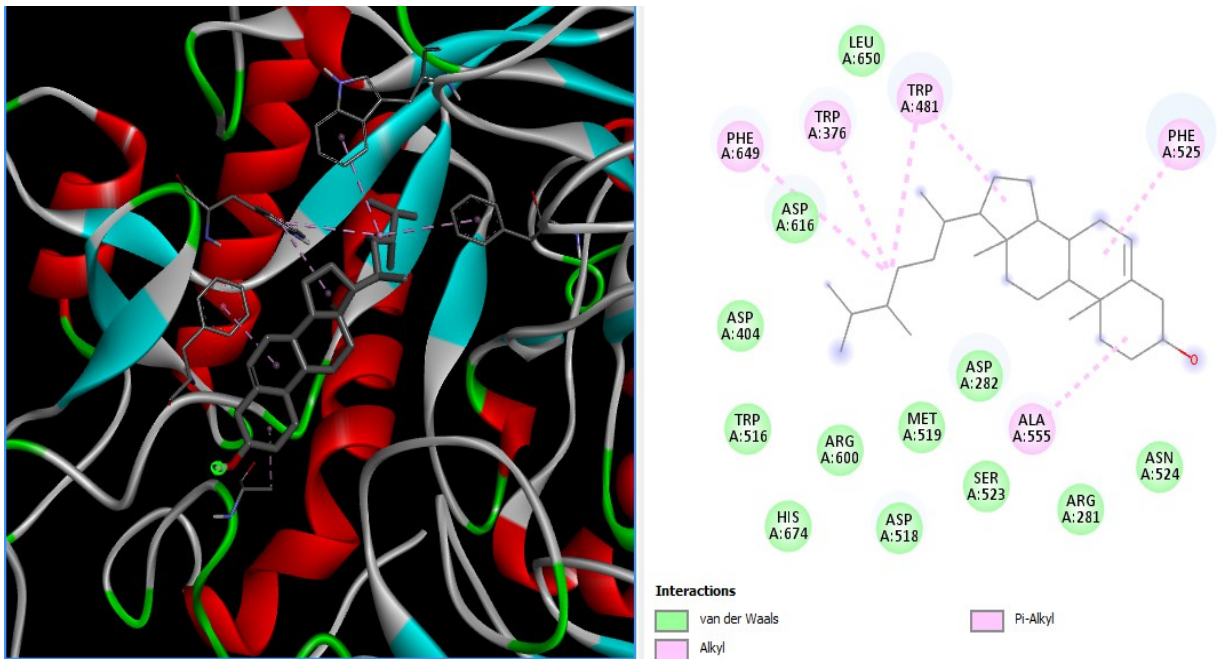

Figure 2.2: 3D (left) and 2D (right) structures and interactions of human α-glucosidase docked with campesterol.

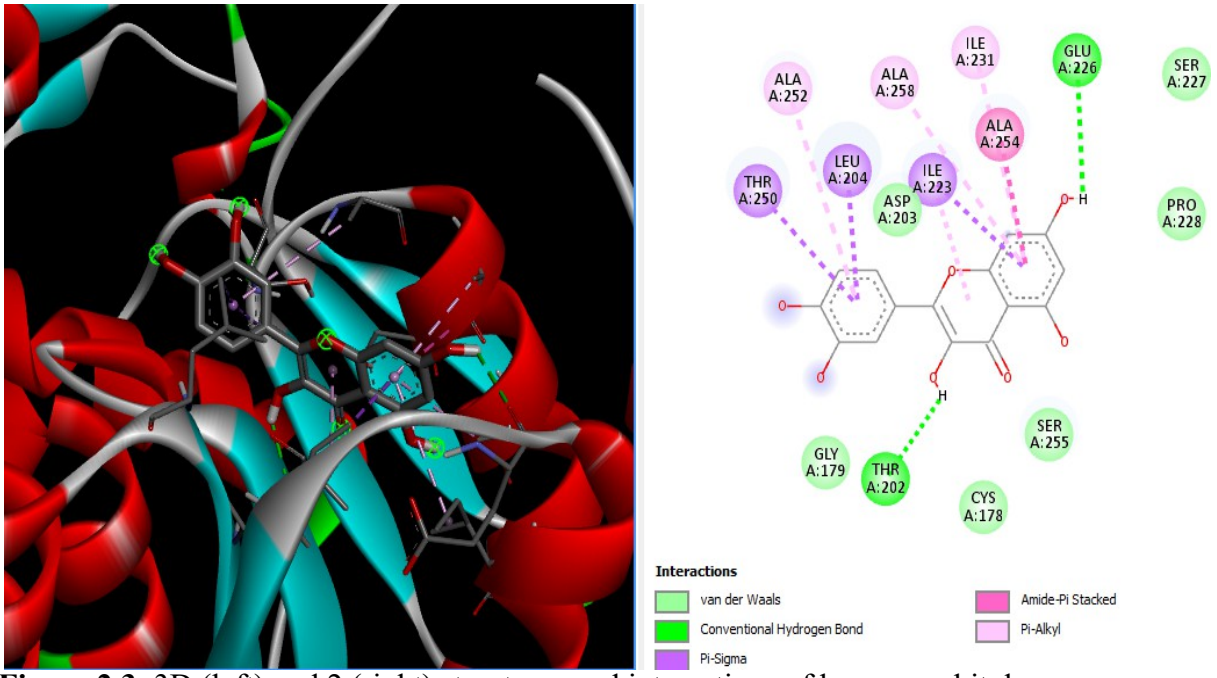

Figure 2.3: 3D (left) and 2 (right) structures and interactions of human sorbitol dehydrogenase docked with quercetin.

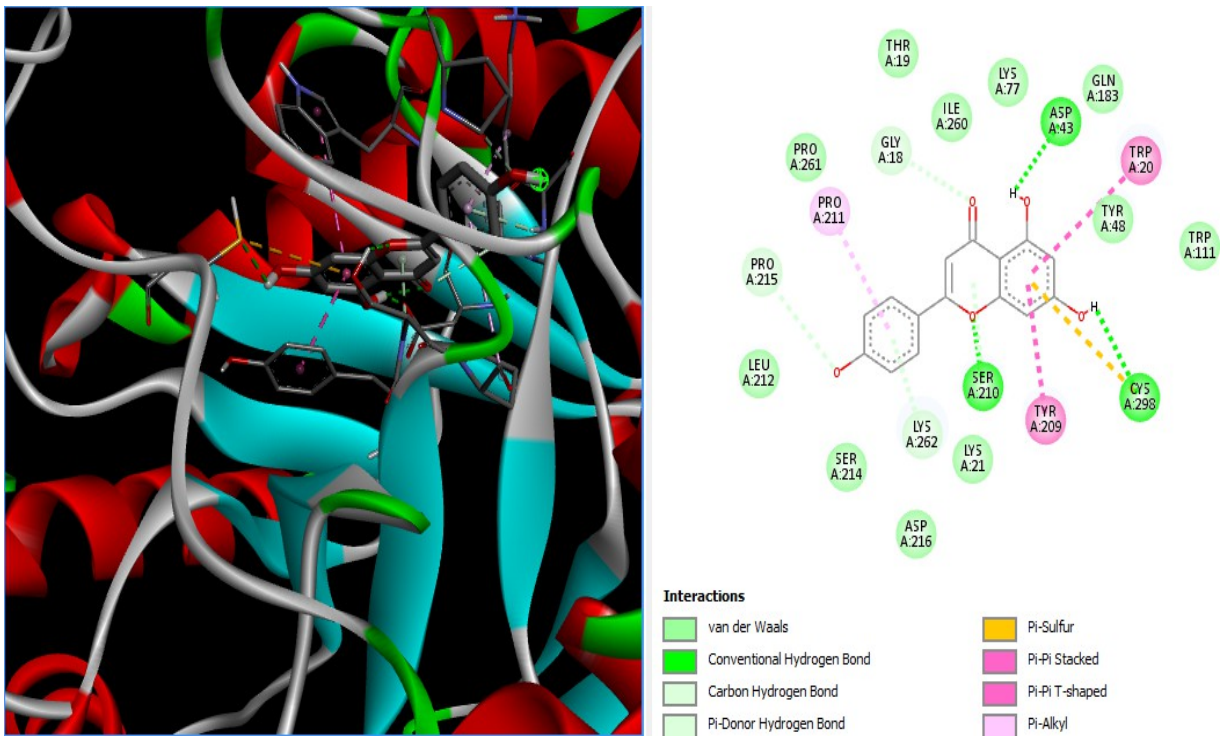

Figure 2.4: 3D (left) and 2D (right) structure and interactions of human aldose reductase docked with apigenin.

The top ten (10) ligands according to their binding affinities (kcal/ mol) are presented in Table 2. The lower the binding energy, the better the binding affinity and ligand. Here, the compound apigenin is revealed as the overall best ligand because of its binding energy of -9.8 kcal/mol.

Table 2: Top ten (10) ligands and their binding affinities with each target protein.

S. No.	Ligands	PubChem ID	Diabetic protein targets α-amylase	α-glucosidase	AR	SDH
1	Apigenin	5280443	-7.5	-7.2	**-9.8**	-7.4
2	Luteolin	5280445	-7.4	-7.0	-9.7	-8.4
3	Kaempferol	5280863	-7.6	-7.0	-9.5	-6.7
4	Quercetin	5280343	**-7.8**	-6.8	-9.5	**-8.5**
5	Capsaicin	1548943	-6.0	-6.3	-9.1	-5.8
6	Campesterol	173183	-7.1	**-8.3**	-5.3	-7.8
7	Stigmasterol	5280794	-7.2	-8.2	-7.4	-8.1
8	Caffeic acid	689043	-6.5	-6.0	-8.2	-6.2
9	26-Hydrocholesterol	99470	-6.5	-8.1	-7.6	-7.0
10	Beta-Sistosterol	22284	-6.8	-8.1	-5.0	-6.9
11	Tolrestat*	53359	-	-	-6.5	-7.3
12	Acarbose*	41774	-4.7	-7.2	-	-

* Denotes standard drugs used in this study.

The physicochemical properties of the best ten (10) ligands embedded in *Musa paradisiaca* aqueous pulp extract are presented in Table 3.1. From the table, the compounds embedded in the plant obeyed the Lipinski rule of five (RO5) which states that a molecule is more likely to be druggable if it has no more than five violations of the following criteria: molecular weight less than 500, logP less than 5, hydrogen bond donors less than 5, hydrogen bond acceptors less than 10, and 10 or fewer rotatable bonds.

The assessment of water solubility and lipophilicity properties of the top ten (10) ligands is presented in Table 3.2. Stigmasterol showed the best logarithm of the partition coefficient (log P) with a value of 5.08. Apigenin, luteolin, quercetin, kaempferol, capsaicin, and caffeic acid are the only ligands predicted to be water-soluble. Meanwhile, all other ligands are also within the ranges away from zero (0), indicating their good lipophilicity properties.

The top ten (10) ligands have a good bioavailability score of 0.55, which is a good drug-likeness property since a minimum of 0.10 bioavailability score is required of a compound to become a drug candidate. All ten ligands obey Lipinski's rule of five (RO5) and Veber. However, only five (5) compounds obeyed Muegge's rule, and six (6) compounds obeyed Egan's rule (Table 3.3).

The medicinal chemical properties of the overall top ten (10) ligands are presented in Table 3.4. Seven of the top ten ligands showed positive pan-assay interference compounds (PAINS), and four ligands showed positive lead-likeness indications. This indicates that the test compounds are not likely to give false-positive results in high-throughput screenings. All the top ten ligands indicated that the synthetic accessibility scored approximately from 1.81 – 6.30, where beta-sitosterol showed the best synthetic accessibility.

The pharmacokinetic properties (Table 3.5) showed low gastrointestinal absorption for three of the ten best ligands, including campesterol, stigmasterol, and beta-sitosterol. Moreso, the blood-brain barrier permeability showed a positive indication for one of these best ten ligands, whereas no ligand was identified as a P-glycoprotein substrate. Five of the best ten ligands were predicted to be CYP34A4 inhibitors. Meanwhile, no ligand was identified as an inhibitor of CYP2C19. Similarly, apigenin, luteolin, kaempferol, quercetin, and capsaicin were identified as inhibitors of CYP1A2 and CYP2D6. Additionally, stigmasterol is the only ligand identified to

be a CYP2C9 inhibitor.

All the selected ligands have a negative indicator for kidney and carcinogenic toxicity. Two of the ten best ligands, including apigenin and caffeic acid, show a negative indicator for respiratory and mitochondrial toxicity. Additionally, luteolin, capsaicin, and caffeic acid have a negative indicator for hepatotoxicity, while all ten ligands have negative indicators for reproductive toxicity (Table 3.6).

The absorption, distribution, metabolism, excretion, and toxicity (ADME/T) properties of the overall top ten (10) ligands are presented in Tables 3.1-3.6.

Table 3.1: Physicochemical properties of active compounds embedded in *Musa paradisiaca* pulp.

Ligands	Molecular Formula	Molecular Weight (g/mol)	NRB	NHBA	NHBD
Apigenin	$C_{15}H_{10}O_5$	270.24	1	5	3
Luteolin	$C_{15}H_{10}O_6$	286.24	1	6	4
Kaempferol	$C_{15}H_{10}O_6$	286.24	1	6	4
Quercetin	$C_{15}H_{10}O_7$	302.24	1	7	5
Capsaicin	$C_{18}H_{27}NO_3$	305.41	10	3	2
Campesterol	$C_{28}H_{48}O$	400.68	5	1	1
Stigmasterol	$C_{29}H_{48}O$	412.69	5	1	1
Caffeic acid	$C_9H_8O_4$	180.16	2	4	3
26-hydroxy cholesterol	$C_{27}H_{46}O_2$	402.65	6	2	2
Beta-sistosterol	$C_{29}H_{50}O$	414.71	6	1	1
Tolrestat*	$C_{16}H_{14}F_3NO_3S$	357.35	6	6	1
Acarbose*	$C_{25}H_{43}NO_{18}$	645.60	9	19	14

* Denotes standard drugs used in this study. NRB = Number of Rotatable Bonds, NHBA = Number of H-bond Acceptors, NHBD = Number of H-bond Donors

Table 3.2: Water solubility and Lipophilicity properties of *Musa paradisiaca* pulp bioactive compounds

S. No.	Ligands	Log S(ESOL)	Log $P_{o/w}$ (iLOGP)
1	Apigenin	-3.94 (Soluble)	1.89
2	Luteolin	-3.71 (Soluble)	1.86
3	Kaempferol	-3.31 (Soluble)	1.70
4	Quercetin	-3.16 (Soluble)	1.63
5	Capsaicin	-3.53 (Soluble)	3.15
6	Campesterol	-7.54 (Poorly soluble)	4.97
7	Stigmasterol	-7.46 (Poorly soluble)	5.08
8	Caffeic acid	-1.89 (Very soluble)	0.97
9	26-hydroxy	-6.44 (Poorly soluble)	4.60
10	Cholesterol Beta-Sitosterol	-7.90 (Poorly soluble)	5.05
11	Tolrestat*	-4.29 (Moderately soluble)	2.42
12	Acarbose*	2.13 (Highly soluble)	1.43

* Denotes standard drugs used in this study.

Table 3.3: Drug-likeness properties of the bioactive compounds embedded in *Musa paradisiaca* pulp.

S.No	Ligands	Lipinski	Ghose	Veber	Egan	Muegge	Bioavailability score
1	Apigenin	Yes; 0 violation	Yes	Yes	Yes	Yes	0.55
2	Luteolin	Yes; 0 violation	Yes	Yes	Yes	Yes	0.55
3	Kaempferol	Yes; 0 violation	Yes	Yes	Yes	Yes	0.55
4	Quercetin	Yes; 0 violation	Yes	Yes	Yes	Yes	0.55
5	Capsaicin	Yes; 0 violation	Yes	Yes	Yes	Yes	0.55
6	Campesterol	Yes; 1 violation: MLOGP>4.15	No; 2 violations: WLOGP>5.6, #atoms>70	Yes	No; 1 violation: WLOGP>5.88	No; 2 violations: XLOGP3>. Heteroatoms<2	0.55
7	Stigmasterol	Yes; 1 violation: MLOGP>4.15	No; 3 violations: WLOGP>5.6, MR>130, #atoms>70	Yes	No; 1 violation: WLOGP>5.88	No; 2 violations: XLOGP3>. Heteroatoms<2	0.55
8	Caffeic acid	Yes; 0 violation	Yes	Yes	Yes	No; 1 violation: MW<200	0.56
9	26-hydroxy Cholesterol	Yes; 1 violation: MLOGP>4.15	No; 2 violations: WLOGP>5.6, #atoms>70	Yes	No; 1 violation: WLOGP>5.88	No; 1 violation: XLOGP3>5	0.55
10	Beta- Sistoster(	Yes; 1 violation: MLOGP>4.15	No; 3 violations: WLOGP>5.6, MR>130, #atoms>70	Yes	No; 1 violation: WLOGP>5.88	No; 2 violations: XLOGP3>. Heteroatoms<2	0.55
11	Tolrestat*	Yes; 0 violation	Yes	Yes	Yes	Yes	0.56
12	Acarbose*	No; 3 violations: MW>500, NorO>10, NHorOH>5	No; 4 violations: MW>48(WLOGP<- 0.4, MR >130, #atoms>70	No; 1violatior TSAP>140	No; 1 violation: TSAP>131.6	No; 5 violations: MW>600, XLOGP<-2, TPSA>150, H-acc>10, H- don>5	0.17

* Denotes standard drugs used in this study.

Table 3.4: Medicinal chemistry prediction of the bioactive compounds embedded in *M. paradisiaca* pulp extract

S.No	Ligands	PAINS	Brenk	Lead-likeness	Synthetic accessibility
1	Apigenin	0 alert	0 alert	Yes	2.96
2	Luteolin	1alert: catechol_A	1 alert: catechol	Yes	3.02
3	Kaempferol	0 alert	0 alert	Yes	3.14
4	Quercetin	1alert: catechol_A	1 alert: catechol	Yes	3.23
5	Capsaicin	0 alert	1 alert: isolated_ alkene	No;2violations: Rotors>7, XLOGP3>3.5	2.32
6	Campesterol	0 alert	1 alert: isolated_ alkene	No;2violations: MW>350, XLOGP3>3.5	6.17
7	Stigmasterol	0 alert	1 alert: isolated_ alkene	No;2violations: MW>350, XLOGP3>3.5	6.21
8	Caffeic acid	1alert: catechol_A	2 alerts: catech michael_acceptor_1	No;1violation: MW<250	1.81
9	26-hydroxy cholesterol	0 alert	1 alert: isolated_ alkene	No;2violations: MW>350, XLOGP3>3.5	6.09
10	Beta-sistosterol	0 alert	1 alert: isolated_ alkene	No;2violations: MW>350, XLOGP3>3.5	6.30
11	Tolrestat*	0 alert	1 alert: thiocarbonyl_group	No; 2 violations: MW>350, XLOGP3>3.5	2.34
12	Acarbose*	0 alert	1 alert: isolated_ alkene	No; 2 violations: MW>350, Rotors>7	7.34

* Denotes standard drugs used in this study.

Table 3.5: Pharmacokinetics of *Musa paradisiaca* pulp extract bioactive compounds.

S.No	Ligands	GI Absorption	BBB Permeant	P-gp Substrate	CYP1A2 inhibitor	CYP2C19 inhibitor	CYP2C9 inhibitor	CYP2D6 inhibitor	CYP3A4 inhibitor
1	Apigenin	High	No	No	Yes	No	No	Yes	Yes
2	Luteolin	High	No	No	Yes	No	No	Yes	Yes
3	Kaempferol	High	No	No	Yes	No	No	Yes	Yes
4	Quercetin	High	No	No	Yes	No	No	Yes	Yes
5	Capsaicin	High	Yes	No	Yes	No	No	Yes	Yes
6	Campesterol	Low	No	No	No	No	No	No	No
7	Stigmasterol	Low	No	No	No	No	Yes	No	No
8	Caffeic acid	High	No	No	No	No	No	No	No
9	26-hydroxy Cholesterol	High	No	No	No	No	No	No	No
10	Beta-Sistosterol	Low	No	No	No	No	No	No	No
11	Tolrestat*	High	No	No	No	No	Yes	No	No
12	Acarbose*	Low	No	Yes	Yes	Yes	No	No	No

* Denotes standard drugs used in this study.

https://doi.org/10.55549/zbs.1638235

Table 3.6: Toxicity Properties of the bioactive compounds embedded in *Musa paradisiaca* aqueous pulp extract.

S.No	Ligands	Carcinogenic Toxicity	Hepato-toxicity	Respiratory Toxicity	Reproductive Toxicity	Mitochondria Toxicity	Acute Oral toxicity
1	Apigenin	-	+	-	+	-	III
2	Luteolin	-	-	+	+	+	II
3	Kaempferol	-	+	+	+	+	II
4	Quercetin	-	+	+	+	+	II
5	Capsaicin	-	-	+	+	+	III
6	Campesterol	-	+	+	+	+	I
7	Stigmasterol	-	+	+	+	+	I
8	Caffeic acid	-	-	-	+	-	IV
9	26-hydroxy Cholesterol	-	+	+	+	+	III
10	Beta-Sistosterol	-	+	+	+	+	I
11	Tolrestat*	-	+	+	+	+	III
12	Acarbose*	-	+	+	+	+	IV

* Denotes standard drugs used in this study. Toxicity category I is highly toxic and severely irritating, Toxicity category II is moderately toxic and moderately irritating, Toxicity category III is slightly toxic and slightly irritating, and Toxicity category IV is practically non-toxic and not an irritant.

The effect of MPAPE on protein concentrations and glucose levels is presented in Table 4. The administration of MPAPE significantly ($p<0.05$) increased and decreased high levels of glucose and protein concentrations, respectively, compared to the STZ untreated group.

Table 4: Effect of MPAPE on Protein concentrations and Glucose levels

Experimental Groups	Protein Conc. [mg/mL]	Glucose Levels [mg/dL]
Control	0.214 ± 0.06^{a}	82.65 ± 5.82^{a}
STZ	0.131 ± 0.03^{b}	287.80 ± 4.49^{b}
STZ + MPAPE	0.256 ± 0.02^{a}	$114.8\ 0 \pm 3.10^{c}$
STZ + Glb	0.185 ± 0.06^{b}	71.74 ± 1.15^{a}

Data are presented as mean ± SEM (n=6), and values with different alphabets in the same column are statistically significant at $p<0.05$. STZ = Streptozotocin, MPAPE = *Musa paradisiaca* aqueous pulp extract, Glb = Glibenclamide.

The effect of MPAPE on lipid profiles is presented in Table 5. The administration of MPAPE significantly ($p<0.05$) increased the high-density lipoprotein cholesterol (HDL-Chol) compared

to the STZ untreated group. Conversely, MPAPE significantly ($p<0.05$) decreased total cholesterol (total-Chol), triglyceride (TRIG), low-density lipoprotein cholesterol (LDL-Chol), and very low-density lipoprotein cholesterol (VLDL-Chol) compared to the STZ untreated group

Table 5: Effect of MPAPE on Lipid profiles

Experimental Groups	Total-Chol [mg/dL]	TRIG [mg/dL)]	HDL-Chol [mg/dL]	LDL-Chol [mg/dL]	VLDL-Chol [mg/dL]
Control	202.6 ± 1.13^{a}	196.2 ± 2.79^{a}	211.4 ± 9.92^{a}	41.74 ± 0.32^{a}	39.24 ± 0.56^{a}
STZ	599.2 ± 0.38^{b}	452.6 ± 39.18^{b}	102.0 ± 0.99^{b}	148.20 ± 11.28^{b}	148.5 ± 9.84^{b}
STZ + MPAPE	250.0 ± 24.40^{a}	189.2 ± 4.28^{a}	163.7 ± 0.59^{c}	78.47 ± 24.67^{a}	37.83 ± 0.86^{a}
STZ + Glb	295.2 ± 5.76^{a}	237.8 ± 14.07^{a}	184.1 ± 5.73^{c}	55.58 ± 2.64^{a}	50.63 ± 2.27^{a}

Data are presented as mean ± SEM (n=6) with different alphabets in the same column are statistically significant at $p<0.05$. STZ=Streptozotocin, MPAPE=*Musa paradisiaca* aqueous pulp extract, Glb=Glibenclamide.

The effect of MPAPE on antioxidant activities is presented in Figure 3. The administration of MPAPE significantly ($p<0.05$) increased both superoxide dismutase and catalase activities compared to the untreated group. The effect of MPAPE on liver enzyme activities is presented in Figure 4. The administration of MPAPE significantly ($p<0.05$) increased both alanine transferase (ALT) and aspartate transferase (AST) activities compared to the STZ-untreated group.

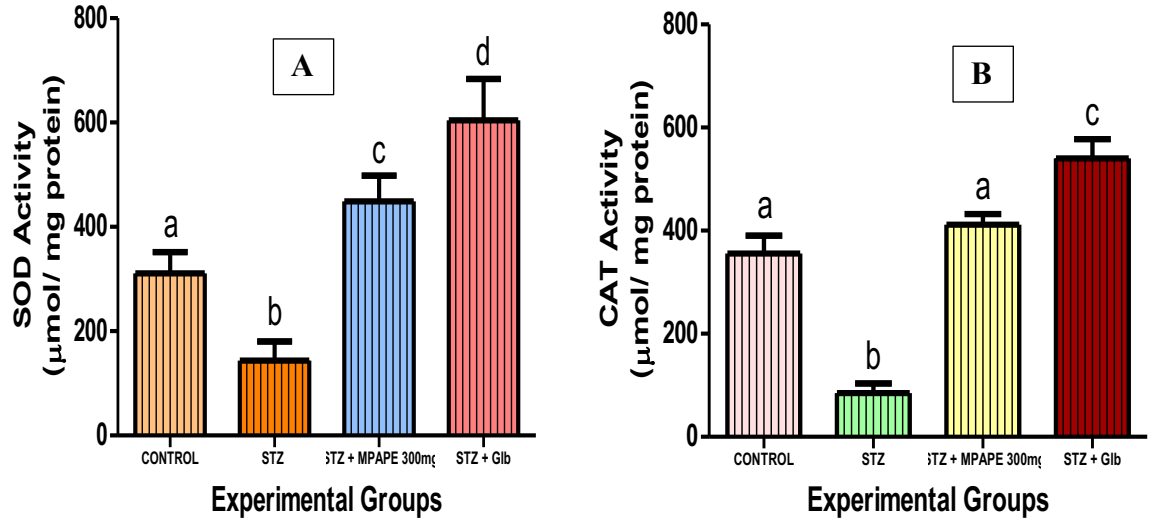

Figure 3: Effects of *Musa paradisiaca* aqueous pulp extract (MPAPE) on antioxidant enzyme: (a) superoxide dismutase and (b) catalase activities in STZ-induced diabetic Wistar rats. Each bar represents mean ± SEM (n=6) and bars with different alphabets are statistically significant at $p<0.05$. STZ=Streptozotocin, Glb=Glibenclamide

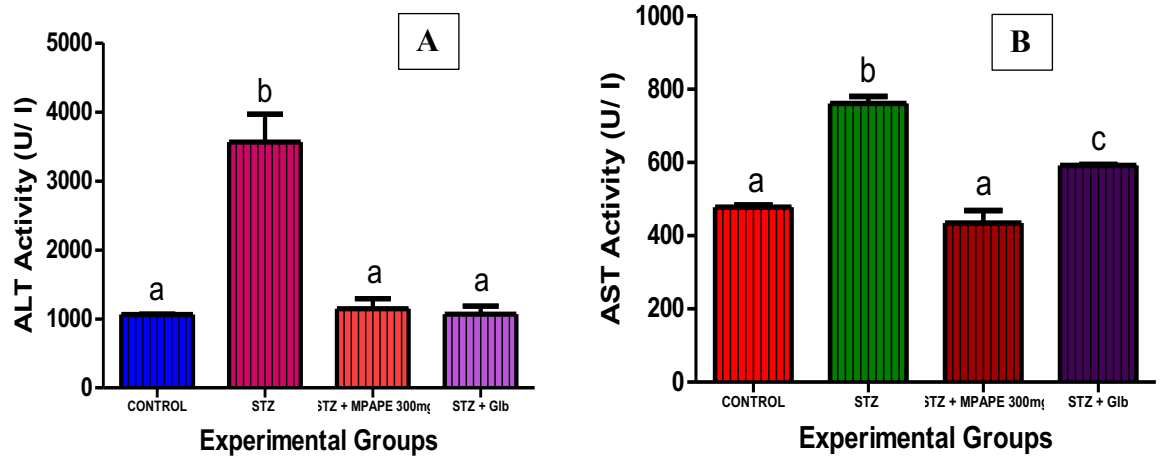

Figure 4: Effects of *Musa paradisiaca* aqueous pulp extract (MPAPE) on liver enzymes: (a) alanine transaminase (ALT) and (b) aspartate transaminase (AST) activities in STZ-induced diabetic Wistar rats. Each bar represents mean ± SEM (n=6), and bars with different alphabets are statistically significant at $p<0.05$. STZ=Streptozotocin, Glb= Glibenclamide

The effects of MPAPE on oxidative stress markers are presented in Table 6. The administration of MPAPE significantly ($p<0.05$) increased glutathione (GSH) compared to the STZ-induced untreated group. Conversely, MPAPE significantly ($p<0.05$) decreased the high hydrogen peroxide (H_2O_2), nitric oxide (NO), and malonaldehyde (MDA) concentration compared to the STZ-induced untreated group.

Table 6: Effects of MPAPE on oxidative stress markers

Experimental Groups	H_2O_2 [mmol/mL]	NO [mmol/mL]	GSH [µmol/mg protein]	MDA [nMoles]
Control	0.053 ± 0.01^a	0.038 ± 0.01^a	339.80 ± 13.78^a	80.02 ± 2.75^a
STZ	0.190 ± 0.04^b	0.156 ± 0.01^b	191.60 ± 7.020^b	197.40 ± 0.87^b
STZ + MPAPE	0.045 ± 0.00^a	0.054 ± 0.01^a	410.30 ± 61.88^c	68.05 ± 0.03^a
STZ + Glb	0.060 ± 0.00^a	0.037 ± 0.00^a	392.50 ± 6.83^a	58.61 ± 2.12^a

Data are presented as mean ± SEM (n=6), and values with different alphabets in the same column are statistically significant at $p<0.05$. STZ=Streptozotocin, MPAPE=*Musa paradisiaca* aqueous pulp extract, Glb=Glibenclamide, MDA=malonaldehyde, GSH=glutathione, NO=nitric oxide, H2O2=hydrogen peroxide.

Discussion

Individuals diagnosed with diabetes mellitus are more likely to develop complications due to hyperglycemia. The use of conventional drugs in the management of diabetes has been associated with adverse effects that are detrimental to the health of individuals, which has given

grounds for the exploration of medicinal plants as an alternative treatment (Idm'hand *et al*., 2020). The phytochemical screening of *M. paradisiaca* aqueous pulp extract confirmed the presence of flavonoids, alkaloids, phenols, tannins, and saponins, but not terpenoids and steroids. These phytochemicals (bioactive compounds) act as antioxidants by exerting their protective effects on the cells of the body and acting as immune regulators, scavengers of reactive oxygen species (ROS), and preventers of ROS generation (Vo *et al*., 2020).

If scientifically proven, the phytochemicals embedded within a medicinal plant that contain biochemical properties with known pharmacological activities are used to develop modern medicine for the treatment and management of various illnesses, including diabetes and its complications (Awuchi, 2019). Alkaloids are a group of nitrogen-containing compounds, obtained from plants that possess pharmacological properties, such as analgesic, anticancer, antibacterial, antimalarial, and antidepressant activities (Adibah and Azzreena, 2019). Flavonoids and phenols are secondary metabolites that also serve as antioxidants that scavenge and eliminate free radicals. They have also shown effective antioxidant, anticancer, antibacterial, and anti-inflammatory properties while improving the immune system (Tungmunnithum *et al*., 2018). The quantitative analysis of the aqueous fruit pulp extract of *Musa paradisiaca* showed a high polyphenolic content of total flavonoids, followed by total phenols and total tannins.

Molecular docking is an essential computational technique in developing new drugs for various disease management and treatment. It forecasts the interactions between a possible medication and its target protein and aids in assessing the feasibility of therapeutic candidates (Riyaphan *et al*., 2021). In this study, to determine the antidiabetic potential and prospects of the phytochemical constituents of *M. paradisiaca* aqueous fruit pulp extracts (MPAPE), an extensive *in silico* approach was employed. The compounds obtained from GC-MS and HPLC analysis of the extract served as the ligands alongside the standard drugs tolrestat and acarbose. All were selected and docked against the catalytic sites of four different diabetic target proteins, and the docking scores were obtained. Figures 2.1 – 2.4 show the interacting amino acids and bonds responsible for the stability of the protein-ligand complex. The active site of each of the proteins contains different amino acid residues, such that α-amylase contains His201, Leu162, Trp59, and Leu165. As well as, Try151, Ile235, Glu233, Ala198, Asp197, His101, Glu60, Tyr62, and Gln63. Some of the amino acid residues present at the active sites of other protein such as α-glucosidase includes Leu650, Asp616, Asn524, Asp404, Asp282, Arg281, Ser253, Met519, Asp518, Arg600, His647, and Trp516; sorbitol dehydrogenase includes Thr250, Leu204, Ile233, Ala252, Ser255, Cys178, Gly179, Glu226, and Pro228, and aldose reductase includes Lys21, Asp216, Ser214, Leu212, Pro261, Thr19, Trp111, Tyr48, Gln183, Lys77, and Ile260. The results showed campsterol, apigenin, and quercetin as the top binding ligands of each protein target.

In the last decade, drug failures due to poor pharmacokinetic profiles, medicinal chemistry properties, efficacy, unmanaged toxicity, and inadequate drug-likeness properties have been on the rise. This led to a focus on improving the drug development process by utilizing ADMET properties at the early stages (Dulsat *et al*., 2023). In this study, the ADMET properties of the top ten (10) ligands resulting from the *in-silico* study were analyzed using SwissADME, admetSAR, and ProTox software. All the best ten (10) ligands obeyed the Lipinski rule of five (RO5) (Lipinski, 2004), which shows that all ten ligands have the potential to be used in the development of new pharmaceuticals (Ivanović *et al*., 2020). Stigmasterol showed the best logarithm of the partition coefficient (log P) with a value of 5.08. Apigenin, luteolin, quercetin, kaempferol, capsaicin, and caffeic acid are the only ligands predicted to be water-soluble. Meanwhile, the remaining ligands, campesterol, stigmasterol, 26-hydro cholesterol, and beta-

sitosterol are within the ranges away from zero (0), indicating their good lipophilicity properties. This aligns with similar studies by Chmiel *et al*. (2019). Drug-likeness properties showed that all ten ligands have a good bioavailability score range of 0.17 to 0.55, since a minimum of 0.10 bioavailability score is required for a compound to become a drug candidate (Ntie-Kang *et al*., 2019).

The medicinal chemistry prediction of the top ten ligands showed that seven of these ligands have positive pan-assay interference compounds (PAINS), and four ligands showed positive lead- likeness indications. This indication may imply that these compounds are not likely to give false-positive results in high-throughput screenings. More so, all the top ten ligands indicated a synthetic accessibility score range of 1.81 to 6.30, where beta-sitosterol showed the best synthetic accessibility. This may imply that this compound can be easily used in the synthesis of a new drug (Stratton *et al*., 2015). Pharmacokinetic properties of the overall top ten ligands showed low gastrointestinal absorption for three of the ten best ligands, including campesterol, stigmasterol, and beta-sitosterol. Additionally, the blood-brain barrier permeability showed a positive indication for one of the ligands, as a result, this compound may be developed and used for central nervous system (CNS) disorders, especially in neurological disorders, including dementia, schizophrenia, and Alzheimer's disease (Małkiewicz *et al*., 2019). Whereas no ligand was identified as a P-glycoprotein substrate. Five of the best ten ligands were predicted to be CYP34A4 (cytochrome P450 3A4) inhibitors. Meanwhile, no ligand was identified as an inhibitor of CYP2C19 (cytochrome P450 2C19). Similarly, apigenin, luteolin, kaempferol, quercetin, and capsaicin were identified as inhibitors of CYP1A2 (cytochrome P450 1A2) and CYP2D6 (cytochrome P450 2D6C). Additionally, stigmasterol is the only ligand identified to be a CYP2C9 (cytochrome P450 2C9) inhibitor.

Streptozotocin (STZ) is a chemical agent used experimentally in the partial or total destruction of pancreatic islet β-cells in animal models to induce either type 1 diabetes mellitus (T1DM) or type 2 diabetes mellitus (T2DM) (Furman, 2015). In this present study, the STZ-induced diabetic Wistar rats exhibited the characteristic hyperglycemia attributed to diabetes mellitus. The induced hyperglycemia was, however, reduced after the oral administration of MPAPE (300 mg/ kg body weight) over 21 days. This suggests that MPAPE has a hypoglycemia potential by increasing the glucose uptake (Taylor *et al*., 2021). On the other hand, STZ intraperitoneal injection also caused a significant ($p<0.05$) decrease in the protein concentration of the STZ-untreated animals compared to the control. However, the oral administration of 300 mg/kg bw of MPAPE and glibenclamide significantly ($p<0.05$) decreased the concentration in the STZ-induced rats.

Initially, the induction of diabetes using STZ resulted in a significant increase in glucose (hyperglycemia), lipids (hyperlipidemia), and alterations in liver enzymes. However, following the administration of MPAPE (300 mg/ kg body weight), a significant decrease ($p<0.05$) was observed in these parameters. This aligns with the findings of Salazar-García and Corona, (2021) who reported similar findings after treatment Superoxide dismutase (SOD) and catalase (CAT) are enzymatic antioxidants that are crucial in the mitigation of free radical-induced oxidative stress (Kumar and Pandey, 2015). SOD facilitates the dismutation of super-oxides produced during enzymatic and non-enzymatic processes in the biological system (Fujii *et al*., 2022). On the other hand, CAT neutralizes the H_2O_2 produced during the dismutation process to prevent oxidative stress and protect the cells (Tehrani and Moosavi-Movahedi, 2018). The treatment of STZ-induced diabetic rats with MPAPE (300 mg/ kg body weight) restored the plasma antioxidant levels.

Hyperglycemia triggered by STZ-induction may lead to an increase in polyunsaturated (PUFA)

fatty acids in the cell membrane, leading to lipid peroxidation (Manirafasha, 2014). In this study, there was a significant increase in the plasma malonaldehyde (MDA), hydrogen peroxide (H_2O_2), and nitric oxide (NO) levels of the STZ untreated animals compared to the control. However, following the administration of MPAPE (300 mg/ kg body weight) and glibenclamide, there was a significant decrease in these parameters. This improvement in oxidative stress markers is most likely attributed to the embedded phytochemicals of MPAPE and its ability to scavenge and neutralize free radicals.

The liver enzymes, alanine transaminase (ALT) and aspartate transaminase (AST), serve as indicators of hyperglycemia-induced liver damage/injury (Mohamed *et al*., 2016). In this study, the activities of the liver enzymes (ALT and AST) significantly ($p<0.05$) increased in the STZ untreated rats, which is an indicator of liver damage or injury. However, treatment with MPAPE (300mg/ kg body weight) and the standard drug, glibenclamide, significantly ($p<0.05$) decreased the activities of the plasma liver enzyme of the STZ untreated animals. Similar findings have been reported by McGill (2016).

Conclusion

In conclusion, the evaluation of *Musa paradisiaca* fruit aqueous pulp extract provided evidence to the traditional claim that the plant contains bioactive compounds that show significant antidiabetic potential. This embedded bioactive compound possesses insulin-releasing properties as indicated by the reduction of glucose levels, in addition to its ability to mitigate oxidative stress induced by reactive oxygen species (ROS) via STZ introduction to a biological system (Wistar rat).

Declaration of Conflict of Interest

The authors of this research declare no known financial or any other conflict of interest.

Authors and Contribution

O.K.A. developed the concept, designed experiments, reviewed, and edited the manuscript.

A.A.A. carried out the investigation and wrote the first draft.

References

Adeniran, A., Anjorin, O. & Chieme, C. (2022). Prevalence and Risk Factor of Diabetes Mellitus among Civil Servants in Abeokuta Town, Ogun State, Nigeria. *Tropical Journal of Medical Research,* 21**,** 29-37.

Adetuyi, B. O., Odine, G. O., Olajide, P. A., Adetuyi, O. A., Atanda, O. O. & Oloke, J. K. (2022). Nutraceuticals: role in metabolic disease, prevention and treatment. *World News of Natural Sciences,* 42**,** 1-27.

Adibah, K. Z. M., & Azzreena, M. A. (2019). Plant toxins: alkaloids and their toxicities. *GSC Biological and Pharmaceutical Sciences*, *6*(2), 21-29.

Awote, O. K., Amisu, K. O., Anagun, O.S., Dohou, F. P., Olokunola, E. R., & Elum, N. O. (2024). *In vitro* and Molecular Docking Evaluation of the Antibacterial, Antioxidant, and Antidiabetic Effects of Silver Nanoparticles from *Cymbopogon citratus* Leaf. *Tropical Journal of Natural Product Research (TJNPR)*, *8*(9): 8400–8411.

Awote, O. K., Adeyemo, A. G., Igbalaye, J. O., Awosemo, R. B., Ibrahim, A. B., Omolaja, B. E., Abdulrafiu, F., & Fajobi, T. (2021a). *In vitro* alpha-amylase inhibitory activity, antioxidant activity and HPLC analysis of Eichhornia crassipes (water hyacinth) methanol extracts.

Awote, O. K., Igbalaye, J. O., & Adeyemo, A. G. (2021b). Effect of *Phragmanthera incana* Leaves Extracts on Lipid Profile in Wistar Rats Fed High-Fat Diet. *International Journal of Formal Sciences: Current and Future Research Trends*, *12*(1), 23-32.

Awuchi, C. G. (2019). Medicinal plants: the medical, food, and nutritional biochemistry and uses. *International Journal of Advanced Academic Research*, *5*(11), 220-241.

Ayeni, E. A., Gong, Y., Yuan, H., Hu, Y., Bai, X. & Liao, X. (2022). Medicinal plants for anti-neurodegenerative diseases in West Africa. *Journal of Ethnopharmacology,* 285**,** 114468.

Azzi, A. (2022). Oxidative stress: what is it? Can it be measured? Where is it located? Can it be good or bad? Can it be prevented? Can it be cured? *Antioxidants,* 11**,** 1431.

Banu, S., & Bhowmick, A. (2017). Therapeutic targets of type 2 diabetes: An overview. *MOJ Drug Des. Dev. Ther*, *1*(11).

Chmiel, T., Mieszkowska, A., Kempińska-Kupczyk, D., Kot-Wasik, A., Namieśnik, J., & Mazerska, Z. (2019). The impact of lipophilicity on environmental processes, drug delivery and bioavailability of food components. *Microchemical Journal*, *146*, 393-406.

Daliri, E. B. M., Oh, D. H., & Lee, B. H. (2017). Bioactive peptides. *Foods*, *6*(5), 32.

Dulsat, J., López-Nieto, B., Estrada-Tejedor, R., & Borrell, J. I. (2023). Evaluation of free online ADMET tools for academic or small biotech environments. *Molecules*, *28*(2), 776.

Fagbohun, O. F., Oriyomi, O. V., Adekola, M. B., & Msagati, T. A. Biochemical applications of *Kigelia africana* (Lam.) Benth. fruit extracts in diabetes mellitus. *Comparative Clinical Pathology*, 2020, 29, 1251-64.

Fasula, J., Adejumo, B., Akhaumere, E., Oke, M., Odionyenma, U., Dimkpa, U. & Abdulkadir, U. 2024. Prevalence and Risk Factors Associated with Diabetes mellitus among children of parents living with Diabetes in Ondo State, Nigeria. *Open Journal of Medical Research (ISSN: 2734-2093),* 5**,** 1-15.

Fujii, J., Homma, T., & Osaki, T. (2022). Superoxide radicals in the execution of cell death. *Antioxidants*, *11*(3), 501.

Furman, B. L. (2015). Streptozotocin-induced diabetic models in mice and rats. *Current protocols in pharmacology*, *70*(1), 5-47.

Ghasemi, A., & Jeddi, S. (2023). Streptozotocin as a tool for induction of rat models of diabetes: A practical guide. *EXCLI journal*, *22*, 274.

Google Search Engine (2025).

Green, L. C., Wagner, D. A., Glogowski, J., Skipper, P. L., Wishnok, J. S., & Tannenbaum, S. R. (1982). Analysis of nitrate, nitrite, and [15N] nitrate in biological fluids. *Analytical biochemistry*, *126*(1), 131-138.

Idm'hand, E., Msanda, F., & Cherifi, K. (2020). Ethnopharmacological review of medicinal plants used to manage diabetes in Morocco. *Clinical Phytoscience*, *6*, 1-32.

Ivanović, V., Rančić, M., Arsić, B., & Pavlović, A. (2020). Lipinski's rule of five, famous extensions and famous exceptions. *Popular Scientific Article*, *3*(1), 171-177.

Jollow, D. J., Mitchell, J. R., Zampaglione, N. A., & Gillette, J. R. (1974). Bromobenzene-induced liver necrosis. Protective role of glutathione and evidence for 3, 4-bromobenzene oxide as the hepatotoxic metabolite. Pharmacology, 11(3): 151-169.

Kemisetti, D., & Rajeswar Das, D. B. B. (2022). A comprehensive review on *Musa paradisiaca* taxonomical, morphological classification and its pharmacological activities. *Journal of Pharmaceutical Negative Results*, 737-749.

Kumar, S., & Pandey, A. (2015). Free radicals: health implications and their mitigation by herbals. *British Journal of Medicine and Medical Research*, *7*(6), 438-457.

Lipinski, CA. (2004). Lead-and drug-like compounds: the rule-of-five revolution. *Drug Discovery Today: Technologies,* 1(4): 337-41.

Lowry, O.H., Rosebrough, N.J., Farr, A.L., Randall, R.J., 1951. Protein measurement with the Folin phenol reagent. Journal of Biological Chemistry, 193: 265–275.

Małkiewicz, M. A., Szarmach, A., Sabisz, A., Cubała, W. J., Szurowska, E., & Winklewski, P. J. (2019). Blood-brain barrier permeability and physical exercise. *Journal of neuroinflammation*, *16*, 1-16.

Manirafasha, C. (2014). *The effects of kolaviron on epididymal and testicular function in streptozotocin induced diabetic wistar rats* (Doctoral dissertation, Cape Peninsula University of Technology).

Marino, A., Battaglini, M., Moles, N., & Ciofani, G. (2022). Natural antioxidant compounds as potential pharmaceutical tools against neurodegenerative diseases. *ACS omega*, *7*(30), 25974-25990.

McGill, M. R. (2016). The past and present of serum aminotransferases and the future of liver injury biomarkers. *EXCLI journal*, *15*, 817.

Mohamed, J., Nafizah, A. N., Zariyantey, A. H., & Budin, S. (2016). Mechanisms of diabetes-induced liver damage: the role of oxidative stress and inflammation. *Sultan qaboos university medical journal*, *16*(2), e132.

Ntie-Kang, F., Nyongbela, K. D., Ayimele, G. A., & Shekfeh, S. (2019). "Drug-likeness" properties of natural compounds. *Physical Sciences Reviews*, *4*(11), 20180169.

Ogunyinka, B.I., Oyinloye, B.E., Osunsanmi, F.O., Opoku, A.R., & Kappo, A.P. (2017). Protective effects of *Parkia biglobosa* protein isolate on streptozotocin-induced hepatic damage and oxidative stress in diabetic male rats. Molecules, 22(10): 1654.

Oladimeji, S.O., Soares, A.S., Igbalaye, J.O., Awote, O.K., Adigun, A.K., & Awoyemi, Z.O. (2022). Ethanolic Root Extract of *Urtica dioica* Exhibits Pro-fertility and Antioxidant Activities in Female Albino Rats. *International Journal of Biochemistry Research & Review*. 31(8):29-38.

Oladimeji, S.O., Igbalaye, J.O., Awote, O.K., Shodimu, B.O., Oladeinde, D.T., Omorowa, V.T., Oluwole, S.M., Akinyemi, Y.A., Shobowale, A.Y., Jimoh, D., & Balogun, S.T. (2023). *Cissampelos pareira* ethanolic extract modulates hormonal indices, lipid profile, and oxidative parameters in transient infertility-induced female albino rats. *Bio-Research*, *21*(2), pp.1961-1972.

Onah, L. U., & Oguche, S. O. (2022). Histopathological Analysis of the Kidney of Alloxan Induced Diabetic Albino (Wistar Strain) Rat Treated with Musa paradisiaca (Plantain) Stem Juice. *Int. J. Sci. Res. in Chemical Sciences, 9*(2): 8-13.

Ortiz, G. G., Huerta, M., González-Usigli, H. A., Torres-Sánchez, E. D., Delgado-Lara, D. L., Pacheco-Moisés, F. P., Mireles-Ramírez, M. A., Torres-Mendoza, B. M., Moreno-Cih, R. I., & Velázquez-Brizuela, I. E. (2022). Cognitive disorder and dementia in type 2 diabetes mellitus. *World Journal of Diabetes*, *13*(4), 319.

Padhi, S., Nayak, A. K., & Behera, A. (2020). Type II diabetes mellitus: a review on recent drug- based therapeutics. *Biomedicine & Pharmacotherapy*, *131*, 110708.

Riyaphan, J., Pham, D. C., Leong, M. K., & Weng, C. F. (2021). In silico approaches to identify polyphenol compounds as α-glucosidase and α-amylase inhibitors against type-II diabetes. *Biomolecules*, *11*(12), 1877.

Saeedi, P., Petersohn, I., Salpea, P., Malanda, B., Karuranga, S., Unwin, N., Colagiuri, S., Guariguata, L., Motala, A. A., Ogurtsova, K. & Shaw, J. E. (2019). Global and regional diabetes prevalence estimates for 2019 and projections for 2030 and 2045: Results from the International Diabetes Federation Diabetes Atlas. *Diabetes research and clinical practice*, *157,* 107843.

Salazar-García, M., & Corona, J. C. (2021). The use of natural compounds as a strategy to counteract oxidative stress in animal models of diabetes mellitus. *International Journal of Molecular Sciences*, *22*(13), 7009.

Shree, R. L., & Selvakumar, P. (2022) Phytochemical and Pharmacological Property Review of

Musa Paradisiaca. *YMER, 21(11): 152-166.*

Singh, A., Kukreti, R., Saso, L., & Kukreti, S. (2022). Mechanistic insight into oxidative stress-triggered signaling pathways and type 2 diabetes. *Molecules*, *27*(3), 950.

Stratton, C. F., Newman, D. J., & Tan, D. S. (2015). Cheminformatic comparison of approved drugs from natural product versus synthetic origins. *Bioorganic & medicinal chemistry letters*, *25*(21), 4802-4807.

Taylor, S. I., Yazdi, Z. S., & Beitelshees, A. L. (2021). Pharmacological treatment of hyperglycemia in type 2 diabetes. *The Journal of clinical investigation*, *131*(2), e142243.

Tehrani, H. S., & Moosavi-Movahedi, A. A. (2018). Catalase and its mysteries. *Progress in biophysics and molecular biology*, *140*, 5-12.

Tungmunnithum, D., Thongboonyou, A., Pholboon, A., & Yangsabai, A. (2018). Flavonoids and other phenolic compounds from medicinal plants for pharmaceutical and medical aspects: An overview. *Medicines*, *5*(3), 93.

Varshney, R., & Kale, R. K. (1990). Effects of calmodulin antagonists on radiation-induced lipid peroxidation in microsomes. *International journal of radiation biology*, *58*(5), 733-743.

Wolff, S. P. (1994). Ferrous ion oxidation in the presence of ferric ion indicator xylenol orange for measurement of hydroperoxides. Methods in Enzymology, 233: 182–189.

World Health Organization. (2019). *Global action plan on physical Activity 2018-2030: More Active People for a healthier world*. World Health Organization.

Vo, T. T. T., Chu, P. M., Tuan, V. P., Te, J. S. L., & Lee, I. T. (2020). The promising role of antioxidant phytochemicals in the prevention and treatment of periodontal disease via the inhibition of oxidative stress pathways: Updated insights. *Antioxidants*, *9*(12), 1211.

Yedjou, C. G., Grigsby, J., Mbemi, A., Nelson, D., Mildort, B., Latinwo, L., & Tchounwou, P. B. (2023). The management of diabetes mellitus using medicinal plants and vitamins. *International Journal of Molecular Sciences*, *24*(10), 9085.

ZEUGMA BIOLOGICAL SCIENCE
2025
v:5 n:2 p:42-71

Ameliorative Potential of Polyphenolic Compounds in *Cucumis sativus* (*Linn.*) Fruit Pulp Extract on Streptozotocin-induced Diabetes in Male Wistar Rats

Olasunkanmi Kayode Awote[1*], Blessing Oluwaseun Ogunyinka[1], Adesegun Gideon Adeyemo[1], Olabisi Olufunmilayo Ogunrinola[1], Ibrahim Oyeyemi Adenekan[2], Babajide David Kayode[3]

[1] Department of Biochemistry, Lagos State University, PMB 0001, Ojo, Lagos State, Nigeria.
[2] Department of Mathematics, University of Louisiana at Lafayette, LA, United States of America.
[3] Department of Medical Biochemistry, Faculty of Basic Medical Sciences, Eko University of Medicine and Health Sciences, Badagry Expressway, Lagos State, Nigeria.

olasunkanmi.awote@lasu.edu.ng

Abstract

Diabetes mellitus continues to be a major global public health concern, underscoring the urgent need for continuous exploration of locally available medicinal plants and functional foods that are affordable, accessible, and capable of supporting effective management and improved health outcomes. This study investigated the effect of *Cucumis sativus* pulp extract (CSPE) on selected oxidative stress and diabetes-related biochemical indices. A total of 24 male Wistar rats were divided into 4 groups (n=6), including control, diabetic-untreated, and diabetic-treated groups (with CSPE or glibenclamide). Oxidative stress indices (hydrogen peroxide [H_2O_2], nitric oxide [NO], malondialdehyde [MDA], glutathione [GSH]); lipid profile (total cholesterol [TC], triglyceride [TRIG], high-density [HDL-Chol, low-density [LDL-Chol], and very-low-density [VLDL-Chol] lipoprotein cholesterol; liver antioxidant (superoxide dismutase [SOD], catalase [CAT]); and liver function (alanine [ALT], and aspartate [AST] aminotransferase) enzymes were evaluated using standard biochemical kits and procedures. PyRx and Biovia Discovery Studio were used for molecular docking studies, while SwissADME and ProTox were used to predict the ADME/T properties. Results showed that treatment with CSPE had a significant (p<0.05) increase in liver antioxidant enzymes, HDL-Chol, and GSH levels and a decrease in plasma ALT and AST, TC, TRIG, LDL-Chol, VLDL-Chol, H_2O_2, MDA, and NO compared to the diabetic-untreated group. β-sitosterol bound well with α-amylase (-8.9 kcal/mol) and aldose reductase (-8.8 kcal/mol) while hesperidin bound to α-glucosidase (-8.8 kcal/mol) and sorbitol dehydrogenase (-10.6 kcal/mol) with favorable ADME and toxicity profiles. In conclusion, CSPE can serve as a therapeutic agent in addition to its known nutritional properties in managing diabetes and its related complications.

Keywords: Diabetes mellitus, *Cucumis sativus* fruit, Phytochemistry, Polyphenols, Hypoglycemic, Hypolipidemic, Functional foods, Lipid profile, Hepatic function, Antioxidant.

Introduction

Diabetes mellitus (DM) is one of the leading causes of death and morbidity worldwide, affecting people of all ages, genders, and geographic areas (Awote *et al*., 2022; Popoviciu *et al*., 2023). DM is a dangerous and chronic condition marked by consistently high blood glucose levels caused by insufficient insulin synthesis or the body's inability to use the generated insulin (Hossain *et al*. 2024). Nearly half of all adults with diabetes are unaware that they have the

https://doi.org/10.55549/zbs.1644267

disease, and an estimated 240 million adults worldwide live with undiagnosed diabetes (Magliano and Boyko, 2022). Meanwhile, 463 million adults have been estimated to be diagnosed with diabetes, which has been projected to increase to 578 and 700 million by the year 2030 and 2045, respectively (WHO, 2019; Awote *et al*., 2023). DM has historically been linked to macrovascular problems, including peripheral artery disease, coronary heart disease, and stroke, as well as microvascular problems like diabetic kidney disease, retinopathy, and peripheral neuropathy (Kulkarni *et al*., 2024).

The mitochondrial electron transport chain produces more free radicals in the form of reactive oxygen species (ROS) when blood glucose levels are elevated in diabetic patients (Mukai *et al.*, 2022). Excessive ROS and their accumulation, as well as the breakdown of antioxidant mechanisms inside cells or tissues, lead to oxidative stress (Afzal *et al.*, 2023). It has been suggested that this redox imbalance is a contributing factor to insulin resistance, β-cell malfunction, and impaired glucose intolerance, all of which can lead to type-2 diabetes (Andres *et al*., 2023, Andres *et al.*, 2024).

Streptozotocin (STZ) is a naturally occurring alkylating antineoplastic drug that is especially harmful to the β-cell of the pancreas in mammals that produce insulin (Haghani *et al*., 2022). Based on its structural similarity to glucose, STZ is injected intraperitoneally and enters pancreatic β-cells through glucose transporter 2 (GLUT2). Depending on the dose, STZ administration causes β-cell necrosis and subsequently a complete or partial loss of insulin production (Singh *et al.*, 2024).

Conventional antidiabetic drugs such as sulfonylureas, biguanides, α-glucosidase inhibitors, agonists for peroxisome proliferator-activated receptor-γ (PPARγ), inhibitors of dipeptidyl peptidase IV (DPP IV), and inhibitors of sodium-glucose co-transporter-2 (SGLT2) are economical and the prolonged use of these medications has been associated with serious side effects including the risk of coma, edema, hypoglycemia, vomiting, bloating, possible weight gain, and issues with the central nervous and cardiovascular systems (Banu and Bhowmick, 2017, Daliri *et al.*, 2017, Padhi *et al.*, 2020). One of such antidiabetic drug is glibenclamide (glyburide). It is an oral sulfonylurea antidiabetic drug that lowers blood glucose by stimulating insulin secretion from pancreatic β-cells, primarily used in managing and/or treating type 2 diabetes mellitus. Therefore, to alleviate these side effects, new therapeutic approaches are required, and natural products have been reported as safe and natural alternatives (Yedjou *et al.*, 2023), including medicinal plants and fruits.

Cucumis sativus belongs to the *Cucurbitacae* family and is commonly called “Cucumber” (Khan *et al.*, 2022). It is referred to as ‘‘Kukumba’’ amongst the Yoruba-speaking tribe of Southwestern Nigeria. Cucumbers are fruits with high water content and low calories, fat, cholesterol, and sodium (Adamu *et al.*, 2021). Numerous phytochemicals, including tannins, cardiac glycosides, phlobotannins, alkaloids, flavonoids, glycosides, steroids, terpenoids, carbohydrates, resins, saponins, and phytosterols, have been reported for the phytochemical screening of cucumber (Sari *et al.*, 2021). Flavonoids such as quercetin, apigenin, kaempferol, luteolin, lignans, and triterpenes; vitamins including biotin, vitamin B1, vitamin K, and pantothenic acid; minerals including copper, magnesium, potassium, manganese, and phosphorus have all been reported to be present in cucumber (Molly *et al.* 2017). The reported antimicrobial, antifungal, cytotoxic, antacid, carminative, hepato-protective, hypoglycemia, blood lipid-lowering, and hypo-lipidemic effects of cucumber have been associated with its embedded phytochemical constituent (Heidari *et al.* 2012).

https://doi.org/10.55549/zbs.1644267

Although several studies have explored the biological activities of *Cucumis sativus* (Linn.), there remains a noticeable gap in understanding its specific antioxidant-boosting, glucose-lowering, and lipid-modulating effects, particularly in streptozotocin-induced diabetes. Furthermore, limited research has integrated both experimental and computational methodologies to unravel or suggest the molecular mechanisms underlying the therapeutic potential of its active ingredients. Therefore, this study aims to comprehensively evaluate *C. sativus* by combining *in vivo* experiments with *in silico* analyses, offering novel insights into its role in managing diabetes and associated metabolic imbalances.

Materials and Methods

Plant Collection and Extraction

Fresh Cucumber (*Cucumis sativus*) was procured in March 2024 from a local market, Iyana-Iba market, Ojo, Lagos State, South-western Nigeria (Latitude: 6.4611° N and 3.2043° E) and identified by a botanist, Dr. K. T. Omolokun of the Department of Botany, Faculty of Science, Lagos State University, Ojo, Lagos State, Nigeria. Seven hundred (700) g of the fruit were rinsed under running water, peeled, and blended using a Kenwood blender (model No: KW505) to obtain a uniform pulp. The pulp was filtered using a muslin cloth, followed by Whatman no. 1 filter paper. The resultant liquid was concentrated under reduced pressure using a rotary evaporator to remove excess water, yielding 600 mg of concentrated cucumber pulp extract.

Phytochemical Screening

The phytochemical components of *Cucumis sativus* were determined using the methods described by Awote *et al.* (2023). Alkaloids, flavonoids, phenols, saponins, steroids, tannins, terpenoids, and glycosides were identified, and the polyphenolics (total flavonoids, total phenolics, and total tannins) were quantified in mg/100g using a standard procedure and conditions.

Gas Chromatography-Mass Spectroscopy (GC-MS) Analysis of *Cucumis sativus* Pulp Extract

An Agilent 5977B GC/MSD system with an Agilent 8860 auto-sampler, a gas chromatograph interfaced to a mass spectrometer (GC-MS) equipped with an Elite-5MS (5% diphenyl/95% dimethyl polysiloxane) fused a capillary column (30 × 0.25µm ID × 0.25µm df) were used to perform the GC-MS analysis of the extract. An electron ionization device with an ionization energy of 70 eV was used in electron impact mode for GC-MS detection. A split ratio of 10:1 was used with an injection volume of 1µL and helium gas (99.999%) as the carrier gas at a steady flow rate of 1 mL/min. To calibrate the GC-MS, five (5) point serial dilution calibration standards (1.25, 2.5, 5.0, and 10.0 ppm) were made from the 40 ppm stock solution. Temperatures were maintained at 300 °C for the injector, 250 °C for the ion source, and 100 °C (isothermal) for 0.5 min in the oven, with a 20 °C/min increase to 280 °C (2.5 min) for the oven. Mass spectra were obtained at 70 eV with a 0.5 s scanning interval and fragments ranging from 45 to 450 Da. GC/MS ran for a total of 21.33 minutes, with a solvent delay of 0 to 3 minutes (Awote *et al.*, 2024).

High-Performance Liquid Chromatography (HPLC) Analysis of *C. sativus* Pulp Extract.

The measurement of flavonoid components in the extracts was carried out using high-performance liquid chromatography (HPLC) on an HPLC-Agilent Technologies 1200 series

https://doi.org/10.55549/zbs.1644267

liquid chromatograph equipped with a UV detector. A Hypersil BDS C18 column (150 × 4.6 mm, 5 µm particle size) prepacked for the reversed-phase was used for the chromatography, which was carried out at 250°C. A (0.1% formic acid in water) and B (HPLC grade acetonitrile) are combined to generate the mobile phase, which has a steady flow rate of 0.75 mL/min. At 0 min, 94% A, 14 min, 83.5% A, 16 min, 83% A, 18 min, 82.5% A, 20 min, 82.5%; 22–24 min,

81.5%; and 27–40 min, 80% A, the linear gradient solvent system began. The detection wavelength was 280 nm (Awote *et al.*, 2024).

In-silico Studies Ligand Modeling

The GC-MS and HPLC-generated ligands' 3D crystal structures were downloaded in sdf format from the PubChem database (https://pubchem.ncbi.nlm.nih.gov/). Also, the ligands' canonical SMILES were downloaded from the PubChem database. Biovia Discovery Studios 2021 was used to convert the ligands to .pdb format, and Open Babel (https://openbabel.readthedocs.io/en/latest/Forcefields/mmff94.html) was utilized in optimizing the energy of the ligand molecules. Following energy minimization, the ligand molecules were converted specifically into pdbqt AutoDock ligand format (Awote *et al.*, 2024).

Protein (Target) Preparation

The selected protein targets were sourced from the Protein Data Bank (https://www.rcsb.org) and a deposited crystal structure of *Homo sapiens* was used as a reference to model the 3D structures of these proteins. The protein grid box coordinates were set at x= 8.689, y= -27.9742, and z= 15.7172; x= -12.1777, y= -35.4768, and z= 88.7572; x= 80.183, y= 62.3450, and z=

3.4609; and x= -0.3408, y= -0.6404, and z= 15. 0471 for human pancreatic α-amylase (PDB ID: 2QMK), human pancreatic α-glucosidase (PDB ID: 5NN8), human pancreatic sorbitol dehydrogenase (PDB ID: 1PL6), and aldose reductase (PDB ID: 3S3G), respectively, to target the active sites of each protein. Biovia Discovery Studio 2021 was used to eliminate heteroatoms, ligand groups, and water molecules from the protein structures and add hydrogen polar to protein structures to prepare them for molecular docking analysis (Awote *et al.*, 2024).

Molecular Docking

The AutoDock Vina tool was utilized for molecular docking studies. The usual diabetes standard drugs, acarbose and tolrestat, and the co-crystallized ligands for the target proteins were utilized. Following the sorting of the ligand molecules according to increasing binding energies, the investigation was based on binding free energy values (Awote *et al.*, 2024).

Absorption, Distribution, Metabolism, Excretion & Toxicity (ADMET) Properties Prediction

Based on binding energy, the top ten ligands were selected, and their drug-likeness parameters, physicochemical properties, pharmacokinetic properties, lipophilicity, water solubility, medicinal chemistry, and toxicity were predicted using SwissADME and admetSAR. These predictive algorithms were used to evaluate the ligands' general eligibility as possible drug candidates and to offer information about their possible safety, pharmacological characteristics, and therapeutic efficacy (Awote *et al.*, 2024).

https://doi.org/10.55549/zbs.1644267

Experimental Animals

Twenty-four (24) male Wistar rats (8 weeks old), with an average weight of 103 g (range of 100–105 g), were sourced from the animal house of the Department of Biochemistry, Faculty of Science, Lagos State University, Nigeria. The rats were kept in regular day/night cycles while they were made to have access to clean drinking water and commercial pelleted feed (Vital feed® Nigeria). Current national and international criteria were followed in the care and usage of the Wistar rats during the study. With the ethical approval number LASU/23/REC/055, the Lagos State University Research Ethics Committee authorized the study procedure.

Induction of Type-2 Diabetes mellitus

Type-2 Diabetes Mellitus (T2DM) was introduced into the overnight fasted rats intraperitoneally at a dose of 60 mg/kg body weight of Streptozotocin (STZ) (Sigma-Aldrich Chemicals Company, St. Louis, MO., U.S.A.) dissolved in freshly prepared 0.1 M of iced-cold citrate buffer (pH 4.5) (Ogunyinka *et al.*, 2017). To prevent hypoglycemia, the rats were maintained with 20% glucose (Unique Pharmaceuticals, Sango Otta, Ogun State, Nigeria) for six hours following the induction and later with 5% glucose for the following 24 hours (Prince and Menon, 2003). On the third day (72 hours) after induction, hyperglycemia was found to be gradually developing, but by the seventh day, all of the rats had stabilized and were consistently hyperglycemic. The rats exhibiting a fasting blood glucose level of 200 mg/dL or higher by the seventh day were classified as diabetic and included in the investigation. The fourth day after STZ induction marked the start of the treatments, which lasted for 28 days. The blood glucose concentrations were measured after drawing blood from the rats' tails using an Accu-Check glucometer. The success rate of induction exceeded 76.9%.

Animal Groupings and Treatments

Animal groupings and treatment were carried out using the modified method of Ogunyinka *et al.* (2017). Before this study, the rats were fasted overnight and divided into four (4) groups (A–D) of six rats each, randomly selected so that the group mean weights were the same.

Group A (normal control) consisted of non-diabetic rats that received 2 mL/kg body weight/day of distilled water orally for 28 days.

Group B (positive control) = streptozotocin (STZ)-induced diabetic rats orally administered 2 mL/kg body weight/ day distilled water for 28 days.

Group C = diabetic rats orally administered 600 mg/kg body weight/ day of *C. sativus* pulp extract for 28 days.

Group D = diabetic rats orally administered 5 mg/kg body weight/ day of glibenclamide (®Daonil, Hoechst Marion Roussel Limited, Mumbai, India) for 28 days.

Blood Collection

After receiving medication for 28 days, each rat was given an injection of 0.2 mL of ketamine to induce anesthesia and then dissected. The gradual lack of corneal and pedal responses confirmed anesthesia. Afterward, a sterile 21 G needle placed on a 5 mL plunger syringe (®Clinject Hypodermic Syringe, Albert David Limited, Mandideep-462046, Raisen District, India) was used to collect fresh blood from the heart chamber and stored in plain sample bottles. The blood was centrifuged immediately for 15 minutes at 2500 rpm. The supernatant (serum)

https://doi.org/10.55549/zbs.1644267

was then removed and stored in the refrigerator until required for biochemical analysis.

Biochemical Assays

The effects of *Cucumis sativus* pulp extracts on STZ-induced diabetic Wistar rats were evaluated using the following biochemical parameters:

Protein Determination

The protein concentration of the various samples was determined using the Lowry method as described by Lowry *et al.* (1951) with a few modifications. In summary, 400 µL of solution C (200 µL solution B (1% copper sulfate ($CuSO_4.5H_2O$) and 2% sodium potassium tartrate) and

9.8 mL of solution A (0.1 M sodium hydroxide and 2% sodium bicarbonate), 40 µL of folin C, and 25 µL of each sample were mixed with 0.5 mg/mL bovine serum albumin (BSA). After thoroughly mixing, the mixture was left to stand. At 650 nm, the absorbance was measured against a blank that contained 60 µl of solution C, water, or buffer. From the Lowry standard curve, the protein concentrations of each group were extrapolated and expressed in mg/mL.

Catalase (CAT) Activity

Catalase activity was determined according to the method of Oladimeji *et al.* (2022). In summary, 10 µL of the homogenate and 590 µL of hydrogen peroxide (590 µL of 19 mM solution) were pipetted into a 1 cm quartz cuvette. The mixture was quickly swirled to mix it thoroughly, and it was then put in a spectrophotometer. The change in absorbance was measured at 240 nm for 10 seconds for 2 minutes. The extinction coefficient of hydrogen peroxide, which is 240 nm, was used to express catalase activity as µmol/mg protein.

Superoxide Dismutase (SOD) Activity

SOD activity was determined by the Epinephrine method reported by Oladimeji *et al.* (2023). In brief, 2.5 mL of 0.05 M phosphate buffer (pH 7.8) was mixed with 0.1 mL of the tissue homogenate supernatant. At the point of absorbance measurement, which was measured at 750 nm for one minute and thirty seconds at intervals of 15 seconds, 0.3 mL of adrenaline solution (0.059%) was then added. After calculation, SOD activity was then expressed as mmol/mg protein.

Lipid Profile Estimation

Using standard diagnostic test kits (Randox Laboratories, Crumlin, U.K.), the lipid profile (triglyceride (TG), total cholesterol (TC), and high-density lipoprotein cholesterol (HDL-c)) of the treated Wistar rats was analyzed in the serum sample. The Friedewald formula was used to determine serum low-density lipoprotein cholesterol (LDL-c) and very-low-density lipoprotein cholesterol (VLDL-c): LDL-c = [TC- (HDL-c + TG/5)], and VLDL-c = TAG/5, respectively (Awote *et al.*, 2021).

Non-Protein Thiol (GSH) Estimation

The level of reduced glutathione (GSH) was estimated according to Jollow *et al.* (1974). Using Ellman's reagent (DTNB), the glutathione (GSH) content was determined calorimetrically. Sulfa-salicylic (4%) was added to the supernatant in a 1:1 ratio to precipitate it. After being stored at 4°C for one hour, the samples were centrifuged for ten minutes at 4°C at 5000 rpm.

https://doi.org/10.55549/zbs.1644267

Phosphate buffer (0.1 M, 550 µL), 100 µL of supernatant, and 100 µL of DTNB were mixed to make up the assay combination. The absorbance was read at 412 nm, and the results were expressed as µmol of GSH/mg protein.

Nitric Oxide (NO) Estimation

After the Griess reaction, the concentrations of nitrite in serum or supernatants were determined by incubating 250 µL of the homogenate with 250 µL of Griess reagent at room temperature for 20 minutes. The spectrophotometric method was used to measure the absorbance at 550 nm. The absorbance of a standard solution containing known amounts of sodium nitrite was compared to determine the nitrite content; the findings were expressed as mmol/L (Green *et al.*, 1983).

Hydrogen Peroxide (H_2O_2) Estimation

In summary, FOX was formed by adding 10 mL of Xylenol, 10 mL of sorbitol, and 50 mL of ammonium ferrous sulfate to 30 mL of distilled water. In the meantime, 10 µL of homogenate and 290 µL of FOX were well mixed by vortexing until foamy. After 30 minutes of room temperature incubation, a faint pink color complex is produced. At a wavelength of 560 nm, the absorbance was measured against a blank (distilled water). The hydrogen peroxide generated was calculated and expressed in mmol/mL (Wolff, 1994).

Lipid Peroxidation Estimation

Lipid peroxidation was determined by measuring the formation of thiobarbituric acid reactive substance (TBARS) according to the method of Varshney and Kale, (1990). Briefly, tissue samples were homogenized in 0.1 M phosphate buffer (pH 7.4) in a ratio of 1:5. 200 µL of the stock reagent—an equal volume of trichloroacetic acid (10%, w/v) and 2-thiobarbituric acid (0.75%, w/v) in 0.1 M HCl was added to 100 µL of homogenate, and the mixture was incubated at 95ºC for an hour using a water bath. After cooling, the solution was centrifuged at 3000 rpm for 10 minutes, and the absorbance of the supernatant was measured at 532 nm and 600 nm. Lipid peroxidation was expressed as nmol.

Determination of Enzymatic Activities

Using commercial diagnostic kits (Randox, U.K.), the activities of alanine transaminase (ALT, EC 2.6.1.2) and aspartate transaminase (AST, EC 2.6.1.1) were measured following the manufacturer's instructions (Fagbohun *et al.*, 2020). At 340 nm, each enzyme's activity was determined using a spectrophotometer.

Statistical Analysis

The results are presented as Mean ± Standard Error of Mean (SEM). For the descriptive statistics, One-way ANOVA was used to compare the treated and control groups using GraphPad Prism 5.0 (GraphPad Prism Software Inc., San Diego, CA, USA). When comparing the treated and control groups, statistically significant differences were identified at $p<0.05$ with a 95% confidence interval. When significant, means were separated using the Bonferroni post-hoc test.

https://doi.org/10.55549/zbs.1644267

Results

Table 1 shows the preliminary phytochemical screening of *Cucumis sativus* pulp extract (CSPE). The qualitative analysis shows the presence of alkaloids, flavonoids, phenols, saponins, tannins, steroids, terpenoids, and glycosides. Furthermore, the polyphenolic quantitative analysis showed that CSPE contained abundant flavonoids, followed by phenolic acids and tannins. Table 2 –3 shows the comprehensive phytochemical screening of CSPE.

Eleven (11) polyphenolic compounds and forty-one (41) secondary metabolites were observed from the HPLC and GC-MS analyses of CSPE, respectively. The GC-MS analysis showed a 99.94 area percentage.

Table 1. Preliminary Phytochemical Profile of *Cucumis sativus* Pulp Extract

SN	Phytochemicals	Qualitative	Polyphenolic content
1	Alkaloids	+	NQ
2	Flavonoids	+	41.8 ± 0.88 (mg QE/ 100g)
3	Phenolics	+	59.4 ± 0.87 (mg GAE/ 100g)
4	Saponins	+	NQ
5	Steroids	+	NQ
6	Tannins	+	45. 5 ± 0.11 (mg GAE/ 100g)
7	Terpenoids	+	NQ
8.	Glycosides	+	NQ

KEY: - = Absent, + = Present, NQ= not quantified, QE= milligrams of quercetin equivalents per 100g extract, GAE= milligrams of gallic acid equivalents per 100g extract

Table 2. HPLC profile of the bioactive compounds present in *Cucumis sativus* pulp extract

SN	Compounds	MW (g/mol)	MF	Conc. (ppm)	Class of Compound
1	Caffeic acid	180.16	$C_9H_8O_4$	0.30	Phenolic acid
2	Chlorogenic acid	354.31	$C_{16}H_{18}O_9$	0.69	Phenolic acid
3	Epigallocatechin	306.21	$C_{15}H_{14}O_7$	0.2	Flavonoid
4	Gallic acid	170.12	$C_7H_6O_5$	0.48	Phenolic acid
5	Hesperidin	610.56	$C_{28}H_{34}O_{15}$	0.34	Flavonoid glycoside
6	Kaempferol	286.24	$C_{15}H_{10}O_6$	1.76	Flavonoid
7	Protocatechuic acid	154.12	$C_7H_6O_4$	0.87	Phenolic acid

https://doi.org/10.55549/zbs.1644267

8	Rutin	610.52	$C_{27}H_{30}O_{16}$	0.65	Flavonoid glycoside
9	Tannic acid	1701.2	$C_{76}H_{52}O_{46}$	2.58	Tannins
10	Vannilic acid	168.15	$C_8H_8O_4$	1.67	Phenolic acid
11	Vitexin	432.4	$C_{21}H_{20}O_{10}$	0.56	Flavonoid glycoside

Table 3. GC-MS profile of bioactive compounds present in *Cucumis sativus* pulp extract

SN	Compounds	MW	MF	RT	Area (%)	Class of compounds
1.	3'-Benzyloxy-5,6,7,4'-tetramethoxyflavone	448.46	$C_{26}H_{24}O_7$	9.83	0.64	Flavonoids
2.	3-Feruloylquinic Acid	368.34	$C_{17}H_{20}O_9$	6.89	3.10	Phenolic acid
3.	3-Methyl-L-histidine	169.18	$C_7H_{11}N_3O_2$	5.4	4.61	Alkaloid
4.	3-p-Coumaroylquinic Acid	338.31	$C_{16}H_{18}O_8$	7.12	4.20	Phenolic acid
5.	5,7-dimethoxyflavone	282.29	$C_{17}H_{14}O_4$	10.25	1.31	Flavonoid
6.	5-Aminolevulinic acid	131.13	$C_5H_9NO_3$	5.12	2.13	Amino acid derivative
7.	5-hydroxyisovanillic acid	184.15	$C_8H_8O_5$	11.59	1.15	Phenolic acid
8.	6-Octadecenoic acid (Z)	282.5	$C_{18}H_{34}O_2$	12.08	0.46	Fatty acid
9.	9,12-Octadecadienoic acid (Z,Z)-, methyl ester	294.5	$C_{18}H_{32}O_2$	54.89	6.91	Fatty acid ester
10.	9-Octadecenoic acid, methyl ester	296.5	$C_{19}H_{36}O_2$	55.03	4.16	Fatty acid ester
11.	10-Octadecenoic acid, methyl ester	296.5	$C_{19}H_{36}O_2$	55.15	8.41	Fatty acid ester
12.	Arachidic acid	312.5	$C_{20}H_{40}O_2$	11.85	1.42	Fatty acid
13.	β-sitosterol	414.71	$C_{29}H_{50}O$	17.6	0.59	Sterol
14.	Catechin	290.27	$C_{15}H_{14}O_6$	8.45	2.10	Flavonoid
15.	Coumaric acid	146.14	$C_9H_6O_2$	4.78	1.80	Phenolic compound
16.	Dodecanoic	200.32	$C_{12}H_{24}O_2$	8.72	9.95	Fatty acid
17.	Fluconazole	306.27	$C_{13}H_{12}F_2N_6O$	56.03	5.15	Synthetic compound
18.	Galactinol	342.3	$C_{12}H_{22}O_{11}$	3.91	0.90	Carbohydrate
19.	Genkwanin	284.26	$C_{16}H_{12}O_5$	16.04	5.93	Flavonoid
20.	Gitoxigenin	390.5	$C_{23}H_{34}O_5$	13.5	1.17	Cardiac glycoside
21.	Hexadecanoic acid, methyl ester	270.5	$C_{17}H_{34}O_2$	49.48	3.23	Fatty acid ester
22.	Hexa-Hydro-farnesol	228.41	$C_{15}H_{32}O$	20.24	0.56	Terpenoid
23.	Hexamethylinositol	264.31	$C_{12}H_{24}O_6$	8.3	0.90	Inositol derivative
24.	Hydroquinine	326.4	$C_{20}H_{26}N_2O_2$	13.57	0.70	Alkaloid
25.	Inosine-1-methyl	282.25	$C_{11}H_{14}N_4O_5$	18.17	0.68	Nucleoside derivative
26.	Isolongifolol	222.37	$C_{15}H_{26}O$	15.78	1.75	Terpenoid

https://doi.org/10.55549/zbs.1644267

SN	Compounds	MW	MF	RT	Area (%)	Class of compounds
27.	Isomyristic	228.37	$C_{14}H_{28}O_2$	11.44	1.12	Fatty acid
28.	Kaempferitrin	578.52	$C_{27}H_3O_{14}$	5.23	2.10	Flavonoid glycoside
29.	L-Arginine	174.2	$C_6H_{14}N_4O_2$	5.58	1.71	Amino acid
30.	Linoleic acid	280.4	$C_{18}H_{32}O_2$	15.8	0.45	Fatty acid
31.	Linoleic acid ethyl ester	308.5	$C_{20}H_{36}O_2$	56.76	1.97	Fatty acid ester
32.	L-Lysine	146.19	$C_6H_{14}N_2O_2$	6.22	1.59	Amino acid
33.	Mangiferin	422.3	$C_{19}H_{18}O_{11}$	10.045	0.51	Phenolic compound
34.	Melibiose	342.3	$C_{12}H_{22}O_{11}$	6.39	2.09	Disaccharide
35.	Methyl-6,7-dimethoxycoumarin -4-acetate	278.26	$C_{14}H_{14}O_6$	10.799	0.52	Coumarin derivative
36.	Octadecanoic acid methyl ester	298.5	$C_{19}H_{38}O_2$	39.13	5.97	Fatty acid ester
37.	Phytol	296.5	$C_{20}H_{40}O$	14.05	0.91	Diterpenoid
38.	Prunin Naringenin-7-O-Glucoside	434.39	$C_{21}H_{22}O_{10}$	6.45	3.50	Flavonoid glycoside
39.	Quercetin-3,5,7,3',4'-pentamethyl ether	372.4	$C_{20}H_{20}O_7$	21.3	0.47	Flavonoid
40.	Stevioside	804.9	$C_{38}H_{60}O_{18}$	7.1	0.87	Glycoside
41.	Vincadifformine	338.4	$C_{21}H_{26}N_2O_2$	9.7	4.05	Alkaloid

MW = Molecular weight (in g/mol), MF = Molecular formula, and RT = Retention time

Figure 1A shows the complex interaction between β-Sitosterol, the ligand with the best binding affinity with human α-amylase protein. The 2D structure illustrates the formation of a pi-sigma bond between the ligand and Tyr62 (amino acid) at the surface of the protein. Additionally, Leu162, His201, Tyr151, and Ile235 formed both alkyl and pi-alkyl bonds with β-Sitosterol. Meanwhile, Glu240, Thr163, His299, Asp197, Arg195, His305, Asp300, Trp58, Trp59, Leu165, Ala198, Glu233 and Lys200 formed van der Waals interaction with β-Sitosterol.

Figure 1B shows the 3D and 2D structures of hesperidin (ligand) – human α-glucosidase (protein) complex interaction. Arg591, Thr593, Arg837, His432, Trp859, and Asp860 formed conventional hydrogen bonds; Glu863 formed an unfavorable acceptor-acceptor interaction; Asp513, Arg591, and Arg437 formed pi-cation and pi-anion interactions while His507 and Arg591 both formed pi-alkyl and alkyl bonds. Additionally, Pro511, Arg436, Leu899, Glu895, Asp861, Gly862, Tyr366, and Thr834 formed van der Waals interactions with hesperidin. Hesperidin (ligand) also formed a complex with sorbitol dehydrogenase (protein). Here in, Cys249, Arg208, Arg298, and Thr121 formed conventional hydrogen bonds while, Gly179, Asp203, Gly181, Ile56, Phe297, Phe59, Pro122, Tyr50, Phe118, Leu274, Ser46, Val296, Val272, His49, Val159, Ile183, Gly45 and Thr250 formed van der Waals interaction with hesperidin (Figure 1C).

Figure 1D shows the complex interaction between β-Sitosterol (ligand) and human aldose reductase (protein). The 2D structure illustrates the formation of pi-alkyl and alkyl interactions between the best-fitting ligand and Cys298, Tyr48, His110, Trp219, Phe122, and Trp20 (amino acids) at the surface of the protein. Meanwhile, Tyr209 and Trp20 formed pi-sigma interaction. Additionally, Ser302, Leu301, Leu300, Trp79, Asn160, Ser159, Trp111, Lys77, Gln183,

https://doi.org/10.55549/zbs.1644267

Asp43, Ile260 and Ser210 formed van der Waals interaction with β-Sitosterol.

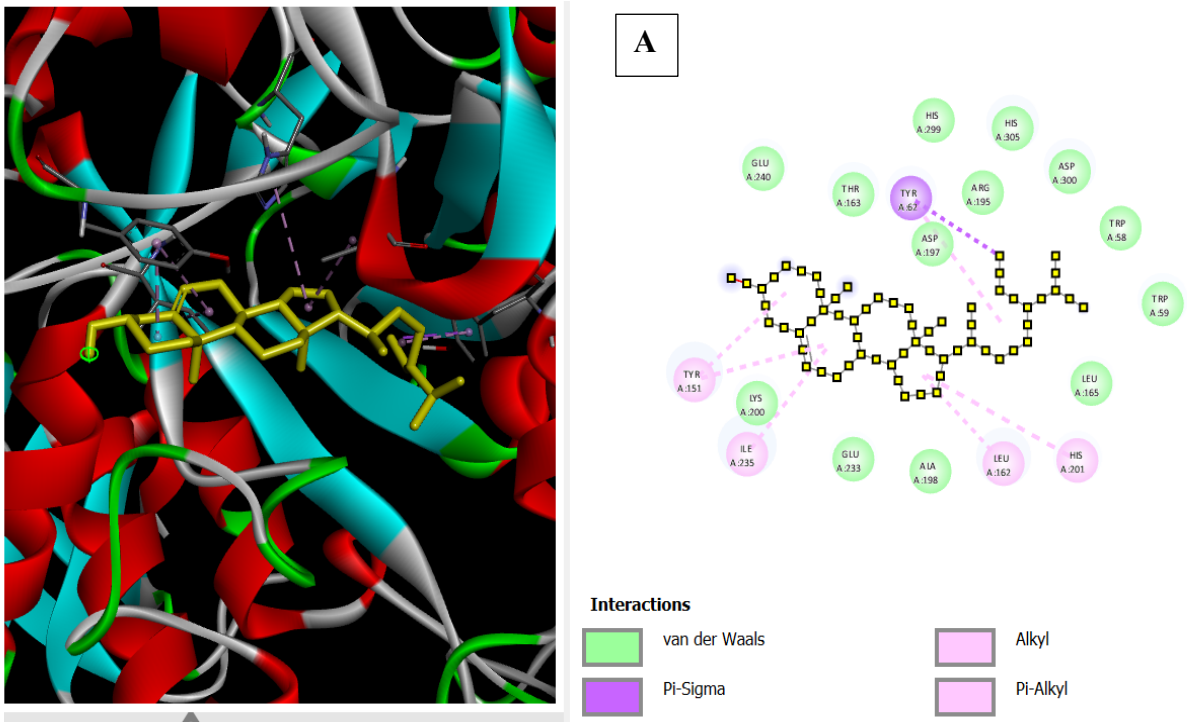

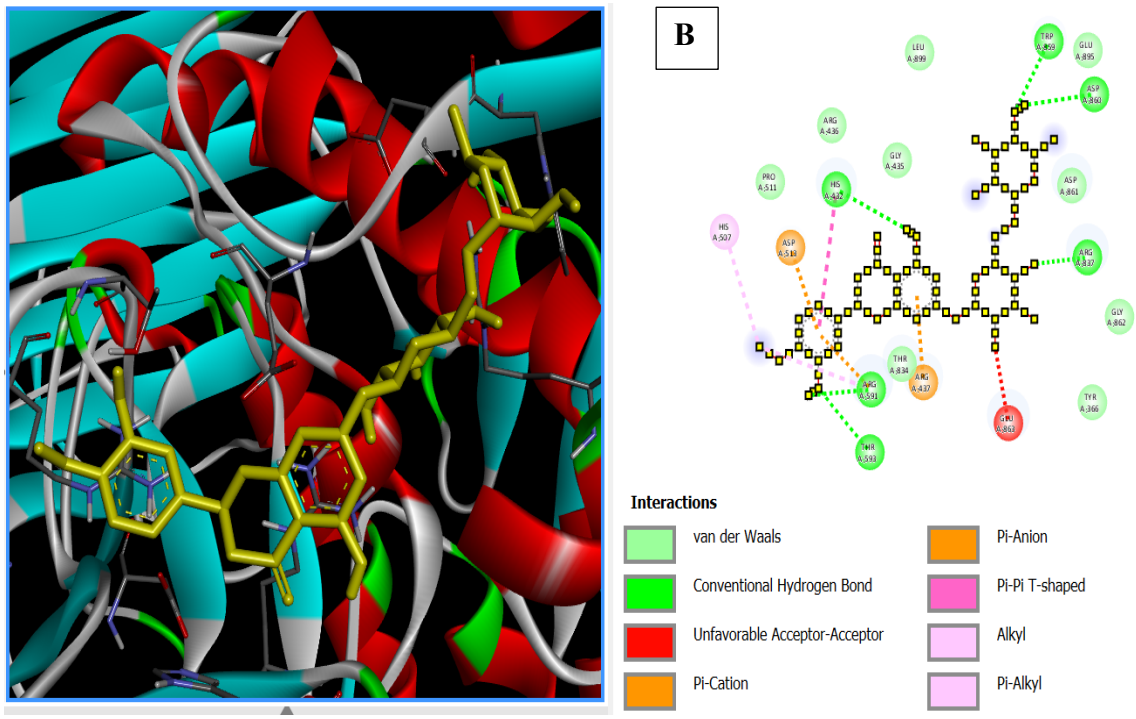

https://doi.org/10.55549/zbs.1644267

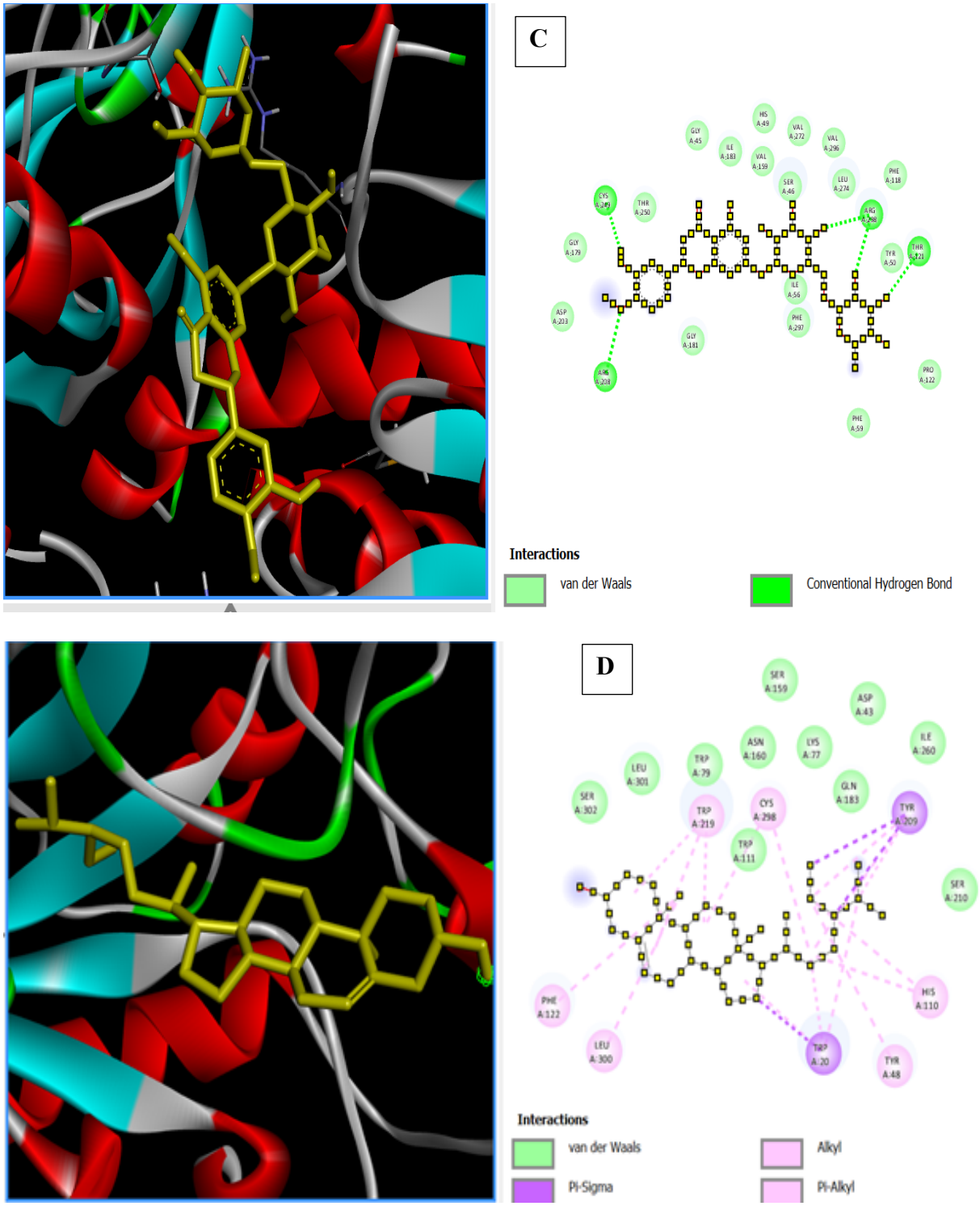

Figure 1. Interaction of (a) β-sitosterol (b) hesperidin (c) hesperidin (d) β-Sitosterol with the active site amino acids of human pancreatic α-Amylase (PDB ID: 2QMK), α-glucosidase (PDB ID: 5NN8), human sorbitol dehydrogenase (PDB ID: 1PL6), and human aldose reductase (PDB ID: 3S3G) shown in 3D (left) and 2D (right) structures.

Table 4 shows the top ten (10) ligands based on their binding affinities. Better ligands and binding affinities result from reduced binding energies. All these 10 ligands showed a better binding affinity with either of the carbohydrate metabolizing enzymes compared to the standard drugs, acarbose, and tolrestat. Here, β-Sitosterol, a molecule from the extract of *Cucumis sativus*, showed a better binding energy of -10.6 kcal/mol and thus better binding affinity

https://doi.org/10.55549/zbs.1644267

compared to the standard drugs used in this study. Additionally, all the top ten ligands showed a better binding affinity with α-amylase and α-glucosidase compared to acarbose, except for 3-Feruloylquinic acid (-6.7 kcal/ mol in α-glucosidase). Furthermore, all the top ten ligands showed a better binding affinity with sorbitol dehydrogenase and aldose reductase compared to the tolrestat, except for 3-Feruloylquinic acid (-6.7 kcal/ mol) and chlorogenic acid (-5.5 kcal/ mol) in sorbitol dehydrogenase.

Table 4. Binding Energies (Kcal/ mol) of the top ten (10) ligands.

No	Ligands	PubChem ID	Diabetes Protein Targets (kcal/mol)			
			α-Amylase	**α-Glucosidase**	**Sorbitol Dehydrogenase**	**Aldose Reductase**
1	β-Sitosterol	222284	**-8.9**	-7.7	-8.4	**-10.6**
2	Genkwanin	5281617	-6.9	-7.1	-7.4	-9.9
3	Epigallocatechin	72277	-6.9	-7.3	-7.6	-9.7
4	Hesperidin	10621	-7.8	**-8.8**	**-8.8**	-9.6
5	Chlorogenic acid	1794427	-8.0	-7.0	-6.7	-9.6
6	Rutin	5280805	-7.5	-8.5	-8.3	-9.6
7	Prunin-Naringenin-7-O-glucosides	92794	-8.8	-8.3	-8.6	-9.5
8	3'-Benzyloxy-5,6,7,4'-tetramethoxyflavone	7020621	-7.6	-8.0	-8.6	-9.4
9	3-Feruloylquinic acid	10133609	-7.8	-6.7	-5.5	-9.3
10	Kaempferitrin	5486199	-7.5	-8.5	-8.6	-9.3
11	Tolrestat*	53359	-	-	-7.0	-7.7
12	Acarbose *	41774	-6.8	-7.2	-	-

KEY: * denotes the standard drugs incorporated in this study

Tables 5.1 – 5.6 show the absorption, distribution, metabolism, excretion, and toxicity (ADMET) properties of the top ten (10) ligands and the standard drugs, acarbose and tolrestat.

Table 5.1 illustrates the physicochemical properties and β-Sitosterol, genkwanin, epigallocatechin, chlorogenic acid, prunin-naringenin-7-O-glucosides, 3'-benzyloxy-5,6,7,4'-tetramethoxy flavone, and 3-feruloylquinic acid obeyed the Lipinski rule of five while hesperidin, rutin, and kaempferitrin disobeyed it. The Lipinski rule of five (RO5) states that a molecule has an increased chance of being druggable if it has no more than two violations of the following demands: molecular weight less than 500, log P less than 5, hydrogen bond donors

https://doi.org/10.55549/zbs.1644267

less than 5, hydrogen bond acceptors less than 10, and rotatable bonds less than 10.

Table 5.2 shows lipophilicity and water solubility predictions of the top ten ligands. With a value of 5.05, the ligand with the highest binding affinity, β-Sitosterol, displayed the best logarithm of the partition coefficient (Log P). All ligands except β-Sitosterol are predicted to be either moderately soluble, soluble, or very soluble.

The pharmacokinetic properties showed in Table 5.3 showed that, of the top ten ligands, only four ligands- genkwanin, epigallocatechin, 3'-benzyloxy-5,6,7,4'-tetramethoxy flavone, and acarbose have high gastrointestinal absorption. In addition, none of the ligands demonstrated positive blood-brain barrier permeability while only five of these top ten ligands were found to be a p-glycoprotein substrate. One of the best ten ligands namely 3'-benzyloxy-5,6,7,4'-tetramethoxy flavone and a standard drug tolrestat were predicted to be CYP2C19 inhibitors. Concurrently, it was discovered that genkwanin and tolrestat are inhibitors of CYP1A2 while genkwanin is the sole inhibitor of CYP2D6. Moreover, genkwanin and 3'-Benzyloxy-5,6,7,4'-tetramethoxy flavone were identified as CYP2C9 and CYP3A4 inhibitors.

Table 5.4 shows the drug-likeness properties of the top ligands with a good bio-availability score range of 0.11 – 0.55. This shows that the top ten ligands have a good drug-likeness property since a minimum of 0.10 bioavailability score is required of a compound to be considered as a drug candidate. Table 5.5 shows the medicinal chemistry properties. Here, three of the top ten ligands – epigallocatechin, chlorogenic acid, and rutin showed indications for positive pan-assay interference compounds (PAINS). Meanwhile, genkwanin and epigallocatechin showed lead-likeness indication. Furthermore, the top ten ligands and the standard drugs showed a good synthetic accessibility score range of 2.34 to 7.34.

The top ten ligands showed a negative and positive indicator for carcinogenic and reproductive toxicity, respectively. The standard drugs and five of the top ligands including, β-sitosterol, epigallocatechin, chlorogenic acid, rutin, and 3-feruloyl quinic acid showed positive indicators for hepatic and respiratory toxicity. Additionally, β-sitosterol, epigallocatechin, chlorogenic acid, prunin-naringenin-7-O-glucosides, acarbose, tolrestat and 3-feruloyl quinic acid predicted mitochondria toxicity while prunin-naringenin-7-O-glucosides predicted nephrotoxicity (Table 5.6).

https://doi.org/10.55549/zbs.1644267

Table 5.1. Physicochemical properties of the top ten ligands

S/N	Ligands	PubChem ID	MF	MW(g/mol)	NRB	NHBA	NHBD
1	β-Sitosterol	222284	$C_{29}H_{50}O$	414.71	6	1	1
2	Genkwanin	5281617	$C_{16}H_{12}O_5$	284.26	2	5	2
3	Epigallocatechin	72277	$C_{15}H_{14}O_7$	306.27	1	7	6
4	Hesperidin	10621	$C_{28}H_{34}O_{15}$	610.56	7	15	8
5	Chlorogenic acid	1794427	$C_{16}H_{18}O_9$	354.31	5	9	6
6	Rutin	5280805	$C_{27}H_{30}O_{16}$	610.52	6	16	10
7	Prunin-Naringenin-7-O-glucosides	92794	$C_{21}H_{22}O_{10}$	434.39	4	10	6
8	3'-Benzyloxy-5,6,7,4'-tetramethoxyflavone	7020621	$C_{26}H_{24}O_7$	448.46	8	7	0
9	3-Feruloylquinic acid	10133609	$C_{17}H_{20}O_9$	368.34	6	9	5
10	Kaempferitrin	5486199	$C_{27}H_3O_{14}$	578.52	5	14	8
11	Tolrestat*	53359	$C_{16}H_{14}F_3NO_3S$	357.3	6	6	1
12	Acarbose *	41774	$C_{25}H_{43}NO_{18}$	645.50	9	19	14

KEY: * denotes the standard drugs incorporated in this study. MF= Molecular formula, MW= Molecular weight, NRB= Number of rotatable bonds, NHBA= Number of hydrogen bond acceptors, and NHBD= Number of hydrogen bond donors.

Table 5.2. Lipophilicity and water solubility properties of the top ten ligands

S/N	Ligands	PubChem ID	Log Po/w (iLOGP)	Log *S* (ESOL)
1	β-Sitosterol	222284	5.05	-7.90 (poorly soluble)
2	Genkwanin	5281617	2.48	-4.14 (Moderately soluble)
3	Epigallocatechin	72277	0.98	-2.08 (Soluble)
4	Hesperidin	10621	2.60	-3.28 (Soluble)
5	Chlorogenic acid	1794427	0.96	-1.62 (Very soluble)
6	Rutin	5280805	1.58	-3.30 (Soluble)
7	Prunin-Naringenin-7-O-glucosides	92794	2.38	-2.97 (Soluble)
8	3'-Benzyloxy-5,6,7,4'-tetramethoxyflavone	7020621	4.23	-5.44 (Moderately soluble)
9	3-Feruloylquinic acid	10133609	1.47	-1.84 (Very soluble)
10	Kaempferitrin	5486199	1.89	-3.33 (Soluble)
11	Tolrestat*	53359	2.42	-4.29 (Moderately soluble)
12	Acarbose *	41774	1.43	2.13 (Highly soluble)

KEY: * denotes the standard drugs incorporated in this study

https://doi.org/10.55549/zbs.1644267

Table 5.3. Pharmacokinetic properties of the top ten ligands

Ligands	GI Absorption	BBB Permeant	P-gp Substrate	CYP1A2 Inhibitor	CYP2C19 Inhibitor	CYP2C9 Inhibitor	CYP2D6 Inhibitor	CYP3A4 Inhibitor
β-Sitosterol	Low	No	No	No	No	No	No	No
Genkwanin	High	No	No	Yes	No	yes	Yes	Yes
Epigallocatechin	High	No	No	No	No	No	No	No
Hesperidin	Low	No	Yes	No	No	No	No	No
Chlorogenic acid	Low	No	No	No	No	No	No	No
Rutin	Low	No	Yes	No	No	No	No	No
Prunin-Naringenin-7-O-glucosides	Low	No	Yes	No	No	No	No	No
3'-Benzyloxy-5,6,7,4'-tetramethoxy flavone	High	No	Yes	No	Yes	Yes	No	Yes
3-Feruloylquinic acid	Low	No	No	No	No	No	No	No
Kaempferitrin	Low	No	Yes	No	No	No	No	No
Tolrestat*	High	No	No	Yes	Yes	No	No	No
Acarbose*	Low	No	Yes	No	No	No	No	No

https://doi.org/10.55549/zbs.1644267

Table 5.4. Drug-likeness properties of the top ten ligands

SN	Ligands	Lipinski	Ghose	Veber	Egan	Mugge	BS
1.	β-Sitosterol	Yes; 1 violation	Yes; 1 violation	Yes	No; 1 violation	No; 2 violations	0.55
2.	Genkwanin	Yes; 0 violation	Yes	Yes	Yes	Yes	0.55
3.	Epigallocatechin	Yes; 1 violation	Yes	Yes	Yes	No; 1 violation	0.55
4.	Hesperidin	No; 3 violations	No; 4 violations	No; 1 violation	No; 1 violation	No; 4 violations	0.17
5.	Chlorogenic acid	Yes; 1 violation	No; 1 violation	No; 1 violation	No; 1 violation	No; 2 violations	0.11
6.	Rutin	No; 3 violations	No; 4 violations	No; 1 violation	No; 1 violation	No; 4 violations	0.17
7.	Prunin-Naringenin-7-O-glucosides	Yes; 1 violation	Yes	No; 1 violation	No; 1 violation	No; 2 violations	0.55
8.	3'-Benzyloxy-5,6,7,4'-tetramethoxy flavone	Yes; 0 violation	Yes	Yes	Yes	Yes	0.55
9.	3-Feruloylquinic acid	Yes; 0 violation	No; 1 violation	No; 1 violation	No; 1 violation	No; 1 violation	0.11
10.	Kaempferitrin	No; 3 violations	No; 4 violations	No; 1 violation	No; 1 violation	No; 3 violations	0.17
	Tolrestat*	Yes; 0 violation	Yes	Yes	Yes	Yes	0.56
	Acarbose*	No; 3 violations	No; 4 violations	No; 1 violation	No; 1 violation	No; 5 violations	0.17

KEY: * denotes the standard drugs incorporated in this study. BS= Bioavailability scores

https://doi.org/10.55549/zbs.1644267

Table 5.5. Medicinal chemistry prediction of the top ten ligands

Ligands	PAINS	Brenk	Leadlikeness	Synthetic availability
β-Sitosterol	0 alert	1 alert: isolated_alkene	No; 2 violations: MW>350, XLOGP3>3.5	6.30
Genkwanin	0 alert	0 alert	Yes	3.03
Epigallocatechin	1 alert: catechol_A	1 alert: catechol	Yes	3.53
Hesperidin	0 alert	0 alert	No; 1 violation: MW>350	6.34
Chlorogenic acid	1 alert: catechol_A	2 alerts: catechol, michael_acceptor_1	No; 1 violation: MW>350	4.16
Rutin	1 alert: catechol_A	1 alert: catechol	No; 1 violation: MW>350	6.52
Prunin-Naringenin-7-O-glucosides	0 alert	0 alert	No; 1 violation: MW>350	4.98
3'-Benzyloxy-5,6,7,4'-tetramethoxy flavone	0 alert	0 alert	No; 3 violations: MW>350, Rotors>7, XLOGP3>3.5	4.05
3-Feruloylquinic acid	0 alert	1 alert: michael_acceptor_1	No; 1 violation: MW>350	4.25
Kaempferitrin	0 alert	0 alert	No; 1 violation: MW>350	6.48
Tolrestat*	0 alert	1 alert: thiocarbonyl_group	No; 2 violations: MW>350, XLOGP3>3.5	2.34
Acarbose*	0 alert	1 alert: isolated_alkene	No; 2 violations: MW>350, Rotors>7	7.34

KEY: * denotes the standard drugs incorporated in this study.

https://doi.org/10.55549/zbs.1644267

Table 5.6. Toxicity prediction of the top ten ligands

Ligands	Carcino-genicity	Hepato-toxicity	Respiratory toxicity	Reproductive toxicity	Mitochondria toxicity	Nephro toxicity	Acute oral toxicity	PPAR Gamma	Eye irritation	Skin irritation
β-Sitosterol	-	+	+	+	+	-	I	+	-	+
Genkwanin	-	-	-	+	-	-	III	+	+	-
Epigallocatechin	-	+	+	+	+	-	IV	+	+	-
Hesperidin	-	-	-	+	-	-	III	+	-	-
Chlorogenic acid	-	+	+	+	+	-	III	+	-	-
Rutin	-	+	+	+	-	-	III	+	-	-
Prunin-Naringenin-7-O-glucosides	-	-	-	+	+	+	III	+	-	-
3'-Benzyloxy-5,6,7,4'-tetramethoxy flavone	-	-	-	+	-	-	III	+	-	-
3-Feruloylquinic acid	-	+	+	+	+	-	III	-	-	-
Kaempferitrin	-	-	-	+	+	-	III	+	-	-
Tolrestat*	-	+	+	+	+	-	III	+	-	-
Acarbose*	-	+	+	+	+	-	IV	+	-	-

KEY: * denotes Standard drug
+ Denotes active
- Denotes inactive
I Denotes highly toxic and highly irritating
II Denotes moderately toxic and moderately irritating
III Denotes slightly toxic and slightly irritating
IV Denotes practically non-toxic and non-irritating

https://doi.org/10.55549/zbs.1644267

Table 6 presents the effect of *Cucumis sativus* peel extract (CSPE) on both protein concentration and glucose levels. The results indicate that administration of 600 mg of CSPE led to a significant ($p<0.05$) increase in protein concentration, suggesting a potential role in enhancing protein synthesis or preserving structural and functional proteins in diabetic conditions. Conversely, glucose levels were significantly reduced ($p<0.05$) compared to both the control and STZ-untreated diabetic groups, indicating the hypoglycemic potential of CSPE. This reduction in glucose levels may be attributed to improved insulin sensitivity, enhanced glucose uptake by peripheral tissues, or modulation of key metabolic pathways involved in carbohydrate metabolism.

Table 6. Effects of CSPE on Protein and Glucose Concentrations

S/N	Experimental Groups	Protein Conc. [mg/ dL]	Glucose Conc. [mg/ mL]
1.	Control	0.25 ± 0.06^{a}	86.15 ± 1.24^{a}
2.	STZ	0.13 ± 0.02^{b}	207.41 ± 4.90^{b}
3.	STZ + CSPE 600 mg	0.29 ± 0.05^{a}	138.30 ± 2.68^{c}
4.	STZ + Glb	0.16 ± 0.03^{b}	79.93 ± 1.05^{a}

Data shows mean ± SEM (n=6) and values with different alphabets (a, b, c) are statistically significant at $p<0.05$. STZ = streptozotocin, CSPE = *Cucumis sativus* pulp extract and Glb = Glibenclamide.

Figure 2 shows the effect of CSPE on antioxidant activities. The administration of 600 mg CSPE significantly ($p<0.05$) increased both superoxide dismutase (SOD) and catalase (CAT) activities compared to the STZ-untreated group. This increase suggests an enhanced antioxidant defense system, which may contribute to the reduction of oxidative stress and protection of cellular components from free radical damage. Figure 3 shows the effect of CSPE on Liver function parameters. The administration of 600 mg CSPE was observed to significantly ($p<0.05$) decrease both aspartate transferase (AST) and alanine transferase (ALT) activities compared to the STZ-untreated group. This reduction indicates a protective effect on liver tissues, potentially preventing hepatocellular injury and improving overall liver function in diabetic conditions.

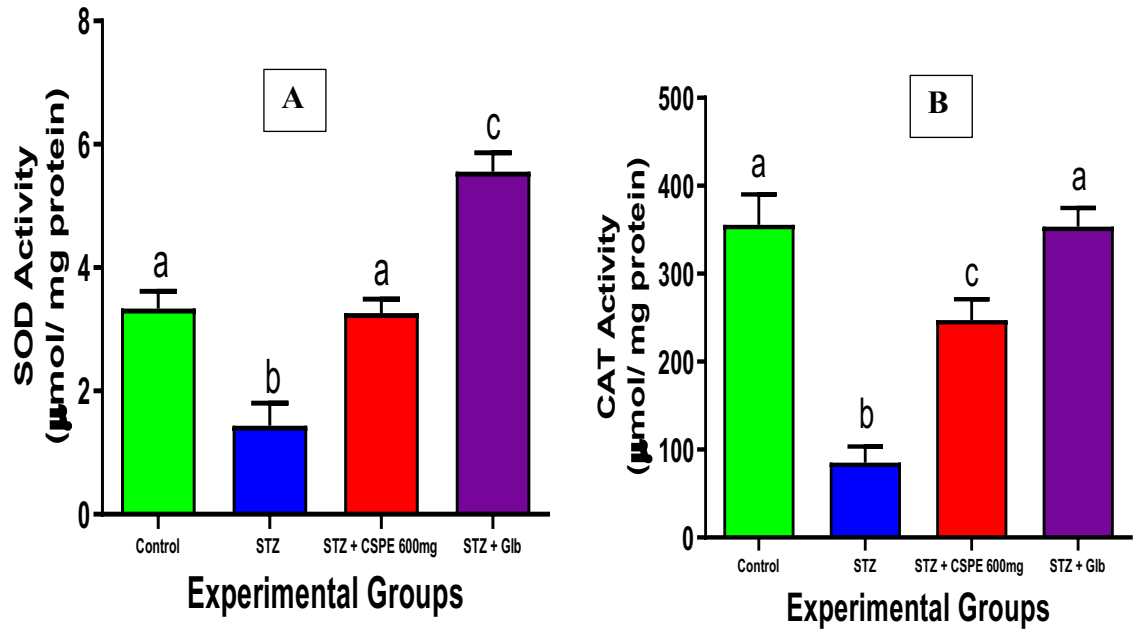

Figure 2. Effect of *Cucumis sativus* pulp extract (CSPE) on antioxidant activities in STZ-induced diabetic Wistar rats. Each bar represents mean ± SEM (n=6) and bars with different alphabets (a, b, c) are statistically significant at $p<0.05$. STZ = streptozotocin, CSPE = *Cucumis sativus* pulp extract and Glb = Glibenclamide.

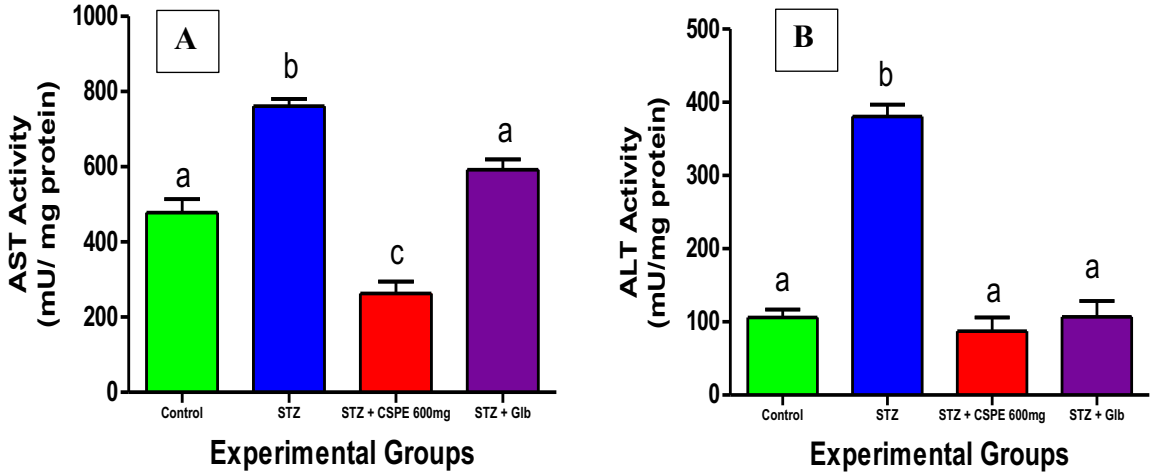

Figure 3. Effect of *Cucumis sativus* Pulp Extract (CSPE) on Lipid enzyme activities in STZ-induced diabetic Wistar rats. Each bar represents mean ± SEM (n=6) and bars with different alphabets (a, b, c) are statistically significant at $p<0.05$. STZ = streptozotocin, CSPE = *Cucumis sativus* Pulp Extract and Glb = Glibenclamide.

Table 7 presents the effect of *Cucumis sativus* peel extract (CSPE) on oxidative stress markers. The results indicate that the administration of 600 mg of CSPE led to a significant ($p<0.05$) increase in non-protein thiol (glutathione) concentration compared to the control and STZ-untreated groups. Glutathione plays a crucial role in cellular antioxidant defense by neutralizing reactive oxygen species (ROS) and detoxifying harmful compounds, suggesting that CSPE may enhance endogenous antioxidant capacity.

Furthermore, the administration of 600 mg of CSPE significantly (p<0.05) decreased the concentrations of hydrogen peroxide (H_2O_2) and malondialdehyde (MDA) compared to both the control and STZ-untreated groups. The reduction in H_2O_2 levels indicates a lower presence of oxidative radicals that could otherwise contribute to cellular damage. Similarly, the decrease in MDA, a well-known marker of lipid peroxidation, suggests that CSPE helps protect membrane lipids from oxidative degradation, thereby preserving cellular integrity and reducing oxidative damage in diabetic conditions.

However, treatment with 600 mg of CSPE did not result in a statistically significant difference (p>0.05) in nitric oxide (NO) levels when compared to the STZ-untreated group. This finding suggests that while CSPE effectively modulates several oxidative stress markers, its impact on NO metabolism may be limited or require a different dosage or duration of treatment to produce noticeable changes. Nitric oxide plays a dual role in oxidative stress, acting as both a signaling molecule and a potential contributor to oxidative damage, depending on its concentration and interaction with other reactive species. Overall, these findings highlight the potential of CSPE in mitigating oxidative stress by enhancing antioxidant defense mechanisms and reducing lipid peroxidation, which may contribute to its protective role in diabetes management.

Table 7. Effects of CSPE on Oxidative stress indices.

S/N	Experimental Groups	H_2O_2 [mmol/ mL]	NO [mmol/ mL]	MDA [nmol]	GSH [µmol/ mg protein]
1.	Control	0.059 ± 0.01^a	0.337 ± 0.00^a	80.02 ± 2.75^a	339.8 ± 13.78^a
2.	STZ	0.194 ± 0.04^b	0.584 ± 0.31^b	297.4 ± 6.87^b	191.6 ± 7.02^b
3.	STZ + CSPE 600 mg	0.081 ± 0.01^a	0.545 ± 0.44^b	132.86 ± 5.91^c	411.5 ± 23.17^c
4.	STZ + Glb	0.076 ± 0.00^a	0.312 ± 0.05^a	108.44 ± 2.12^c	302.5 ± 6.830^a

Data shows mean ± SEM (n= 6) and values with different alphabets (a, b, c) in the same column are statistically significant at p<0.05. STZ = streptozotocin, CSPE = *Cucumis sativus* pulp extract and Glb = Glibenclamide.

Table 8 presents the effect of CSPE on lipid profile indices. The administration of 600 mg of CSPE resulted in a significant (p<0.05) reduction in total cholesterol, triglycerides, low-density lipoprotein cholesterol (LDL-C), and very-low-density lipoprotein cholesterol (VLDL-C) concentrations compared to the STZ-untreated diabetic animals. This suggests that CSPE may play a beneficial role in lipid metabolism by lowering harmful lipids that are commonly elevated in diabetic dyslipidemia, thereby potentially reducing the risk of cardiovascular complications associated with diabetes.

Interestingly, the administration of CSPE resulted in a statistically significant (p<0.05) increase in high-density lipoprotein cholesterol (HDL-C) levels compared to the STZ-untreated diabetic animals. Moreso, there was no statistical significance (p>0.05) between the animals treated with the extract or standard drug, glibenclamide. However, the treated groups were statistically significantly (p<0.05) lower than the normal control. This may indicate that CSPE may help improve lipid profile balance by targeting elevated cholesterol and triglyceride levels. HDL-C

is considered beneficial and good cholesterol as it facilitates reverse cholesterol transport and protects against atherosclerosis. This suggests that while CSPE effectively modulates harmful lipid fractions, it does not significantly enhance protective lipoproteins within the dosage and duration of treatment used in this study.

Table 8. Effects of CSPE on Lipid profile indices

S/N	Experimental Groups	Total-Chol [mg/ dL]	TRIG [mg/ dL]	HDL-Chol [mg/ dL]	LDL-Chol [mg/ dL]	VLDL-Chol [mg/dL]
1.	Control	202.6 ± 1.13^{a}	196.2 ± 2.79^{a}	211.4 ± 9.90^{a}	41.77 ± 0.29^{a}	39.24 ± 0.56^{a}
2.	STZ	599.2 ± 0.376^{b}	452.6 ± 39.18^{b}	59.0 ± 0.84^{b}	148.2 ± 11.28^{b}	148.5 ± 9.84^{b}
3.	STZ + CSPE 600 mg	196.4 ± 1.32^{a}	287.4 ± 36.45^{c}	145.04 ± 0.16^{c}	39.95 ± 7.71^{a}	57.48 ± 7.29^{a}
4.	STZ + Glb	295.2 ± 5.755^{c}	237.8 ± 14.07^{a}	167.1 ± 5.725^{c}	55.58 ± 2.64^{a}	50.63 ± 2.27^{a}

Data shows mean ± SEM (n=6) and values with different alphabets (a, b, c) in the same column are statistically significant at $p<0.05$. STZ = streptozotocin, CSPE = *Cucumis sativus* pulp extract and Glb = Glibenclamide.

Discussion

The choice of 600 mg/kg body weight of *Cucumis sativus* pulp extract used in this study was based on the yield obtained from the extract preparation process and also from a previous study by Saidu *et al.* (2014), who used 500 mg/kg body weight of methanol fruit pulp extract of *C. sativus* for the treatment of alloxan-induced diabetic rats (AIDRs). Meanwhile, the dose of glibenclamide (5 mg/kg body weight) used in this study was based on the dose of each tablet consumed by diabetic patients according to the manufacturer's prescription. Bioactive compounds, including flavonoids, phenolics, tannins, and saponins, were present and abundant in CSPE. These substances have all been linked to glucose and lipid-lowering activities and considerable antioxidant potential (Oloruntoba and Ayodele, 2022). This study showed abundant total flavonoids (TFC), total phenols (TPC), and total tannins (TTC), which are known to scavenge free radicals and reduce oxidative stress, a major contributor to diabetes complications (Quranayati *et al.*, 2023). HPLC further validated the polyphenolic content of CSPE, and their capacities to control glucose metabolism, reduce oxidative stress, and scavenge free radicals have been reported (Chaudhary *et al.* 2023). Various volatile compounds were also observed via GC-MS analysis, and compounds such as sterols, fatty acid compounds, glycosides, and terpenoids were detected. Terpenoids are known to have lipid-lowering properties, hence, the presence of steroids and terpenoids implies that these compounds may be involved in regulating lipid metabolism (Mannino *et al*., 2021). These comprehensive analyses suggest that *Cucumis sativus* may affect glucose and lipid metabolism.

The induction of diabetes (type 2) with 60 mg/kg body weight of STZ resulted in partial pancreatic failure, but treatment with *Cucumis sativus* pulp extract (CSPE) significantly ($p<0.05$) reduced and increased the blood glucose and protein concentrations, respectively, compared to STZ-untreated diabetic animals. Since the glucose is only reduced in the treated animals, it is justifiable and appropriate to associate this activity with the fruit's embedded phytochemicals, especially the high polyphenolic content. These polyphenolics may have resulted in improved insulin sensitivity, glucose utilization and metabolic functioning, and overall cell health, respectively, in the treated rats. These findings corroborate the report of

Thabti *et al.* (2012), who suggested that phenolics and flavonoids have blood sugar-lowering bioactivity.

Antioxidant enzymes (SOD and CAT) regulate oxygen and hydrogen peroxide levels by neutralizing radicals and organic peroxides caused by STZ exposure. In this study, STZ-induced diabetes impaired hepatic antioxidant enzymes, with SOD converting superoxide radicals to H2O2 and O2, while CAT removes H2O2 (Drabińska, 2024). The reduced liver SOD and CAT activities observed in diabetic animals may result from increased ROS generation, including superoxide ($O2^{-}$) and hydroxyl (OH^{-}) radicals, induced by STZ. These free radicals may have inactivated these enzymes, weakening antioxidant defenses against ROS damage. However, the treatment of the STZ-induced diabetic animals with CSPE significantly ($p<0.05$) increased the activities of these antioxidant enzymes. In contrast, hydrogen peroxide (H_2O_2) and malondialdehyde (MDA) levels significantly ($p<0.05$) decreased, reflecting reduced oxidative stress. Furthermore, treatment with CSPE significantly ($p<0.05$) increased non-protein thiol (GSH) concentrations, reinforcing the defense against oxidative stress. These findings may indicate that *Cucumis sativus* fruit pulp extract may help reduce oxidative stress, a critical factor in the progression of diabetes complications (Heidari *et al.*, 2016).

In diabetic conditions, the elevated activities of liver function markers such as aspartate aminotransferase (AST) and alanine aminotransferase (ALT) have been associated with liver dysfunction leading to liver necrosis (Farid *et al.*, 2022). As a result, the increase in serum AST and ALT activity in diabetic untreated control animals may be attributed to the leakages of these enzymes from the liver cytosol into the bloodstream, indicating the hepatotoxic action of STZ.

Conversely, administration of CSPE to the STZ-induced diabetic animals reduced the activity of these enzymes compared to the STZ-induced untreated animals (Mbatha *et al.*, 2022).

In addition to a significant increase in the animal's blood glucose (hyperglycemia) and liver enzyme dysfunction observed following the induction of diabetes using STZ, a significant ($p<0.05$) increase in lipids (hyperlipidemia) was also observed in the STZ-induced diabetic animals. This is in agreement with the report of Nabi *et al.* (2013). However, treatment with CSPE regulated the lipid profile by significantly ($p<0.05$) reducing the total cholesterol, triglycerides, LDL-cholesterol, and VLDL-cholesterol levels. Meanwhile, a significant ($p<0.05$) increase in HDL-cholesterol was observed with the treatment with CSPE. A similar trend has been reported by Al-Snafi *et al.* (2019).

The *in-silico* study provided more insight into the molecular mechanism of *Cucumis sativus* bioactive compounds and the selected diabetes-related protein targets. Molecular docking is an essential computational tool in the field of drug discovery and development for comprehending the interactions that occur between small molecules and target proteins (Sahu *et al.*, 2024). From all the ligands (bioactive compounds) generated from GC-MS and HPLC analyses of *C. sativus*, β-sitosterol and hesperidin showed stronger binding affinities for α-amylase, α-glucosidase, sorbitol dehydrogenase, and aldose reductase than the standard drugs incorporated in this study (acarbose and tolrestat). These enzymes (protein targets) are essential for the regulation of insulin and the metabolism of carbohydrates (Dubey *et al.*, 2020), and inhibiting them can decrease blood glucose and increase insulin sensitivity like that of current anti-diabetic medications (Bhosale *et al.*, 2024). β-sitosterol showed the strongest inhibitory effect against α-amylase and aldose reductase, and hesperidin showed the best affinity for α-glucosidase and sorbitol dehydrogenase, indicating that the two ligands can regulate or manage diabetes mellitus through these enzymes.

In the last decade, drug failures due to poor pharmacokinetic profiles, medicinal chemistry properties, efficacy, unmanaged toxicity, and inadequate drug-like properties have been on the rise. This led to a focus on improving the drug development process by utilizing ADMET properties at the early stages (Dulsat *et al*., 2023). In this study, the ADMET properties of the top ten (10) ligands resulting from the *in-silico* study were analyzed using SwissADME, admetSAR, and ProTox software. The physicochemical properties of the top ten (10) ligands showed that β-sitosterol obeyed the Lipinski rule of five while hesperidin disobeyed it (Lipinski, 2004), which shows that all ten ligands have the potential to be used in the development of new pharmaceuticals (Ivanović *et al*., 2020).

The assessment of the water-soluble properties showed that the ligand with the best binding affinity, β-sitosterol, is poorly soluble in water, meanwhile, its lipophilicity property showed the best solubility in lipids with a value of 5.05 and this may be advantageous because drug potency and lipid solubility improve as the values move away from zero. This aligns with similar studies by Chmiel *et al*. (2019). The evaluation of the drug-likeness properties showed that the top ten ligands had good bioavailability scores of 0.55, which is encouraging because a chemical must have a bioavailability score of at least 0.10 to be classified as a drug candidate (Ntie-Kang *et al*., 2019; Awote *et al.*, 2024). Three of the top ten ligands – epigallocatechin, chlorogenic acid, and rutin showed positive pan-assay interference compounds (PAINS) indication. Meanwhile, genkwanin and epigallocatechin showed lead-like indications. Furthermore, all the best ten ligands and the standard drugs have a synthetic score ranging from

2.34 to 7.34, where acarbose demonstrated the best synthetic accessibility. This may imply that this compound can be easily used in the synthesis of a new drug (Stratton *et al*., 2015). The blood-brain barrier permeability showed a negative indication for all the ligands, as a result, this compound may not be developed for use in the treatment of central nervous system (CNS) disorders, especially in neurological disorders, including dementia, schizophrenia, and Alzheimer's disease (Małkiewicz *et al*., 2019). SwissADME and admetSAR predictions revealed that all of the top ten ligands have a negative indicator for carcinogenic toxicity and a positive indicator for reproductive toxicity. Seven compounds, including β-sitosterol, epigallocatechin, chlorogenic acid, rutin, tolrestat, acarbose, and 3-feruloylquinic acid, showed a positive indicator for hepatotoxicity and respiratory toxicity. In addition, β-sitosterol, epigallocatechin, chlorogenic acid, prunin-naringenin-7-O-glucosides, acarbose, tolrestat, and 3-feruloylquinic acid predicted mitochondrial toxicity, while prunin-naringenin-7-O-glucosides predicted nephrotoxicity.

Conclusion

In conclusion, the findings from this study suggest *Cucumis sativus* fruit as a functional food with possible natural medicinal therapeutic properties for the management and treatment of diabetes, particularly in reducing oxidative stress, improving liver function, and regulating glucose and lipid metabolism. Additionally, its antioxidant properties likely play a crucial role in protecting pancreatic and hepatic tissues from oxidative damage, thereby supporting overall metabolic health.

While these results demonstrate promising antidiabetic effects, further studies are required to isolate and characterize the active phytochemicals responsible for these effects, elucidate their precise molecular mechanisms, and evaluate their long-term safety and efficacy through clinical trials. Future research should also explore the potential synergistic effects of *Cucumis sativus* with existing antidiabetic medications and its application in functional food formulations. These insights could contribute to the development of novel nutraceutical strategies for diabetes

prevention and management.

Declaration of Conflict of Interest

The authors of this research declare no known financial or any other conflict of interest.

Authors and Contribution

O.K.A. developed the concept and designed experiments. B.O.O. carried out the investigation and wrote the first draft. A.G.A. conducted the *in-silico*/ bioinformatics analyses. I.O.A. performed the statistical analysis. O.O.O. and B.D.K. reviewed and edited the manuscript.

References

Adamu, A. U., Abdulmumin, Y., & Mustapha, R. K. (2021). Green Synthesis, Characterization and Phytochemicals Analysis of Silver Nano-Particles Using Aqueous Peel Extract of Cucumis sativus. *J. Mater. Environ. Sci*, *12*(12), 1627-1636.

Andrés, C. M. C., Lastra, J. M. P. D. L., Juan, C. A., Plou, F. J., & Pérez-Lebeña, E. (2023). Chemical insights into oxidative and nitrative modifications of DNA. *International Journal of Molecular Sciences*, *24*(20), 15240.

Andrés, C. M. C., Pérez de la Lastra, J. M., Juan, C. A., Plou, F. J., & Pérez-Lebeña, E. (2024). Antioxidant Metabolism Pathways in Vitamins, Polyphenols, and Selenium: Parallels and Divergences. *International Journal of Molecular Sciences*, *25*(5), 2600.

Afzal, S., Abdul Manap, A. S., Attiq, A., Albokhadaim, I., Kandeel, M., & Alhojaily, S. M. (2023). From imbalance to impairment: the central role of reactive oxygen species in oxidative stress-induced disorders and therapeutic exploration. *Frontiers in Pharmacology*, *14*, 1269581.

Awote OK, Amisu KO, Anagun OS, Dohou FP, Olokunola ER and Elum NO. (2024). *In vitro* and Molecular Docking Evaluation of the Antibacterial, Antioxidant, and Antidiabetic Effects of Silver Nanoparticles from *Cymbopogon citratus* Leaf. *Tropical Journal of Natural Product Research (TJNPR)*, *8*(9): 8400–8411.

Awote, O.K., Kazeem, M.I., Ojekale, A.B., Ayanleye, O.B., & Ramoni, H.T. (2023). Prospects of silver nanoparticles (AgNPs) synthesized by *Justicia secunda* aqueous extracts on diabetes and its related complications. Proc Nig Acad Sci., 16(1): 87-105.

Awote, O.K., Apete, S.K., Igbalaye, J.O., Adeyemo, A.G., Dele-osedele, P.I., Thomas-Akinwale, K., Boniwey, T.S., Ogunbamowo, A.A., Ebube, S.C., Folami, S.O. (2022). Phytochemical Screening, Antioxidant, and α-Amylase Inhibitory Activities of *Acacia nilotica* Seed Methanol Extract. Adv J Curr Res., 7(8): 1-27.

Awote, O. K., Igbalaye, J. O., & Gideon, A. (2021). Effect of *Phragmanthera incana* Leaves Extracts on Lipid Profile in Wistar Rats Fed High-Fat Diet. *International Journal of Formal Sciences: Current and Future Research Trends*, *12*(1), 23-32.

Banu, S., & Bhowmick, A. (2017). Therapeutic targets of type 2 diabetes: An overview. *MOJ Drug Des. Dev. Ther*, *1*(11).

Bhosale, H. J., Mamdapure, S. V., Panchal, R. B., & Dhuldhaj, U. P. (2024). α-Amylase, α-glucosidase, and aldose reductase inhibitory and molecular docking studies on Tinospora cordifolia (Guduchi) leaf extract. *Future Journal of Pharmaceutical Sciences*, *10*(1), 107.

Chaudhary, P., Janmeda, P., Docea, A. O., Yeskaliyeva, B., Abdull Razis, A. F., Modu, B., Calina, D., & Sharifi-Rad, J. (2023). Oxidative stress, free radicals and antioxidants: Potential crosstalk in the pathophysiology of human diseases. *Frontiers in chemistry*, *11*, 1158198.

Chmiel, T., Mieszkowska, A., Kempińska-Kupczyk, D., Kot-Wasik, A., Namieśnik, J., & Mazerska, Z. (2019). The impact of lipophilicity on environmental processes, drug delivery and bioavailability of food components. *Microchemical Journal*, *146*, 393-406.

Daliri, E. B. M., Oh, D. H., & Lee, B. H. (2017). Bioactive peptides. *Foods*, *6*(5), 32. Drabińska, N. (2024). Current Perspective About the Effect of a Ketogenic Diet on Oxidative

Stress–a Review. *Polish Journal of Food and Nutrition Sciences*, *74*(1), 92-105.

Dubey, K., Dubey, R., Gupta, R., & Gupta, A. K. (2020). α-Amylase, α-Glucosidase and Aldose reductase Inhibitory Potential of Betanin for the Management of Diabetes and its complications. *Journal of Advanced Scientific Research*, *11*(03), 92-95.

Dulsat, J., López-Nieto, B., Estrada-Tejedor, R., & Borrell, J. I. (2023). Evaluation of free online ADMET tools for academic or small biotech environments. *Molecules*, *28*(2), 776.

Farid, M. M., Aboul Naser, A. F., Salem, M. M., Ahmed, Y. R., Emam, M., & Hamed, M. A. (2022). Chemical compositions of Commiphora opobalsamum stem bark to alleviate liver complications in streptozotocin-induced diabetes in rats: Role of oxidative stress and DNA damage. *Biomarkers*, *27*(7), 671-683.

Green, L. C., Wagner, D. A., Glogowski, J., Skipper, P. L., Wishnok, J. S., & Tannenbaum, S.

R. (1982). Analysis of nitrate, nitrite, and [15N] nitrate in biological fluids. *Analytical biochemistry*, *126*(1), 131-138.

Haghani, F., Arabnezhad, M. R., Mohammadi, S., & Ghaffarian-Bahraman, A. (2022). Aloe vera and streptozotocin-induced diabetes mellitus. *Revista Brasileira de Farmacognosia*, *32*(2), 174-187.

Heidari, H., Kamalinejad, M., & Eskandari, M. R. (2012). Hepatoprotective activity of Cucumis sativus against cumene hydroperoxide induced-oxidative stress. *Research in Pharmaceutical Sciences*, *7*(5), 936.

Hossain, M. J., Al-Mamun, M., & Islam, M. R. (2024). Diabetes mellitus, the fastest growing global public health concern: Early detection should be focused. *Health Science Reports*, *7*(3), e2004.

Ivanović, V., Rančić, M., Arsić, B., & Pavlović, A. (2020). Lipinski's rule of five, famous extensions and famous exceptions. *Popular Scientific Article*, *3*(1), 171-177.

Jollow, D. J., Mitchell, J. R., Zampaglione, N. A., & Gillette, J. R. (1974). Bromobenzene-induced liver necrosis. Protective role of glutathione and evidence for 3, 4-bromobenzene oxide as the hepatotoxic metabolite. Pharmacology, 11(3): 151-169.

Khan, A., Mishra, A., Hasan, S. M., Usmani, A., Ubaid, M., Khan, N., & Saidurrahman, M. (2022). Biological and medicinal application of Cucumis sativus Linn.–review of current status with future possibilities. *Journal of Complementary and Integrative Medicine*, *19*(4), 843-854.

Kulkarni, A., Thool, A. R., & Daigavane, S. (2024). Understanding the Clinical Relationship Between Diabetic Retinopathy, Nephropathy, and Neuropathy: A Comprehensive Review. *Cureus*, *16*(3):e56674.

Latha, P. S., Sangeetha, S., Vijayakarthikeyan, M., & Shankar, R. (2024). Prevalence and influencing factors of metabolic syndrome among rural adult population in a district of South India. *Journal of Family Medicine and Primary Care*, *13*(8), 3122-3128.

Lipinski, CA. (2004). Lead-and drug-like compounds: the rule-of-five revolution. *Drug Discovery Today: Technologies,* 1(4): 337-41.

Lowry, O.H., Rosebrough, N.J., Farr, A.L., Randall, R.J., 1951. Protein measurement with the Folin phenol reagent. Journal of Biological Chemistry, 193: 265–275

Magliano, D. J., & Boyko, E. J. (2022). IDF diabetes atlas.

Małkiewicz, M. A., Szarmach, A., Sabisz, A., Cubała, W. J., Szurowska, E., & Winklewski, P.

J. (2019). Blood-brain barrier permeability and physical exercise. *Journal of neuroinflammation*, *16*, 1-16.

Mannino, G., Iovino, P., Lauria, A., Genova, T., Asteggiano, A., Notarbartolo, M., Porcu, A., Serio, G., Chinigò, G., Occhipinti, A. and Capuzzo, A., Medana, C., Munaron, L., & Gentile, C. (2021). Bioactive triterpenes of *Protium heptaphyllum* gum resin extract display cholesterol-lowering potential. *International Journal of Molecular Sciences*, *22*(5), 2664.

Mbatha, B., Khathi, A., Sibiya, N., Booysen, I., & Ngubane, P. (2022). A Dioxidovanadium Complex cis-[VO2 (obz) py] Attenuates Hyperglycemia in Streptozotocin (STZ)-Induced Diabetic Male Sprague-Dawley Rats via Increased GLUT4 and Glycogen Synthase Expression in the Skeletal Muscle. *Evidence-Based Complementary and Alternative Medicine*, *2022*(1), 5372103.

Molly, J., Edison, S., Vijajaraghavan, R., & Ajith, T. A. (2017). Effect of curry leaves and cucumber fruit on lipid profile in menopausal women with hyperlipidemia: a randomized controlled pilot study. *Int J Clin Trials*, *4*(1), 7-13.

Mukai, E., Fujimoto, S., & Inagaki, N. (2022). Role of reactive oxygen species in glucose metabolism disorder in diabetic pancreatic β-cells. *Biomolecules*, *12*(9), 1228.

Ntie-Kang, F., Nyongbela, K. D., Ayimele, G. A., & Shekfeh, S. (2019). “Drug-likeness” properties of natural compounds. *Physical Sciences Reviews*, *4*(11), 20180169.

Ogunyinka, B.I., Oyinloye, B.E., Osunsanmi, F.O., Opoku, A.R., & Kappo, A.P. (2017). Protective effects of *Parkia biglobosa* protein isolate on streptozotocin-induced hepatic damage and oxidative stress in diabetic male rats. Molecules, 22(10): 1654.

Oladimeji, S.O., Soares, A.S., Igbalaye, J.O., Awote, O.K., Adigun, A.K., & Awoyemi, Z.O. (2022). Ethanolic Root Extract of *Urtica dioica* Exhibits Pro-fertility and Antioxidant Activities in Female Albino Rats. *International Journal of Biochemistry Research & Review*. 31(8):29-38.

Oladimeji, S.O., Igbalaye, J.O., Awote, O.K., Shodimu, B.O., Oladeinde, D.T., Omorowa, V.T., Oluwole, S.M., Akinyemi, Y.A., Shobowale, A.Y., Jimoh, D., & Balogun, S.T. (2023). *Cissampelos pareira* ethanolic extract modulates hormonal indices, lipid profile, and oxidative parameters in transient infertility-induced female albino rats. *Bio- Research*, *21*(2), pp.1961-1972.

Oloruntola, O. D., & Ayodele, S. O. (2022). Phytochemical, proximate, and mineral composition, antioxidant and antidiabetic properties evaluation and comparison of mistletoe leaves from moringa and kolanut trees. *Turkish journal of agriculture-food science and technology*, *10*(8), 1524-1531.

Padhi, S., Nayak, A. K., & Behera, A. (2020). Type II diabetes mellitus: a review on recent drug-based therapeutics. *Biomedicine & Pharmacotherapy*, *131*, 110708.

Popoviciu, M. S., Paduraru, L., Nutas, R. M., Ujoc, A. M., Yahya, G., Metwally, K., & Cavalu,

S. (2023). Diabetes mellitus secondary to endocrine diseases: an update of diagnosticand treatment particularities. *International Journal of Molecular Sciences*, *24*(16), 12676.

Prince, P.S.M., & Menon, V.P., (2003). Hypoglycaemic and hypolipidaemic action of alcohol extract of *Tinospora cordifolia* root in chemical-induced diabetes in rats. Phytotherapy Research 17: 410–413.

Quranayati, Q., Iqhrammullah, M., Saidi, N., Nurliana, N., Idroes, R., & Nasution, R. (2023). Extracts from Phyllanthus emblica L stem barks ameliorate blood glucose level and pancreatic and hepatic injuries in streptozotocin-induced diabetic rats. *Arabian Journal of Chemistry*, *16*(9), 105082.

Sahu, M. K., Nayak, A. K., Hailemeskel, B., & Eyupoglu, O. E. (2024). Exploring recent updates on molecular docking: Types, method, application, limitation & future prospects. *International Journal of Pharmaceutical Research and Allied Sciences*, *13*(2-2024), 24-40.

Saidu, A. N., Oibiokpa, F. I., & Olukotun, I. O. (2014). Phytochemical screening and hypoglycemic effect of methanolic fruit pulp extract of Cucumis sativus in alloxan-induced diabetic rats. *Journal of Medicinal Plants Research*, *8*(39), 1173-1178.

Sari, T. A., Chandra, B., & Rivai, H. (2021). Overview of traditional use, phytochemical, and pharmacological activities of cucumber (*Cucumis sativus* L.). *International Journal of Pharmaceutical Sciences and Medicine*, *6*(3), 39-49.

Singh, R., Gholipourmalekabadi, M., & Shafikhani, S. H. (2024). Animal models for type 1 and

type 2 diabetes: advantages and limitations. *Frontiers in Endocrinology*, *15*, 1359685.

Sood, A., Kaur, P., & Gupta, R. (2012). Phytochemical screening and antimicrobial assay of various seeds extract of Cucurbitaceae family.

Stratton, C. F., Newman, D. J., & Tan, D. S. (2015). Cheminformatic comparison of approved drugs from natural product versus synthetic origins. *Bioorganic & medicinal chemistry letters*, *25*(21), 4802-4807.

Thabti, I., Elfalleh, W., Hannachi, H., Ferchichi, A., & Campos, M. D. G. (2012). Identification and quantification of phenolic acids and flavonol glycosides in Tunisian Morus species by HPLC-DAD and HPLC–MS. *Journal of Functional Foods*, *4*(1), 367-374.

Varshney, R., & Kale, R. K. (1990). Effects of calmodulin antagonists on radiation-induced lipid peroxidation in microsomes. *International journal of radiation biology*, *58*(5), 733-743.

Wolff, S.P. (1994). Ferrous ion oxidation in the presence of ferric ion indicator xylenol orange for measurement of hydroperoxides. Methods in Enzymology, 233: 182–189.

World Health Organization. (2019). *Global action plan on physical Activity 2018-2030: More Active People for a healthier world*. World Health Organization.

Yedjou, C. G., Grigsby, J., Mbemi, A., Nelson, D., Mildort, B., Latinwo, L., & Tchounwou, P.

B. (2023). The management of diabetes mellitus using medicinal plants and vitamins. *International Journal of Molecular Sciences*, *24*(10), 9085.